The spectrum of cosmic rays underground and at sea-level

F. Ashton

THE SPECTRUM OF COSMIC RAYS UNDERGROUND AND AT SEA-LEVEL

A thesis submitted to the University
of Durham for the Degree of
Doctor of Philosophy

by

F.Ashton

September, 1959

Abstract

From a measurement of the momentum spectrum of cosmic rays at different depths in the atmosphere and underground, information can be obtained on the interaction properties of the primary radiation and on the energy loss relation at high energies. Measurements of the spectra at 37.7 m.w.e. below sea-level and at sea-level have been made with magnetic spectrographs employing the new technique of neon flash-tubes to locate the trajectories at the detecting levels. From a comparison of the spectrum at sea-level with that at 37.7 m.w.e. information has been gained on the energy loss of μ-mesons in the range 3-12 GeV. A study of the energy loss up to 158 GeV has also been made from a comparison of the sea-level spectrum with the depth-intensity curve. The conclusion of these experiments is that up to 158 GeV the energy loss of μ-mesons is in accord with that expected theoretically.

Preface

In this thesis an account is given of the research carried out at the University of Durham by the author, under the supervision of Dr.A.W.Wolfendale, between September 1956 and September 1959. The construction of the prototype spectrograph was carried out in collaboration with Dr.S.Kisdnasamy who made the flash-tubes, the author being responsible for the electronic circuits and the mechanical construction of the instrument. The operation of the spectrograph and the interpretation of the results at sea-level and underground was the sole responsibility of the author.

The work carried out at sea-level with the Durham High Energy Spectrograph was performed with the help of Messrs. J.L.Lloyd, D.G.Jones, F.E.Taylor and P.J.Hayman. The author was responsible for the collection of the experimental data and the interpretation of the results.

The work on the prototype spectrograph has been published and two further papers on the spectrum underground have been submitted for publication.

Ashton F., Kisdnasamy S. and Wolfendale A.W., 1958, Nuovo Cimento, 8, 615.

Ashton F., Nash W.F. and Wolfendale, A.W., 1959, Proc.Roy.Soc., (in the press)

Ashton F., Nash W.F. and Wolfendale, A.W., 1959, Proc.Moscow Conference. (in the press)

CONTENTS

CHAPTER 1

Introduction

The phenomenological aspect of the cosmic radiation, such as the nature of the primary radiation, the mechanism of the interaction of the primary radiation with air nuclei at the top of the atmosphere, and the subsequent development of the cascade through the atmosphere and underground, is now moderately well understood. The primary radiation consists predominantly of protons which on entering the earth's atmosphere interact with air nuclei in approximately the first 100 gm. cm.$^{-2}$ to produce π-mesons and a small fraction of heavier mesons and hyperons. The $\pi^{\pm}$ mesons produced in these interactions either decay into μ-mesons or interact further to produce more π-mesons which subsequently decay into μ-mesons. As μ-mesons are weakly interacting and have a comparatively long lifetime they reach sea-level and penetrate underground. The radiation underground consists almost entirely of μ-mesons and their secondaries as nuclear interacting particles are rapidly absorbed. The π°-mesons produced in the primary interaction decay into two γ-rays which if of sufficiently high energy multiply rapidly to produce the electron-photon component of the large extensive air showers. At sea-level these showers are characterized by a high density of low energy electrons. Thus at sea-level the radiation of momentum > 500 MeV/c consists predominantly of μ-mesons with a small flux ($\sim 1\%$) of protons (Mylroi and Wilson, 1951).

The sea-level momentum spectrum of cosmic rays is of considerable interest, since, by developing a diffusion equation for the propagation of the radiation in the atmosphere, it is possible to gain information on the production spectrum of π-mesons in high energy nuclear collisions and also the nature of the high energy primary cosmic ray spectrum. Further, information on the energy loss of high energy μ-mesons can be obtained from a comparison of the sea-level momentum spectrum and the momentum spectrum of μ-mesons underground or the depth-intensity curve.

Several experiments have been performed to measure the sea-level spectrum, the most accurate being those of Caro, Parry and Rathgeber (1951) and Owen and Wilson (1955). In the range 0.5 - 20 GeV/$_c$ there is a discrepancy between these two spectra, the Owen and Wilson spectrum lying below that of Caro et al. for $p < 7$ GeV/$_c$ and above it for $p > 7$ GeV/$_c$. More recently, using higher momentum resolution, Rodgers (1956) has extended the measurements of Owen and Wilson and gained information on the shape of the spectrum up to 240 GeV/$_c$. The results of Rodgers indicate that at momenta > 50 GeV/$_c$ the energy loss of μ-mesons is greater than that expected theoretically and that also there are more particles present than can be accounted for by a π-μ decay process only. The excess of particles is attributed to the increased production of K-mesons in high energy nuclear collisions.

The underground spectrum has been measured at 57 m.w.e. (George and Shrikantia, 1956) and at ~ 40 m.w.e. (Dayon and Potapov, 1959).

One of the difficulties of measuring the momentum spectrum of cosmic rays underground and for momenta > 10 GeV/c at sea-level is the low flux of particles. To overcome this a spectrograph with a large solid-angle of collection and a high maximum detectable momentum which will work reliably over long periods of time is required. Recently Conversi et al. (1955) have introduced a new technique for the location of ionising particle trajectories which is ideally suited for use in a cosmic ray spectrograph. In Chapter 3 the development of a prototype spectrograph is described which uses this technique and later the use of the spectrograph to measure the momentum spectrum of cosmic rays at 37.7 m.w.e. is described. Finally the measurement of the sea-level spectrum using a much larger spectrograph is described and the results are considered in some detail.

CHAPTER 2

The measurement of the momenta of cosmic rays

Previous measurements of the momentum spectrum of cosmic rays have been made using the following techniques.

(a) Measurement of the angular deflection of the particles on traversing a magnetic field, using geiger counters, cloud chambers or nuclear emulsions as detectors.

(b) Measurement of multiple scattering in multiplate cloud chambers or nuclear emulsions.

The accuracy with which the momentum of a particle can be determined using the magnetic deflection technique can be seen by considering the relation between momentum, p (ev/c) magnetic deflection, θ (radians) and the line integral of the magnetic field along the particle trajectory, $\int H\,dl$ (gauss-cm.).

$$p = \frac{300 \int H\,dl}{\theta} \qquad (1)$$

(for a particle travelling in the plane perpendicular to the magnetic field)

Thus for a given magnet the maximum momentum that can be measured is determined by the accuracy of measurement of the angular deflection, θ. The limit of measurement, called the maximum detectable momentum, m.d.m., is defined as that value of p in equation (1) for which θ is the standard deviation of the uncertainty in the angular measurements.

Hyams et al. (1950) use the probable error in θ in defining the maximum detectable momentum but it is considered that the probable error gives an underestimate of the uncertainty. For a Gaussian distribution the standard deviation is 1.48 times the probable error.

In the determination of the sea-level spectrum Owen and Wilson used a tray of geiger counters of diameter 3.6 cm. at each of three detecting levels symmetrically placed about two magnets. With this arrangement they achieved an m.d.m. of 31 GeV/c (probable error). Caro et al. used two trays of counters above their magnet and one tray below. By employing two layers of overlapping counters of diameter 1.35 cm. at each level (equivalent to one layer of diameter 0.45 cm.) they achieved an m.d.m. of 100 GeV/c. It should be noted that spurious events caused by one particle traversing two detecting levels and a different one traversing the third within the resolving time of the coincidence circuits could not be recognised by either apparatus. With detectors at a fourth level this could have been done; for instance, in the Caro spectrograph, the requirement would have been that the projected incident and emergent trajectories should show only a small displacement at the centre of the magnetic field.

Extending the measurements of Owen and Wilson to higher momenta Rodgers placed shallow flat cloud chambers at the detecting levels of the Manchester spectrograph and achieved an m.d.m. of 240 GeV/c, corresponding to a location accuracy

of 1 mm. at each level.

In the emulsion spectrograph as developed by Apostolakis and Macpherson (1957) a very high m.d.m. can be attained but the technique is not very flexible as the particles of known momentum which emerge from the spectrograph cannot be used for further experiments other than a study of their interactions in a block of emulsion below the spectrograph.

The m.d.m. which can be attained by studying the multiple scattering in a multiplate cloud chamber is $\sim$ 4 GeV/$_c$. This limit is set mainly by track distortion due to gas movement. The nuclear emulsion limit is a little higher, being set by the distortion which occurs in processing.

In conclusion it can be said that the most powerful and flexible of the techniques for the measurement of high momenta is that of Rodgers where shallow flat cloud chambers are used as the detecting elements. In the next chapter a new technique is described which replaces the cloud chambers by arrays of neon flash-tubes giving an instrument of higher precision and greater reliability.

It should be noted that the so called sea-level spectra are not in fact measured at sea-level. The laboratories at ground level at which measurements have been made are however at such heights above sea-level ($<$ 500 ft.) that the spectra there are not significantly different from that at sea-level. The usual terminology - sea-level spectrum -

will be used throughout.

CHAPTER 3

The Prototype Spectrograph

3.1. Introduction

As stated in Chapter 1 the measurements of Rodgers on the sea-level spectrum for momenta > 50 GeV/c indicate the possibility of a new process contributing to the energy loss of high energy μ-mesons and also to the increased production of K-mesons in high energy nuclear collisions. Rodgers' spectrum above 50 GeV/c is based on the measurement of only 222 particles and is subject to a number of uncertainties. To substantiate the preliminary conclusions in the high energy region it is necessary to measure the spectrum accurately in this region; the design of a spectrograph to do this, using neon flash-tubes at the detecting levels, has been considered in detail by Kisdnasamy (1958). Before constructing such a spectrograph it was considered necessary to build a prototype so that in the large spectrograph the neon flash-tubes could be operated under their optimum conditions. The construction and performance of the prototype spectrograph will now be described.

3.2 The neon flash-tube

The neon flash-tube developed by Conversi et al. (1955) consists of a glass tube filled with neon gas. If several tubes are placed side by side between parallel metal electrodes then under certain conditions the tubes through which an ionising particle has passed can be made to flash. Normally several layers are mounted one above the other so that the path of the

particle is seen as a series of flashes. See figure 3.1 for a typical record.

The mechanism of operation of such an array is as follows. An ionising particle on traversing the array leaves a trail of ions in the gas and on the application of a pulsed electric field of ~ 6 KV/cm. the initial ionisation is multiplied and a visible discharge develops. A geiger counter coincidence system is used to trigger the high voltage pulsing circuit which applies the electric field to each layer of flash-tubes. The layer efficiency for particle detection is defined as the ratio of the number of single flashes observed in a given layer to the total number of times that an ionising particle has traversed that layer. The layer efficiency depends on the following factors.

1. The time delay between the passage of the particle and the application of the pulse.
2. The rise time of the pulse.
3. The height of the pulse.
4. The pressure and purity of the neon gas.

These factors have been studied extensively by Conversi et al. (1955), Gardener at al. (1957) and Coxell et al. (private communication). Briefly the result of these investigations is to show that high efficiency results from short time delays and rise-times, large pulses and pure gas at high pressure. The apparatus was constructed in such a way as to attain high efficiency of tube operation.

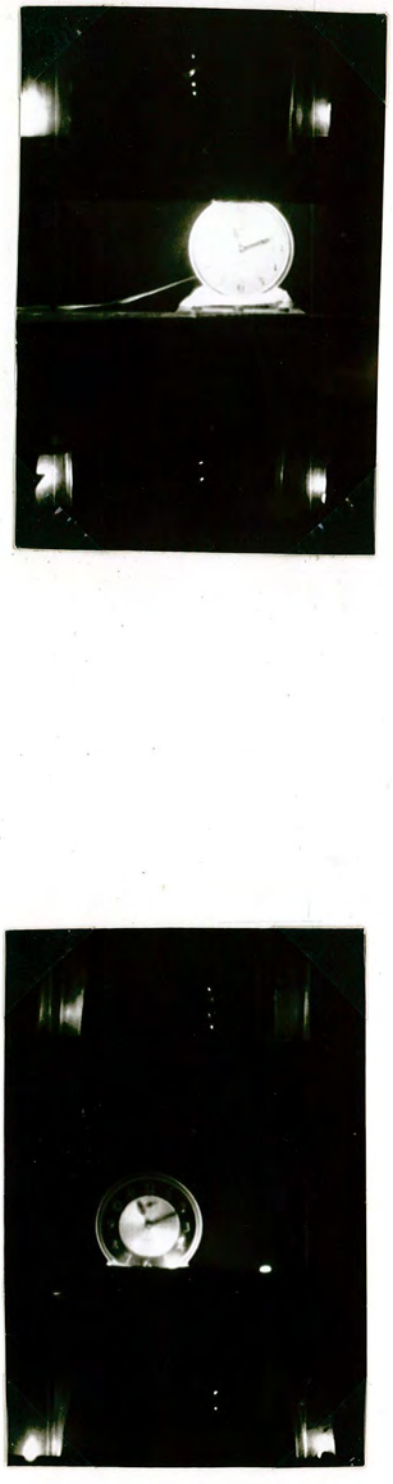

Figure 3.1 Typical record - prototype spectrograph.

In designing a detecting array to locate the trajectory to high accuracy consideration must be given to the optimum tube diameter and the number of layers of tubes required. A study of this problem was made graphically and it was found that for tubes having 100% internal detection efficiency and infinitesimal wall thickness that n layers of tubes of diameter d gave approximately the same location accuracy as n/3 layers of diameter d/3. Further considerations of the gas pressure required to give a reasonable number of ion pairs and the difficulties involved in manipulating tubes having very thin walls dictate a tube diameter of several millimetres. The tubes used in the experiments to be described had internal diameter 5.9 mm. and external diameter 7.7 mm.

3.3 The construction of the spectrograph

A scale diagram of the spectrograph as operated in a noise-level experiment at ground level in Durham is shown in figure 3.2. Let θ_1 be the angle that the incident trajectory makes with the vertical and θ_2 the angle that the trajectory makes with the vertical after passing through the magnetic field. Then the angular deflection is given by $\theta = \theta_1 - \theta_2$. The value of $\int H dl$ is measured using a search coil and fluxmeter and the momentum of the particle calculated from equation (1), Chapter 2.

θ_1 and θ_2 are measured by locating both the incident and emergent trajectories at two points by the arrays of flash-tubes A, B above the magnet and C,D below the magnet. The

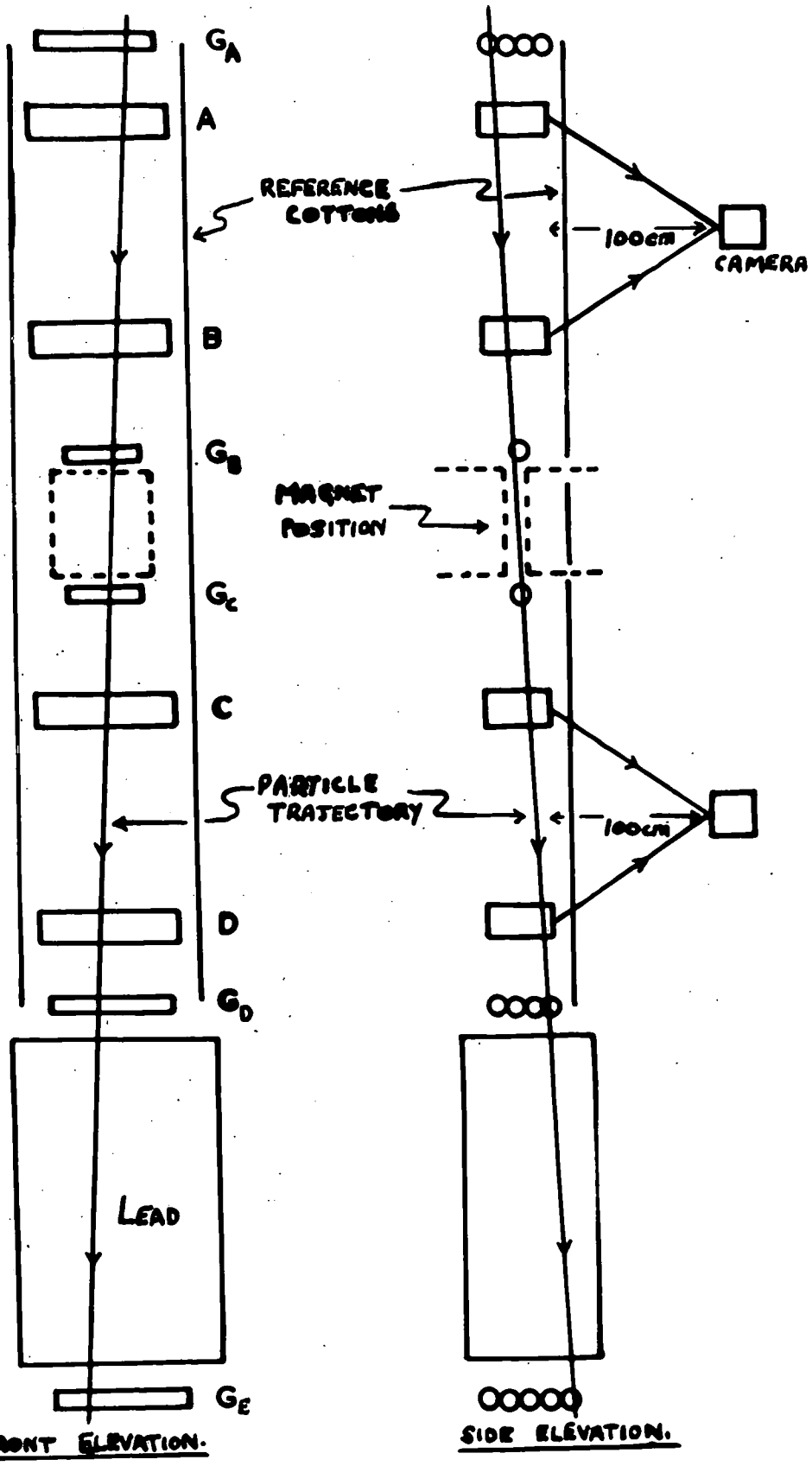

Figure 3.2 The prototype spectrograph as operated in the noise-level experiment in Durham. Scale = 1/11 full size.

reference line against which these angles are measured is provided by a length of weighted cotton hanging under gravity.

In figure 3.2, G_A, G_B, G_C, G_D are geiger counters which define the solid angle of acceptance of the spectrograph and A, B, C, D are arrays of flash-tubes. A and D contain 5 layers of tubes with 27 tubes per layer while B and C have 5 layers of tubes with 15 tubes per layer. All the flash-tubes are of length 15 cm., internal diameter 5.9 mm. and external diameter 7.7 mm. Each tube is coated with black paint to prevent light from one tube triggering an adjacent tube. All the tubes are filled with neon at a pressure of 65 cm. Hg and the tubes in a given layer are accurately located in parallel slots, the perpendicular distance between the axes of adjacent tubes being 8 mm. Hence looking down onto a layer of tubes the ratio of area covered by neon gas to area covered by glass and air = $\frac{5.9 \text{ mm.}}{8.0 \text{ mm.}}$ = 0.74. Thus the maximum possible layer efficiency that can be attained in practice = 74%.

The arrays A, B, C, D are adjusted so that the tubes in all arrays are parallel to one another. This is achieved by having two plates containing locating holes mounted on each array. The adjustment for the parallelism of all tubes is then achieved by two reference cottons hanging under gravity through the holes in the plates.

The mechanism of operation of the spectrograph is as follows: A particle traversing the spectrograph is selected by a four-fold coincidence from the geiger counters G_A, G_B, G_C,

G_D, This is achieved by a conventional Rossi circuit and the coincidence pulse is used to trigger a hydrogen thyratron which allows a condenser bank of capacity 0.012μF, charged to 8 KV, to discharge through the primary of a pulse transformer. The pulse developed across a resistance chain in parallel with the secondary is then fed across each layer of flash-tubes. The total capacity of the flash-tube array is 900 pF.

The time delay between the passage of the particle and the start of the pulse is 2μs. Of this 1μs occurs in the coincidence circuit and 1μs in the high voltage pulse forming network. The characteristics of the pulse are; rise time 0.5μs (defined as the time taken for it to reach 75% of its peak height), height 6 KV/cm. and length 4μs (defined as the length at 50% of its height).

Under these conditions the mean layer efficiency of all 20 layers of flash-tubes is (52 ± 2)% (corresponding to an internal efficiency of $52 \times \frac{8}{5.9} = 70\%$). The reason why the measured layer efficiency is less than the maximum expected value of 74% can best be understood by considering the way in which the tubes work.

The mechanism of operation of the tubes is thought to be as follows. A relativistic particle on the average produces ~ 10 ion pairs in traversing the diameter of a tube. Only electrons are useful in producing the breakdown of a tube as Ne^+ ions never gain sufficient energy to reach the ionisation potential of neon. During the time between the passage of the

particle and the application of the pulse the electrons diffuse and those reaching the walls stick and are lost. As a tube will not flash if there are no free electrons present when the pulse is applied the time delay of 2μs accounts for the reduction in layer efficiency. There is also a slight loss of efficiency due to the finite rise time, 0.5μs, of the pulse.

The tubes in a particular array are not stacked vertically one above the other, but the layers are staggered. The angle of stagger of the arrays A, B, C, D is 16° with respect to the vertical. The staggering angle was chosen by studying the problem graphically.

In determining the optimum staggering angle to employ it was assumed that the internal efficiency was 100% out to 0.70 of the internal tube radius and zero after that. In figure 3.3 the optimum stacking of the tubes is reproduced and in figure 3.4 the angles of incidence for which particles can traverse an array without producing any flashes is shown. In the use of the apparatus to measure the momentum spectrum of cosmic rays at 37.7 m.w.e. the range of angles that an accepted particle can make with the vertical is ± 9.2° (see Chapter 4). Thus the geometry of stacking chosen ensures that no geometrical bias due to the flash-tubes can occur.

3.4 The noise-level experiment

The spectrograph was first used to determine the accuracy with which the layers of flash-tubes could locate

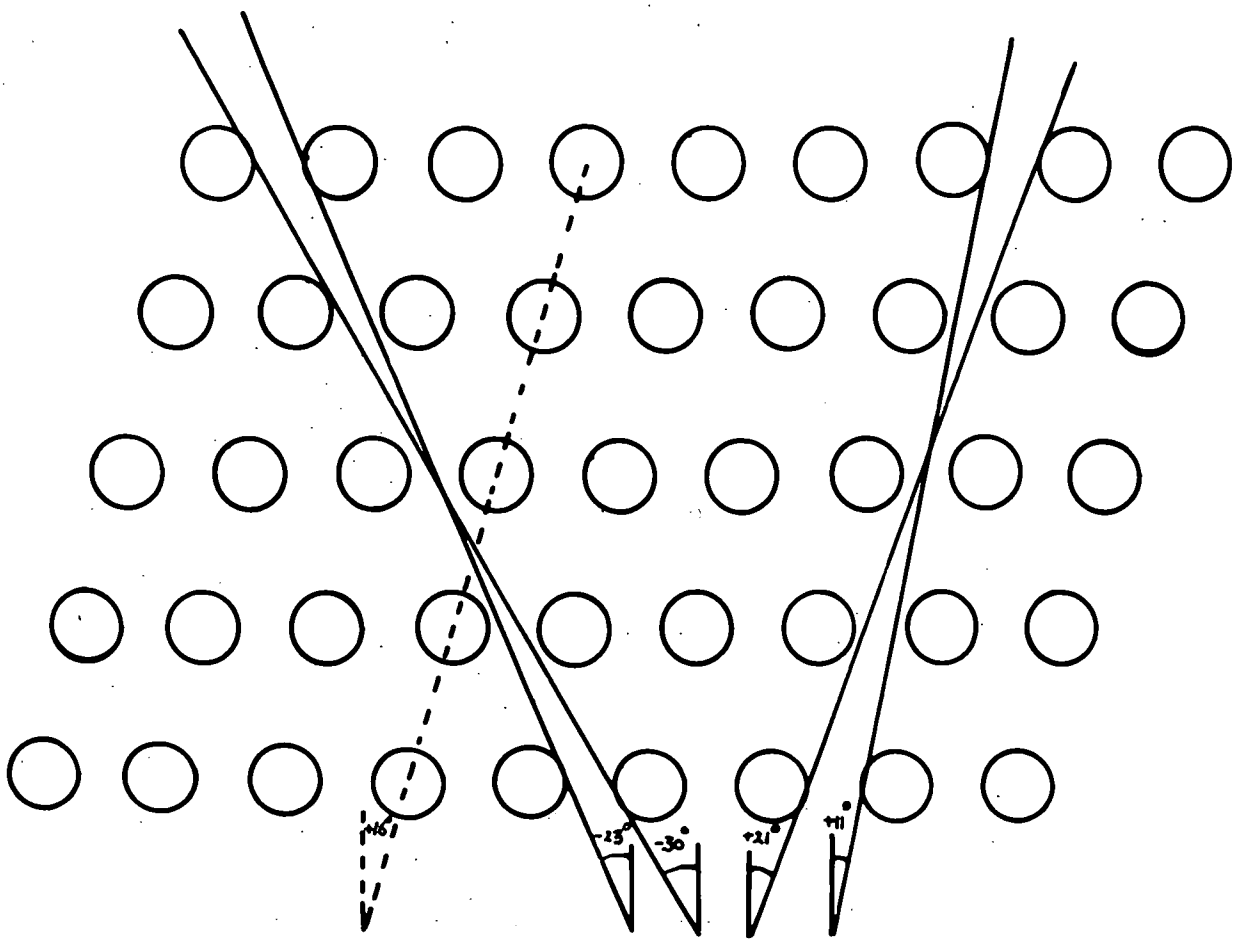

Figure 3.3 The staggering of the flash-tubes

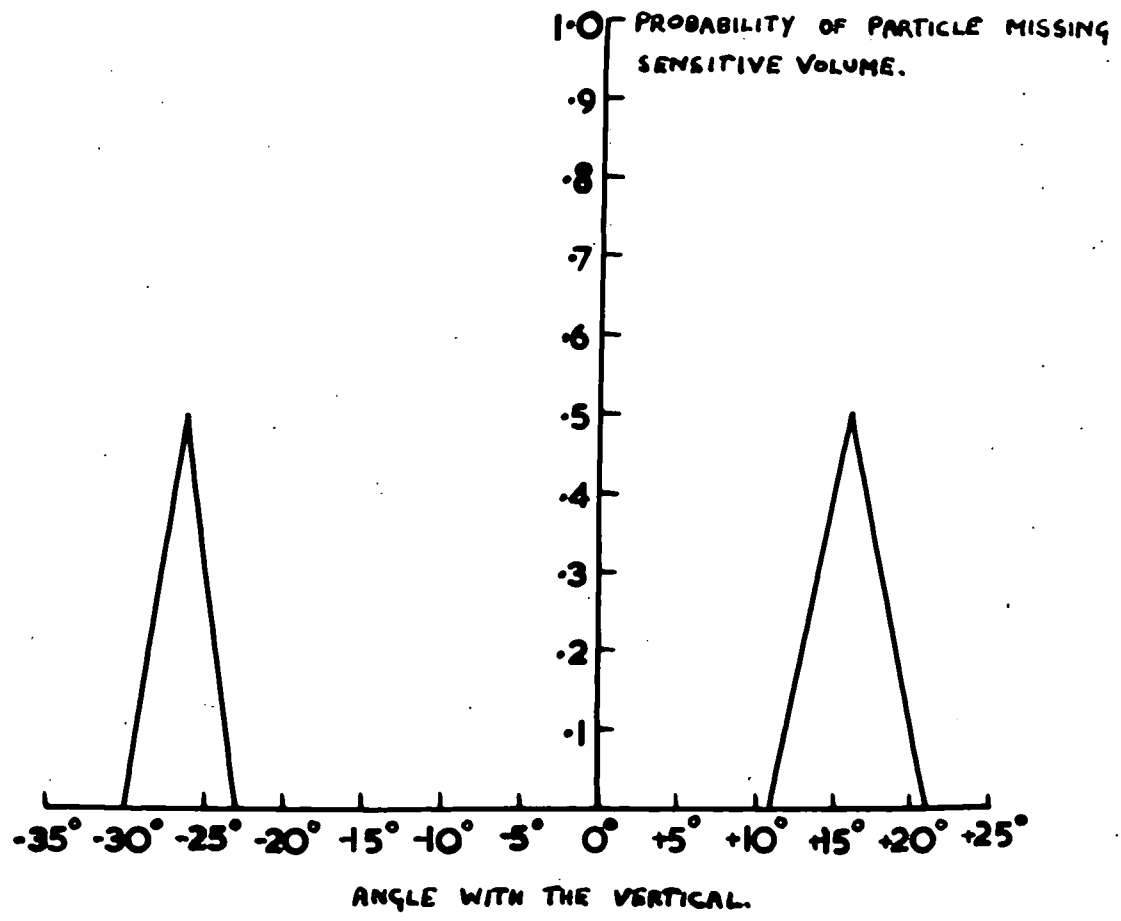

Figure 3.4 The sensitive volume of an array

the trajectory of a particle. This experiment was carried out at sea-level with the magnet removed. Particles with momentum greater than ~ 800 MeV/c were selected. The angle which the trajectory made with the vertical as measured by the arrays A, B was then compared with the angle it made with the vertical as measured by arrays C, D. The fact that in general these angles are different is due to three causes.

1. The best estimate of the trajectory found from the flash-tube data does not in general coincide with the actual trajectory. This error is referred to as the location error.

2. The particle suffers multiple scattering in arrays B, C and geiger counters G_B, G_C. The effect of scattering in the arrays A, D is merely to alter the direction of incidence and emergence of the particle and this does not add noise to the measured deflection.

3. The error of setting the measuring device on the best estimate of the trajectory.

Three methods of measuring the trajectories were investigated:

1. The centre of gravity of the pattern formed by the centres of the tubes which flashed at each level was calculated and the inclination of the line joining the appropriate pairs determined.

2. A scale diagram of the tube assembly was drawn and a length of cotton adjusted until it gave the best estimate of the track direction.

3. The photographic records were projected onto a rotatable screen ruled with close parallel lines and the required angles were measured with a protractor.

The criterion in 2 and 3 was that the best line should give maximum path length in the flashed-tubes.

Methods 2 and 3 were found to give consistent results while method 1 was inferior to these because of the reduction in uncertainty at one level arising from the knowledge of the approximate direction given by the information from the two levels taken together.

In the noise level experiment 93 acceptable photographs have been taken and the frequency distribution of the difference in the two angles is shown in figure 3.5. The results shown are those obtained with method 2 but the protractor results are similar. The distribution is centred about zero, as expected, and has r.m.s. deflection $\sigma_\perp = 0.33° \pm 0.02°$.

The problem now is to derive the contribution to σ arising from the inherent error in track location.

Let $\sigma_{scatt.}$ = r.m.s. contribution to σ due to multiple scattering in arrays B, C and the geiger counter G_B, G_C.

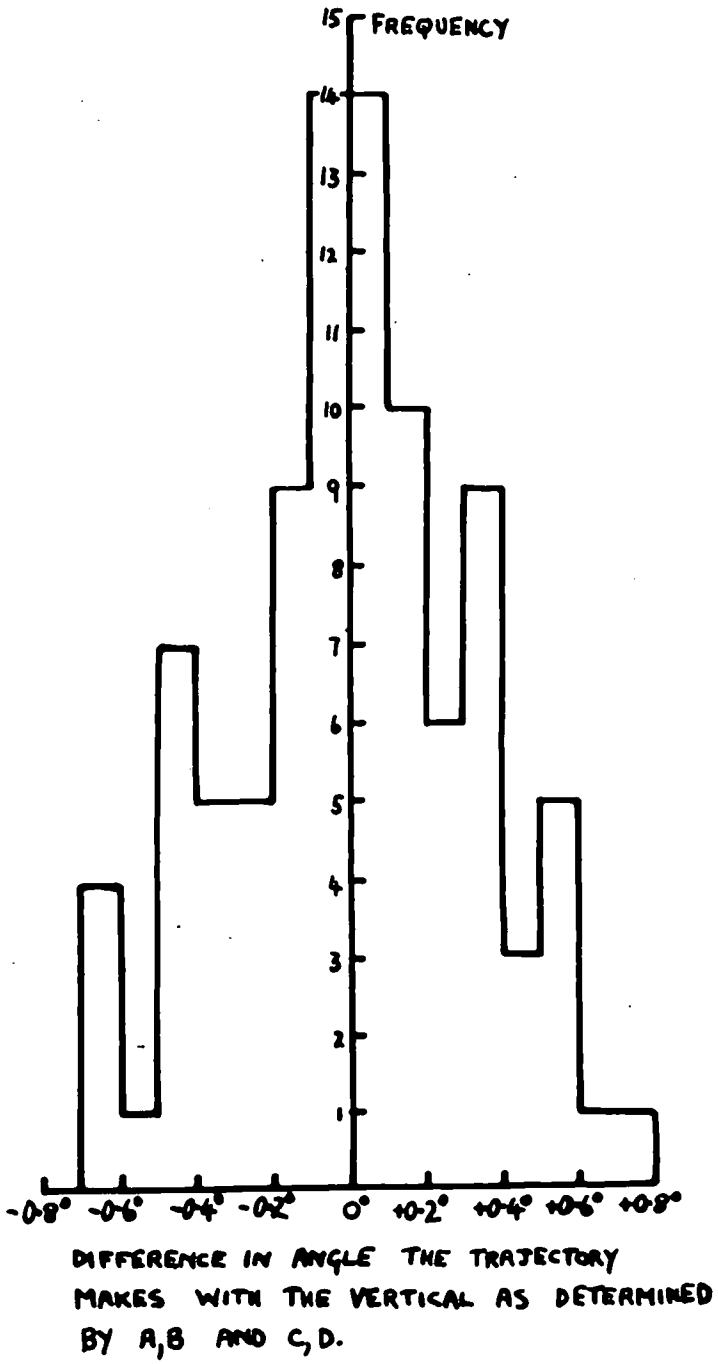

Figure 3.5 Noise-level distribution

Let σ_{sett} = r.m.s. contribution to σ due to errors of setting.

Let σ_I = r.m.s. contribution to σ due to the location error. Then

$$\sigma^2 = \sigma^2_{scatt} + \sigma^2_{sett} + \sigma_I^2 \qquad (2)$$

$\sigma^2_{scatt.}$ can be calculated and is given by

$$\sigma^2_{scatt.} = \frac{\int_{800}^{\infty} N(p)\,\theta_p^2\,dp}{\int_{800}^{\infty} N(p)\,dp}$$

where $\theta_p = \sum \frac{K t^{1/2}}{p\beta}$ and the sum is taken over the whole of the scattering material in arrays B, C and the geiger counters G_B, G_C. θ_p is the r.m.s. projected angle of scatter of a particle of momentum p and N(p) is the number of particles having momentum p in the sea-level spectrum (Owen and Wilson, 1955). The integration has been performed numerically from the low momentum cut off, of 800 MeV/c, due to the 53 cm. Pb below the spectrograph, to infinity and the result is $\sigma_{scatt.} = 0.22°$.

$\sigma_{sett.}$ was found by repeated measurements on several trajectories; $\sigma_{sett.} = 0.14°$.

From equation (2) σ_I can now be found.

$$\sigma_I = 0.20° \pm 0.03°$$

It is usual to quote the uncertainty as that of the position at a single level and this can be calculated. It must be borne in mind however that this uncertainty is less

than would be observed if the single level alone were used. This is because of the information on direction given by the combined data from the two levels taken simultaneously. The r.m.s. uncertainty, δ at a single level is given by

$$\delta = \frac{\sigma_x h}{2}$$

where h is the separation of the centres of each pair of detecting levels. The result is

$$\delta = (0.62 \pm 0.10) \text{ mm.}$$

In calculating $\sigma_{scatt.}$ the integration was performed over all particles in the sea-level spectrum with momentum > 800 MeV/c. This is not strictly true as the rate of particles with momentum just above 800 MeV/c will be reduced somewhat by scattering in the 53 cm. absorber so that the value of δ is expected to be a slight overestimate. In Chapter 4 the location error at the centre of each tube array is found by an independent method and this value, (0.92 ± 0.23) mm., is in fact rather higher than the value given above.

The experimental value of the location accuracy can in principle be compared with that expected from the geometry of the arrangement . Limiting forms of the variation of efficiency across the tube diameter were considered and the expected value of δ determined graphically for two limiting cases, as follows:

(a) The efficiency has a constant value of 70% (equal to the measured mean internal efficiency of the tubes) across the whole internal diameter of the tube. This gives $\delta = 0.75$ mm.

(b) The efficiency is equal to 100% for $r < 0.70a$ and zero for $r > 0.70a$., a is the radius of the tube and r is the distance from centre. This gives $\delta = 0.46$ mm.

The variation of efficiency with the distance of the trajectory from the centre of the tube was then studied experimentally by placing the array B of flash-tubes between the arrays C and D. The flashes in C,D were used to locate the trajectory of the particle and the variation of efficiency with the distance of the trajectory from the centres of the tubes in B was measured. The result is given in figure 3.6.

In figure 3.7 the results of the experimental and theoretical determination of the location accuracy of an array of tubes are compared. It is seen that the experimental variation of efficiency with r is intermediate between the two extremes assumed in the theoretical discussion; thus the result is not inconsistent with the location accuracy of (0.92 ± 0.23) mm. measured experimentally.

It will be appreciated that it is possible for the geiger telescope to be triggered by two unassociated particles, one which traverses G_A, G_B and the other which traverses G_C, G_D within the resolving time of the coincidence circuit, (see figure 3.8). Such spurious events can be recognized by

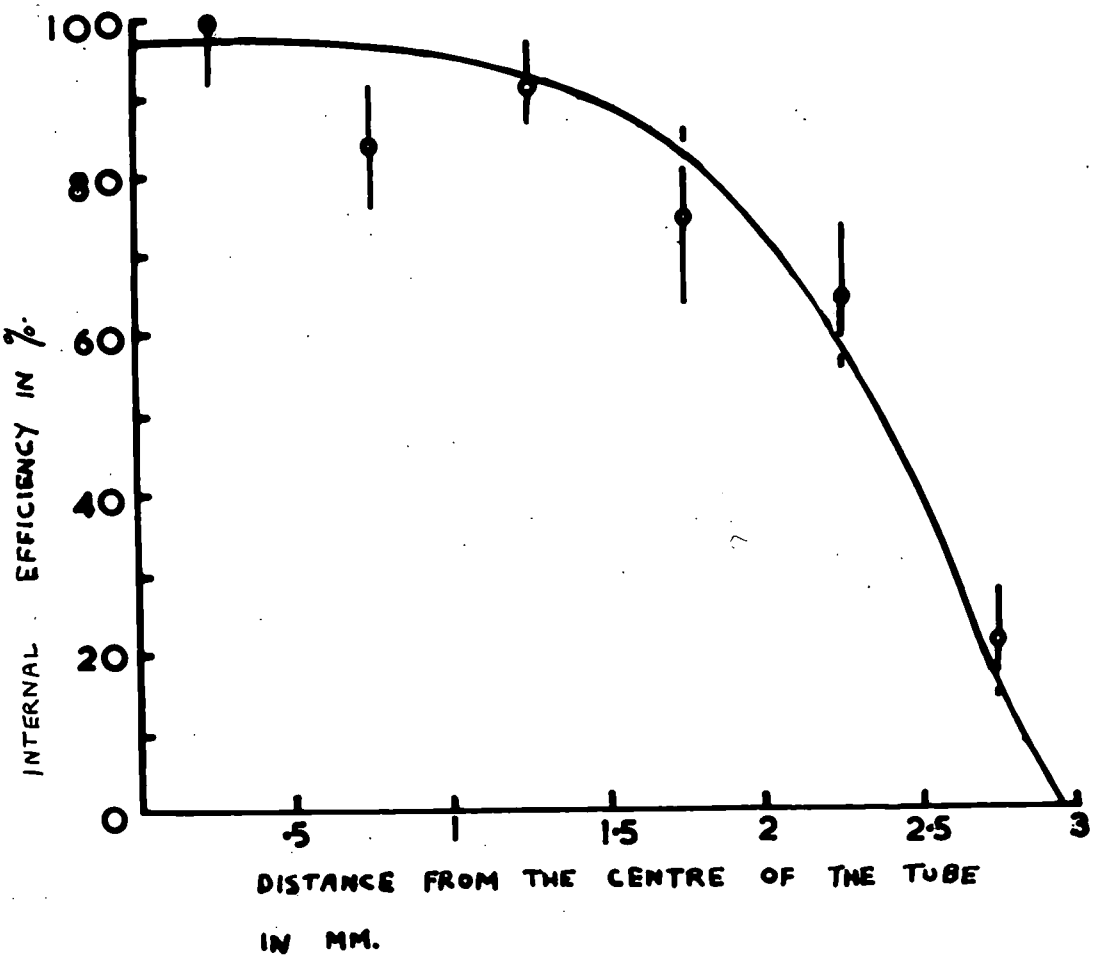

Figure 3.6 Variation of internal efficiency across the tube diameter

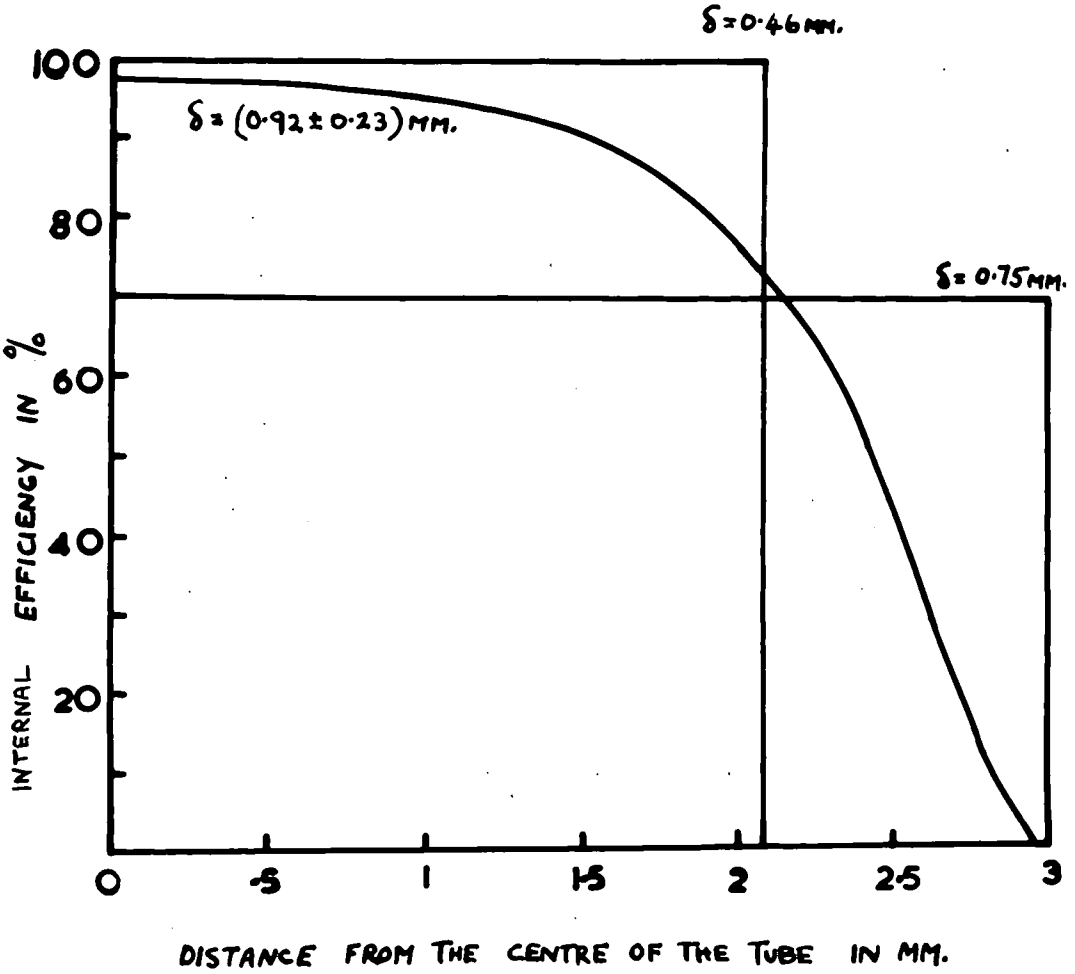

Figure 3.7 Comparison of the theoretical and experimental efficiency variations. The values of δ refer to the corresponding r.m.s. location errors for an array

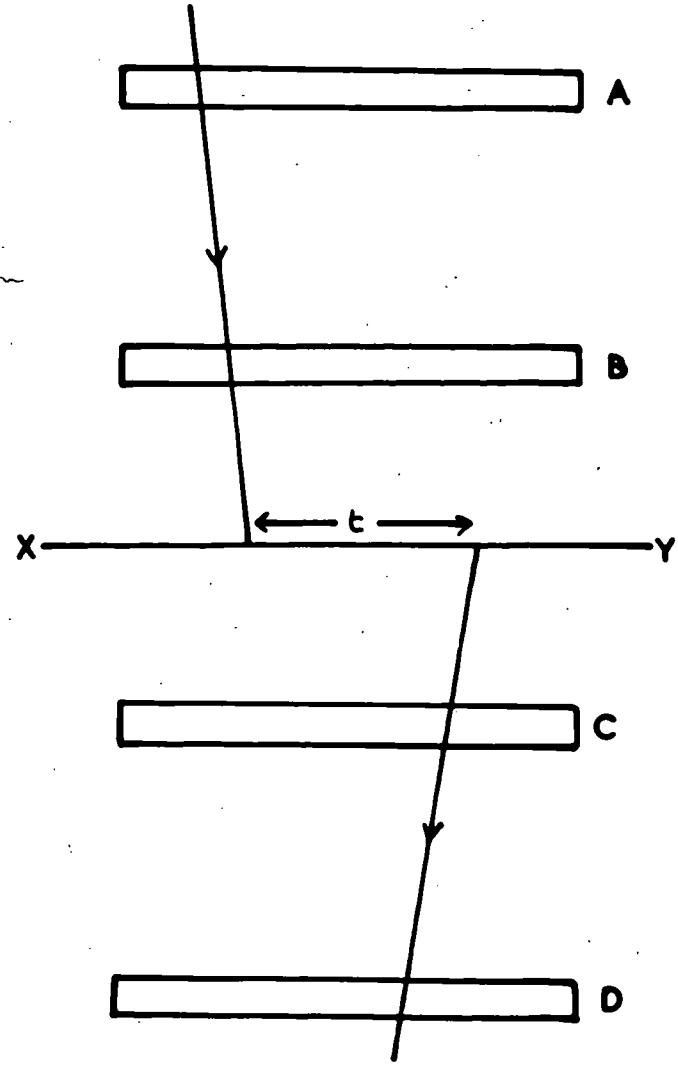

Figure 3.8 Schematic diagram showing how spurious events are recognised

determining the points of intersection of the trajectories determined by the flashes in A, B and the flashes in C, D with the line XY. For genuine four-fold coincidences the separation, t, of the projections of the two trajectories onto the line XY will be small. Figure 3.9 shows the observed frequency distribution of t for the 93 events accepted for measurement in the noise-level determination. From this distribution it can be concluded that no spurious events have been recorded during the noise-level experiment.

The flash-tube arrays, as described, are merely two dimensional devices, i.e. only the projected angle made by the trajectory with the vertical in the plane of the front of the flash-tubes is determined. The lack of information of the precise direction of the trajectory in space is not important in this case as is shown below. Consider a set of rectangular cartesian axes x, y, z. Suppose the lines of magnetic flux are parallel to the y axis and consider a trajectory making an angle α with the z-x plane. The resolved component of the momentum in this plane is p cos α while the resolved component parallel to the y axis is p sin α. By Fleming's left hand rule the magnetic field only exerts a force on the component of the motion in the z-x plane. Hence the deflection of the particle in the z-x plane is given by

$$p \cos \alpha = \frac{300 \int H dl}{\theta}$$

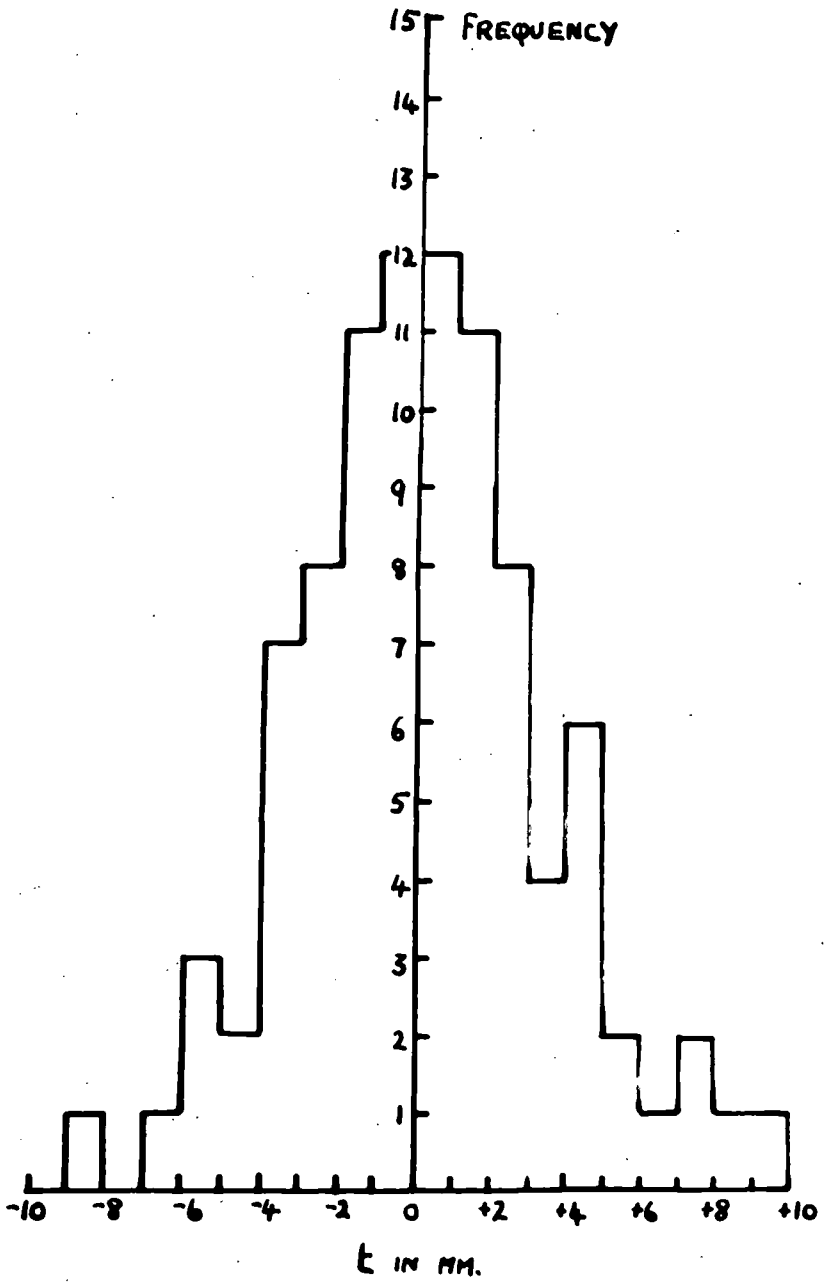

Figure 3.9 Noise-level distribution of the separation of the trajectories on XY

The z-x plane in the spectrograph is the plane containing the fronts of the flash-tubes and as the geiger telescope limits the maximum angle that a trajectory can make with this plane to 3.8° the maximum error introduced is 0.2%. Thus the effect is negligible.

3.5 Conclusions

It is now possible to compare the relative merits of the neon flash-tube and cloud chamber for use as the detecting elements in a high energy cosmic ray spectrograph. The location accuracy of (0.92 ± 0.23) mm. obtained with the neon flash-tube array is rather better than that obtainable with shallow, flat cloud chambers. The other advantages of the neon flash-tube array are:

1. The system has no moving parts and hence it is inherently more reliable than a cloud chamber.

2. The area and hence the solid angle covered by an array can be large. This is obviously very important in cosmic ray experiments where the flux of particles is low and as large a collecting area as possible is used.

3. Although the collecting area is large all the information is presented in one plane. This is important as it eliminates depth of focus problems and the need for stereoscopic photography.

4. The dead time of the flash-tubes, is small (< 1 sec.).

Also it is apparent that a further reduction in error of location can be made in a flash-tube array by increasing the

number of layers, an upper limit being set by the maximum tolerable scattering uncertainty. In cosmic ray experiments however, the limit is liable to be set more by lack of a sufficient flux of particles of small magnetic deflection than the difficulty in measuring the deflections.

CHAPTER 4

The momentum spectrum of cosmic rays at 37.7 m.w.e.

4.1 Introduction

Using the apparatus already described the momentum spectrum of cosmic rays has been measured in a cave under Castle Rock, Nottingham. The rock is of sandstone of density (1.90 ± 0.03) gm. cm.$^{-3}$ with a mean atomic number, $Z = 10$, and a mean atomic weight, $A = 20$. The distance from the roof of the cave to ground level is (19.85 ± 0.03) metres, corresponding to an absorber thickness of (37.7 ± 0.6) m.w.e.

The momentum spectrum at this depth is of interest for two reasons.

(a) When the experiment was started no precise measurements had been performed to determine the rate of energy loss of relativistic charged particles of energy > 5 GeV. Information on this point can be obtained by the comparison of a precise ground level spectrum and a precise spectrum at 37.7 m.w.e.

(b) Several experiments on the large-angle scattering of μ-mesons have been performed underground (e.g. McDiarmid, 1954). In order to analyse the results of such experiments it is necessary to know the momentum spectrum of the incident particles before they are scattered and hitherto all experimenters have calculated this spectrum from an assumed energy loss relation and a knowledge of the sea-level spectrum. As the r.m.s. angle of scatter of a particle is inversely proportional to momentum

it follows that if the flux of low momentum particles is underestimated then the number of large-angle scatters will be overestimated. Thus, a direct measurement of the energy loss of μ-mesons will give a check on the conclusions of such experiments.

The geometry of the spectrograph was altered slightly when the apparatus was moved to the cave in Nottingham and figure 4.1 shows the experimental arrangement.

4.2 Measurement of the trajectories

The arrays of flash-tubes A, B and C,D were photographed by two separate cameras. Measurements of particle trajectories were made by projecting the photographs back to exactly full size. To measure the angle that a particle trajectory made with the vertical before entering the magnetic field a millimetre scale was placed at the position of the geiger counters G_A and also one at the position corresponding to the centre of the magnetic field, WX. The required angle was then found by successively aligning the measuring fibre with the reference cotton and the flashes. In this way not only was the angle obtained but also the position of intersection of the trajectory with a line drawn through the centre of the magnetic field and the geiger counters G_A; this is useful additional information. The same procedure of measurement was used for the bottom half of the spectrograph and an algebraic subtraction of the two measured angles gave the magnitude of the magnetic deflections and the charge of the incident particles. This technique of

Figure 4.1 The prototype spectrograph as operated underground. Scale = 1/8 full size.

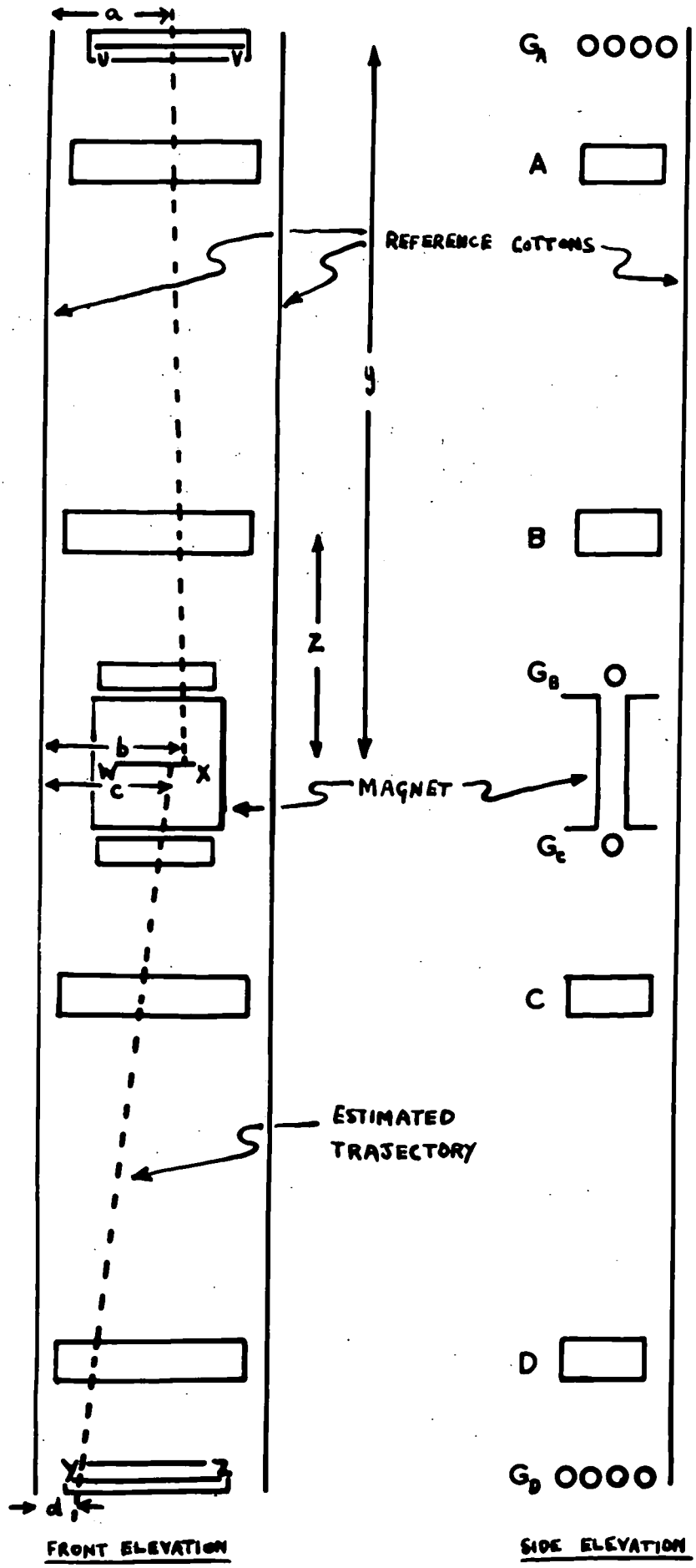
a
U
V
G_A OOOO
A
REFERENCE COTTONS
y
B
Z
G_B O
b
W
X
c
MAGNET
G_C O
C
ESTIMATED TRAJECTORY
D
Y
Z
G_D OOOO
d
FRONT ELEVATION
SIDE ELEVATION

measurement was quicker and yielded more information than the techniques investigated in the noise-level measurements.

Referring to figure 4.1 if a, b, c, d are the co-ordinates of a trajectory at the measuring levels then the angular deflection θ of the particles in traversing the magnetic field is given, in the small angle approximation by $\theta = \frac{\Delta}{y}$ where $\Delta = (a-b) - (c-d)$.

For all accepted particle trajectories $\int H dl$ is constant to 1% and equal to 1.09 10^5 gauss cm. Thus a 1 GeV/c particle suffers an angular deflection of 1.88° in traversing the magnetic field and a displacement of 2.84 cm. in Δ .

In all magnetic spectrographs the momentum spectrum of particles traversing the apparatus differs from the spectrum of particles that would traverse the same counter telescope if the magnet were removed. The reason for this is that some low momentum particles are bent out of the telescope by the magnetic field, while others are bent in. The result of this is a bias against particles of low momentum. However, this bias can be accurately corrected if the geometry of the spectrograph is known. Therefore in measuring the recorded events only those particles are accepted which traverse the solid angle defined by the lines UV, WX, YZ in figure 4.1. The calculation of the magnetic bias is carried out in section 4. 5(a) of this Chapter.

4.3 Uncertainties in the measured magnetic deflection

The measured angular deflection derived from the flashes is not the true magnetic deflection but a combination of magnetic deflection, scattering deflection and a component due to the location error arising from the finite diameter of the flash-tubes. The setting error is minimised by taking the mean of three independent measurements of each angle. It will be appreciated that it is necessary to know the magnitude of these uncertainties.

(a) Scattering error

The r.m.s. projected angle of scattering $\langle\phi\rangle$ of a particle of momentum p in traversing the spectrograph is given by

$$\langle\phi\rangle = \frac{1}{\sqrt{2}} \sum \frac{K t^{\frac{1}{2}}}{p\beta} \qquad (3)$$

where $K = 22$ MeV and t is measured in radiation lengths. The sum is taken over all the material in arrays B,C and the geiger counters G_B, G_C.

Dividing (3) by (1) (Chapter 2) gives

$$\frac{\langle\phi\rangle}{\theta} = \frac{1}{\sqrt{2}} \frac{\sum K t^{\frac{1}{2}}}{300 \int H d\ell} \frac{1}{\beta} \qquad (4)$$

$$= 0.22 \text{ for } \mu\text{-mesons with } \beta \to 1, \text{ i.e. } p > 0.5 \text{ GeV/c}$$

Thus the momentum estimate of each particle has an uncertainty of standard deviation 22% due to multiple scattering. The effect of this is to smear out any fine structure effects

that may occur in the spectrum. However it should be noted that in the evaluation of the true spectrum at 37.7 m.w.e., as distinct from that measured by the apparatus, the effect of multiple scattering can be allowed for, since the form of the scattering distribution, $P(\phi)\,d\phi$ is accurately known.

$$P(\phi)d\phi = \frac{1}{\sqrt{2\pi}\langle\phi\rangle} \exp\left(-\frac{\phi^2}{2\langle\phi^2\rangle}\right) d\phi$$

This point is discussed in section 5 (b).

(b) The location accuracy of the flash-tubes

As the momentum of a particle increases the magnetic angular deflection decreases. Hence a momentum will be reached at which the flash-tubes can no longer resolve the small angular deflection. The maximum detectable momentum, p_m, is given by $p_m = \frac{300 \int H dl}{\sigma_\theta}$ where σ_θ is the r.m.s. uncertainty in the measurement of the angular deflection. The location error has been studied in the noise-level experiment at ground level in Durham and found to be $\delta = (0.62 \pm 0.10)$ mm. at the centre of an array. σ_θ and δ are related by $\delta = \frac{h\sigma_\theta}{2}$ where h is the separation of the centres of the detecting arrays.

It is obviously better to determine the magnitude of the two effects described above under the present experimental conditions, and not to rely on theoretical and predicted values. Estimates can, in fact, be made from the differences in the measurements of b and c.

In figure 4.2 it is assumed that all the scattering material in array B and G_B is concentrated at EF and that in C and G_C is concentrated at HI, where Z = 28 cm. Consider a particle traversing the spectrograph when there is no deflecting field. Suppose the r.m.s. projected angle of scatter of the particle by EF and HI is $\langle\gamma\rangle$. First suppose that the flashes locate the trajectory precisely so that the discrepancy BC is due entirely to scattering.

$$BC = b - c$$
$$= Z\,(\alpha - \beta)$$
$$\sigma_{BC}^2 = z^2(\sigma_\alpha^2 + \sigma_\beta^2)$$
$$= 2z^2\langle\gamma^2\rangle$$

There will be a contribution to BC from the location error, of magnitude σ.

$$\sigma_{BC}^2 = 2z^2\langle\gamma^2\rangle + \sigma^2$$

σ is related to the r.m.s. uncertainty, σ_Δ in Δ by $\sigma = k\sigma_\Delta$ where k is a constant whose value depends on the distance of the centre of the arrays A,D to the measuring levels G_A, G_D and the distance of the centres of the arrays B,C to the measuring level at the centre of the magnetic field. From equation (4), section 4.3(a) of this Chapter

$$\frac{\langle\phi\rangle}{\theta} = \frac{K_1}{\beta} \qquad \text{where} \quad \langle\phi\rangle = \sqrt{2}\langle\gamma\rangle$$
$$\sigma_{BC}^2 = \frac{z^2 K_1^2 \theta^2}{\beta^2} + k^2\sigma_\Delta^2$$
$$= \frac{z^2 K_1^2}{y^2}\,\frac{\Delta^2}{\beta^2} + k^2\sigma_\Delta^2$$

Thus if σ_{BC}^2 is plotted against $\frac{\Delta^2}{\beta^2}$ the slope of the graph will

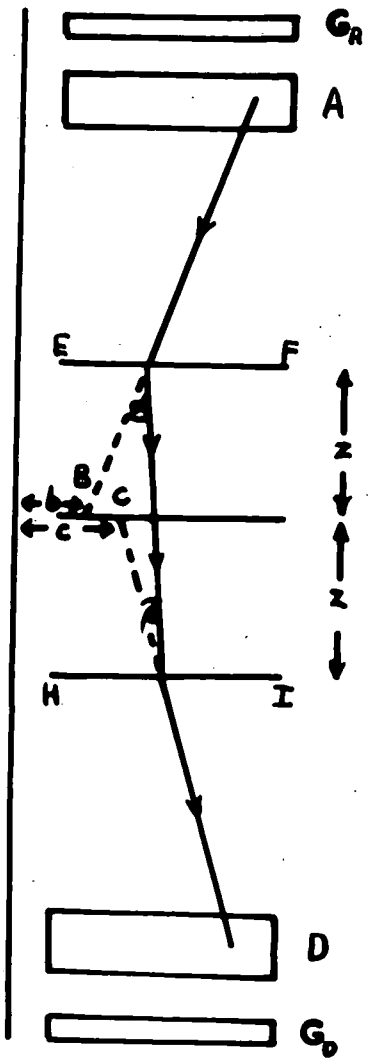

Figure 4.2 Determination of the noise-level of the deflection measurements

give the ratio of the scattering deflection to the magnetic deflection, K_1, and the intercept will give the r.m.s. uncertainty in the measured magnetic deflection, σ_Δ due to the location error. In figure 4.3 the results have been grouped in cells of σ_{BC}^2 and $\frac{\Delta^2}{\beta^2}$, the experimental points being plotted at the mean values of the cells.

The intercept of figure 4.3 gives $\sigma_\Delta = (3.55 \pm 0.90)$ mm. and the slope $K_1 = (0.16 \pm 0.04)$.

These values can now be compared with expectation. $\sigma_\Delta = (3.55 \pm 0.90)$ mm. corresponds to an r.m.s. location error at the centre of each array of flash-tubes of (0.92 ± 0.23) mm. The maximum detectable momentum of the spectrograph with $\sigma_\Delta = 3.55$ mm. is 8.0 GeV/c. The value found for the scattering factor, $(16 \pm 4)\%$ is not far from the theoretical result of 22% found from a knowledge of the atomic constants of the scattering layers.

A graph of the uncertainty in magnetic deflection σ_M can now be plotted as a function of Δ. This is found by adding the component uncertainties due to scattering, $\frac{.16\,\Delta}{\beta}$, and location error, σ_Δ, in quadrature:

$$\sigma_M^2 = \left(\frac{.16\,\Delta}{\beta}\right)^2 + \sigma_\Delta^2$$

The variation of σ_M with Δ is shown in figure 4.4.

4.4 Experimental results.

The apparatus was operated continuously for a period of three months during which time the rate of particles was

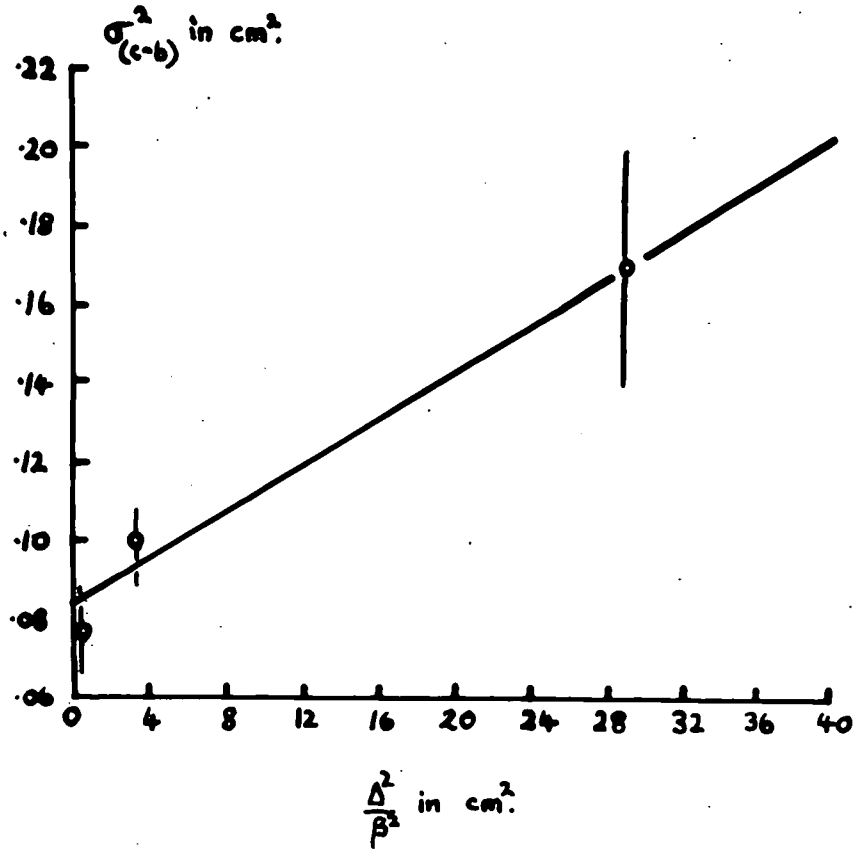

Figure 4.3 The combination of location and scattering errors

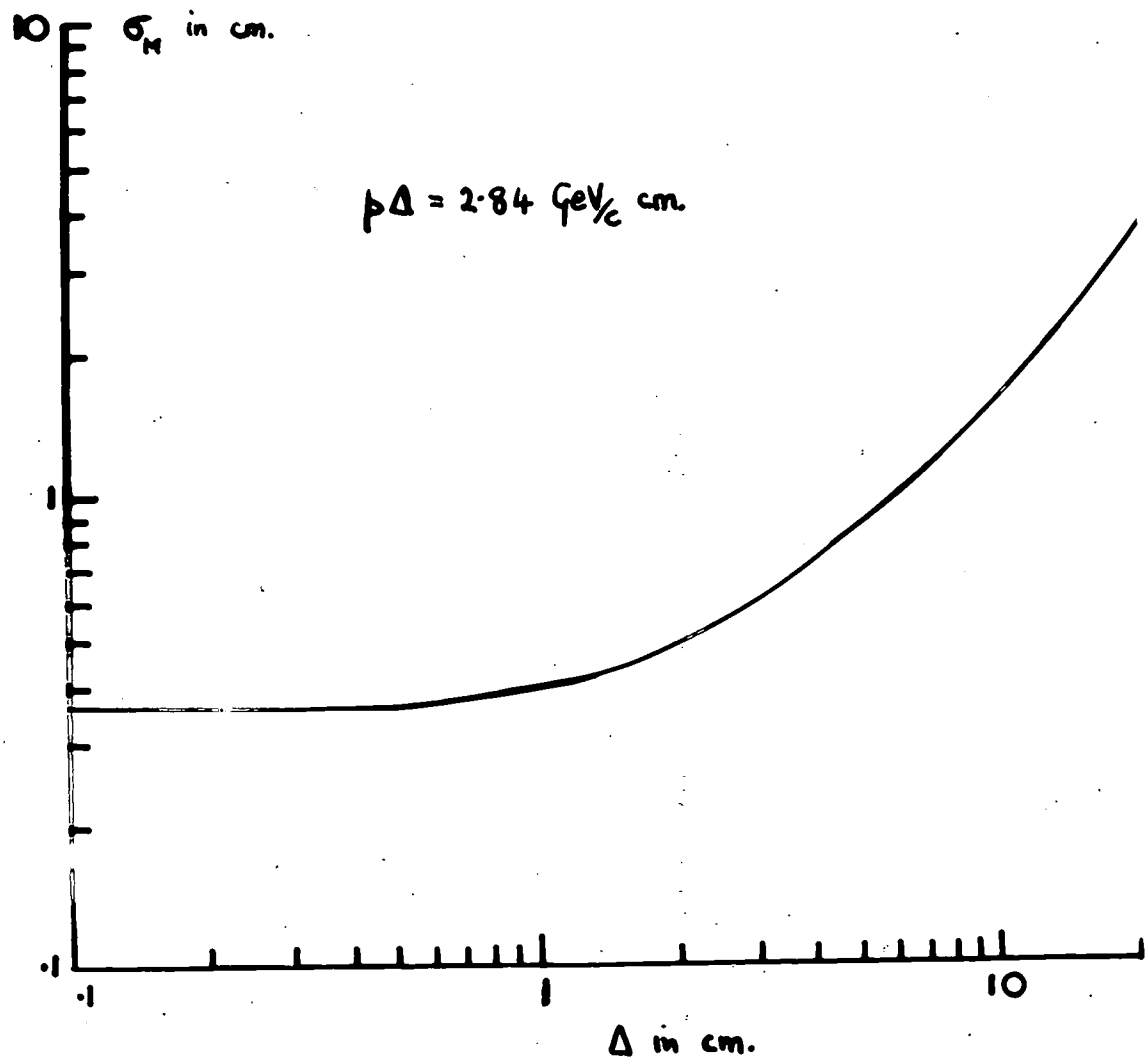

Figure 4.4 The r.m.s. uncertainty in magnetic deflection as a function of the magnetic deflection

(0.536 ± 0.017) hr.$^{-1}$. In all 1,010 trajectories were measured; their distribution in momentum is given in Table 4a.

Grouping together all the particles with momenta between 0.25 GeV/c and 8 GeV/c gives a positive-negative ratio,

$$\frac{N^+ (.25,8)}{N^- (.25,8)} = 1.42 \pm 0.11$$

The most accurate measurements of the positive-negative ratio underground have been made by Filosofo et al. (1954). The above value of 1.42 ± 0.11 is not inconsistent with their value of 1.24 ± 0.01 at a similar depth.

In order to derive the momentum spectrum from the results of table 4a the experimental bias arising from various factors must be considered. These will now be discussed.

4.5 Experimental bias

(a) Magnetic bias

The geometry of acceptance of particles traversing the magnetic field is shown in figure 4.5 where L = 9 cm., ℓ = 5 cm. and y = 86.5 cm. It is required to find the probability of acceptance of a particle of momentum, p, relative to a particle with infinite momentum. Particles with infinite momenta can be incident over the whole length of WX for angles of incidence between $\pm \tan^{-1}\left(\frac{L-\ell}{y}\right)$. For angles of incidence, $\alpha > \tan^{-1}\left(\frac{L-\ell}{y}\right)$, the length of WX over which these particles can be incident is given by $2(L - y \tan \alpha)$ which falls to zero when $\alpha = \tan^{-1} \frac{L}{y}$. The area under the graph of the length of

Momentum interval GeV/c	No.of positive particles, N^+	No.of negative particles, N^-	Total
.25 - .50	15	14	29
.50 - .75	20	14	34
.75 - 1	31	20	51
1 - 2	107	65	172
2 - 3	72	57	129
3 - 4	51	37	88
4 - 5	46	30	76
5 - 6	36	24	60
6 - 7	24	19	43
7 - 8	21	18	39
8	133	156	289
	556	454	1,010

TABLE 4a

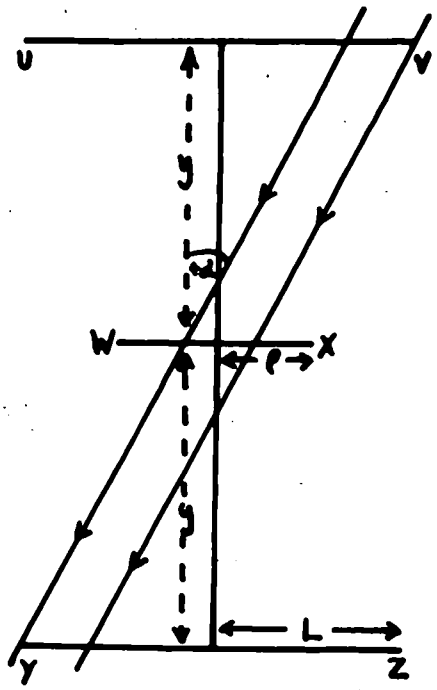

Figure 4.5 Magnetic bias

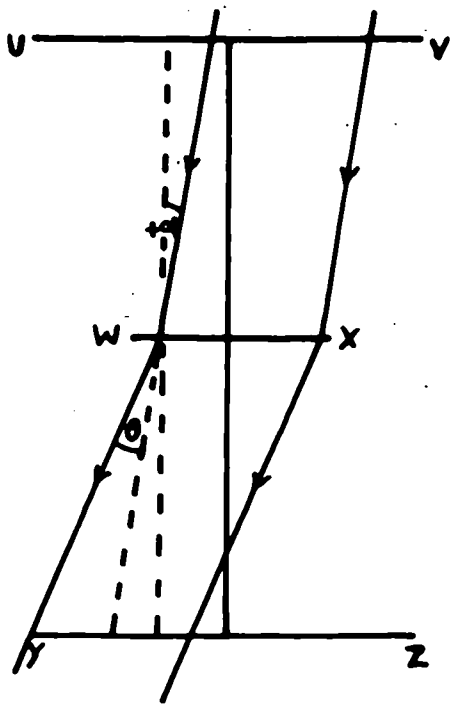

Figure 4.6 Magnetic bias

WX over which particles can be incident versus the angle of incidence gives a measure of the probability of acceptance of particles with momentum, p. The probability of acceptance of particles with infinite momentum, p_∞ is given by

$$P(p_\infty) = 2.2\ell \tan^{-1}\left(\frac{L-\ell}{y}\right) + 2\int_{\tan^{-1}\left(\frac{L-\ell}{y}\right)}^{\tan^{-1}\left(\frac{L+\ell}{y}\right)} 2(L - y\tan\alpha)\, d\alpha$$

Consider a negatively charged particle with momentum p which suffers an angular deflection θ in traversing the magnetic field such that $\theta < \tan^{-1}\left(\frac{L-\ell}{y}\right)$. (See figure 4.6). Firstly consider only positive angles of incidence. The particle can be incident over the whole length of WX for angles of incidence between 0 and $+\alpha_1$ where $\alpha_1 = \tan^{-1}\left(\frac{L-\ell}{y}\right) - \theta$. For angles of incidence between $\alpha = \alpha_1$ and $\alpha = \tan^{-1}\left(\frac{L-\ell}{y}\right)$ the length of WX over which the particle can be incident is given by $(L+\ell) - y\tan(\theta+\alpha)$. This is the case shown in figure 4.6. For angles of incidence $> \tan^{-1}\left(\frac{L-\ell}{y}\right)$ the distance is $2L - y(\tan\alpha + \tan(\theta+\alpha))$, which falls to zero at $\alpha = \frac{L}{y} - \frac{\theta}{2}$ in the small angle approximation.

Consider now negative angles of incidence. For angles of incidence between 0 and $\tan^{-1}\left(\frac{L-\ell}{y}\right)$ the length of WX over which particles can be accepted is 2ℓ. For values of α between $\tan^{-1}\left(\frac{L-\ell}{y}\right)$ and $\alpha_2 = \theta + \tan^{-1}\left(\frac{L-\ell}{y}\right)$ the distance is $(L+\ell)$ - y tan α and for angles $> \alpha_2$ the distance is $2L - y\tan(\alpha - \theta) - y\tan\alpha$ which falls to zero at $\alpha_2 = \theta/2 + L/y$.

The total probability of acceptance for a particle of momentum p with magnetic deflection $\theta < \tan^{-1}\left(\frac{L-\ell}{y}\right)$

is therefore given by:

$$P(p) = 2\ell\left[\tan^{-1}\left(\frac{L-\ell}{y}\right) - \theta\right] + \int_{\tan^{-1}\left(\frac{L-\ell}{y}\right)-\theta}^{\tan^{-1}\left(\frac{L-\ell}{y}\right)} \left[(L+\ell) - y\tan(\theta+\alpha)\right] d\alpha$$

$$+ \int_{\tan^{-1}\left(\frac{L-\ell}{y}\right)}^{L/y - \theta/2} \left[2L - y\{\tan\alpha + \tan(\theta+\alpha)\}\right] d\alpha \quad + 2\ell \cdot \tan^{-1}\left(\frac{L-\ell}{y}\right)$$

$$+ \int_{\tan^{-1}\left(\frac{L-\ell}{y}\right)}^{\theta + \tan^{-1}\left(\frac{L-\ell}{y}\right)} \left\{(L+\ell) - y\tan\alpha\right\} d\alpha \quad + \int_{\theta + \tan^{-1}\left(\frac{L-\ell}{y}\right)}^{\theta/2 + L/y} \left\{2L - y\tan(\alpha-\theta) - y\tan\alpha\right\} d\alpha$$

The calculation has been repeated for magnetic deflections in the range 0 to $2\tan^{-1}\left(\frac{L+\ell}{y}\right)$. The integrals have been evaluated both analytically and numerically and also a check has been made by determining P(p) with a scale model. A correction factor defined as $\frac{P(p)}{P(p_\infty)}$ has been calculated and the result is shown in figure 4.9.

(b) Scattering bias

A particle traversing the spectrograph suffers an angular deflection due to multiple scattering as well as a deflection due to the magnetic field. The effect of the projection of this scattering angle on the plane in which the magnetic deflection takes place is to produce an error in the momentum estimate and also to scatter some particles out of the limits defined for acceptance and scatter other particles in. The effect in the plane parallel to the magnetic field

is similar and the resultant effect is to introduce a bias against particles of low momentum.

The probability that a particle of momentum p will be scattered through a spatial angle α in the interval α to $\alpha + d\alpha$ is given to sufficient accuracy by the expression given by Rossi and Greisen (1941):

$$P(\alpha)d\alpha = \frac{1}{\sqrt{2\pi}\langle\alpha\rangle} \exp\left(-\frac{\alpha^2}{2\langle\alpha^2\rangle}\right) d\alpha$$

where $\langle\alpha\rangle = \frac{E_s t^{1/2}}{p\beta}$, $E_s = 21$ MeV and t is measured in radiation lengths. For projected angles, ϕ, the relation is

$$\langle\phi^2\rangle = \frac{\langle\alpha^2\rangle}{2}$$

In deriving the spectrum of particles incident on the apparatus an attempt has been made to allow for the effects of bias as follows. An assumed incident spectrum is taken and this is first corrected for bias due to particles being scattered out of the geiger telescope in the plane parallel to the magnetic field. The resulting spectrum is then broadened in the usual manner to account for the projected component of the scattering in the plane in which the magnetic deflection takes place. Finally the corrections due to magnetic bias and 'noise' of measurement are applied. The resulting momentum distribution is then compared with the measured distribution.

<u>The correction due to scattering in the plane parallel to the magnetic field.</u>

The geometry of acceptance in this plane is shown in figure 4.7, where X = 5.6 cm., x = 1.4 cm. and y = 86.5 cm. To simplify the calculation it is assumed that all the

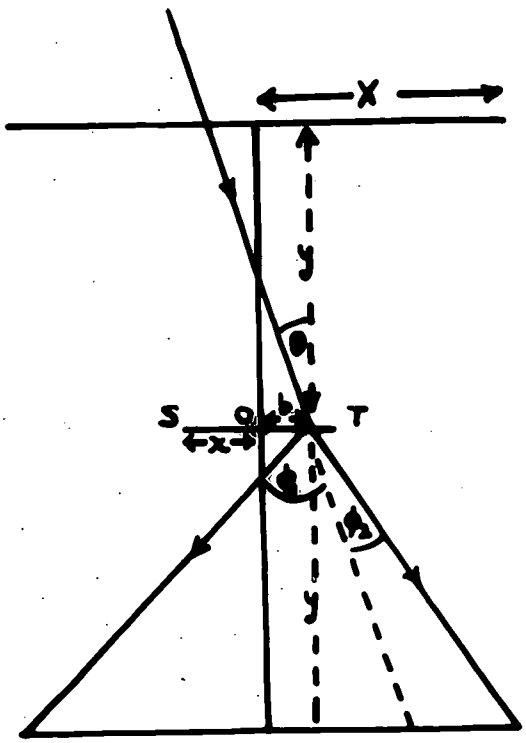

Figure 4.7 Scattering bias

scattering material in the arrays of flash-tubes B,C and the geiger counters G_B, G_C is concentrated at ST at the centre of the magnetic field. The scattering in the array of flash-tubes A and the geiger counters G_A is ignored. The justification for this simplification is that the r.m.s. angle of scatter in A, G_A is $\sqrt{2}$ times smaller than the same angle for B,C,G_B,G_C.

Consider a particle incident on the scattering material at a distance b from O. Suppose the particle has momentum p and that its projected r.m.s. angle of scattering in ST is $\langle\phi\rangle$. The probability that it will be scattered so that it remains in the solid angle defined by the geiger telescope is

$$P(\theta, b) = \int_0^{\phi_1} P(\phi)\,d\phi + \int_0^{\phi_2} P(\phi)\,d\phi$$

where $$P(\phi)\,d\phi = \frac{1}{\sqrt{2\pi}\,\langle\phi\rangle} \exp\left(-\frac{\phi^2}{2\langle\phi^2\rangle}\right) d\phi$$

$$\phi_1 = \tan^{-1}\left\{\frac{X+b}{y}\right\} + \theta$$

$$\phi_2 = \tan^{-1}\left\{\frac{X-b}{y}\right\} - \theta$$

For angles of incidence $> \tan^{-1} X/y$

$$P(\theta, b) = \int_0^{\phi_1} P(\phi)\,d\phi - \int_0^{\phi_2} P(\phi)\,d\phi$$

For a given value of b the probability for all angles of incidence is

$$\int_{\tan^{-1}\frac{X+b}{y}}^{\tan^{-1}\frac{X-b}{y}} P(\theta, b)\,d\theta$$

To obtain the total probability of acceptance, P(p) this integral must also be taken over b.

$$P(p) = \int_{-X}^{X} \int_{\tan^{-1}\frac{X+b}{y}}^{\tan^{-1}\frac{X-b}{y}} P(\theta, b)\,d\theta\,.\,db$$

The multiple scattering distribution $P(\emptyset)\, d\emptyset$ cannot be integrated analytically so it has been evaluated numerically using error function tables. The correction factor to be applied to particles of momentum p is defined as $\frac{P(p)}{P(P_\infty)}$ and its variation with momentum is shown in figure 4.9.

4.6 The trial spectrum

The trial spectrum has been obtained by taking the known sea-level spectrum and from this predicting the shape of the spectrum at 37.7 m.w.e. To a good approximation it can be assumed that particles which reach 37.7 m.w.e. with momentum between 1 GeV/c and 8 GeV/c have lost a constant momentum p_o in the rock. However for momenta below 1 GeV/c the variation of the rate of momentum loss, $\frac{dp}{dx}$, with p must be taken into account and also the effects of multiple scattering in the rock. A further possible correction is for the effect of μ - e decay. The magnitude of these effects will now be considered.

(a) μ - e decay

The probability of μ - e decay can be shown to be

$$\left(\frac{p+p_o}{p}\right)^{-\frac{z_o}{c\tau_o}\cdot\frac{m_\mu c^2}{p_o c}} \qquad \text{(Janossy, 1950)}$$

Here p is the momentum at 37.7 m.w.e. and p_o is the momentum loss in the rock. The other symbols have their usual meanings. With p = 100 MeV/c the probability of decay is 0.003, thus the effect is negligible in the present experiment.

(b) The variation of $\frac{dp}{dx}$ with p for $p < 1$ GeV/c

Suppose the ground level spectrum is given by $N(p_g)\,dp_g$. If p_g is such that the mesons reach 37.7 m.w.e. with $p < 1$ GeV/c then they will be spread over a wider momentum cell because of the increase in $\frac{dp}{dx}$ as p decreases below 1 GeV/c. The effect of this is to produce a peak in the spectrum at low momentum. Suppose they are spread over a momentum cell with limits p to p + dp at 37.7 m.w.e.

$$N(p_g)\,dp_g = N(p)\,dp$$

$$N(p) = N(p_g)\,\frac{dp_g}{dp}$$

$$= N(p_g)\,\frac{\left(\frac{dp}{dR}\right)_{p+p_0}}{\left(\frac{dp}{dR}\right)_p}$$

Now $\left(\frac{dp}{dR}\right)_{p+p_0} = K$ where K is a constant and

$$\left(\frac{dp}{dR}\right)_p = K\,\frac{\left[1+\left(\frac{pc}{mc^2}\right)^2\right]^{3/2}}{\left(\frac{pc}{mc^2}\right)^3} \qquad \text{(Rossi and Greisen, 1941)}$$

$$\therefore N(p) = N(p_g)\,\frac{\left(\frac{pc}{mc^2}\right)^3}{\left[1+\left(\frac{pc}{mc^2}\right)^2\right]^{3/2}}$$

The variation of the factor $\frac{\left(\frac{pc}{mc^2}\right)^3}{\left[1+\left(\frac{pc}{mc^2}\right)^2\right]^{3/2}}$ with p is shown in figure 4.9.

(c) Scattering in the rock

Particles which are incident vertically at sea-level suffer multiple scattering in traversing the rock and are scattered away from the vertical. However some particles are scattered into the vertical from the inclined flux at sea-level. To reach the cave with a certain momentum an

inclined particle must have a higher momentum at sea-level than a vertical particle which reaches the cave with that momentum. Thus as the flux of such inclined particles is less than the flux of vertical particles it is seen that more particles will be scattered away from the vertical than will be scattered back from inclined angles. The effect of this is to produce a reduction in the near vertical spectrum at low momentum.

The maximum angle that an accepted particle trajectory can make with the vertical in the plane perpendicular to the magnetic field is ± 9.2° while the maximum angle in the perpendicular plane is ± 4.5°. The problem then is to calculate the spectrum of particles in this solid angle.

If p is the momentum of a particle at 37.7 m.w.e., which has lost momentum p_o in the rock, then its mean square projected angle of scatter in traversing the rock is given by

$$\langle \beta^2 \rangle = \frac{E_s^2}{2} \int_{p+p_o}^{p} - \frac{1}{\frac{dp}{dt}} \frac{dp}{p^2 \frac{v^2}{c^2}}$$

where $\frac{dp}{dt}$ = 66 MeV/c / radn. length and E_s = 21 MeV; from this equation $\langle \beta \rangle$ = 2.58 $\left\{ \frac{p_o}{p(p+p_o)} \right\}$ radians.

The majority of the scattering arises as the particle slows down and to a fair approximation it can be assumed that it all takes place at the roof of the cave. Figure 4.8 gives a diagrammatic representation. T_s is the trajectory of an incident particle and it is required to find the

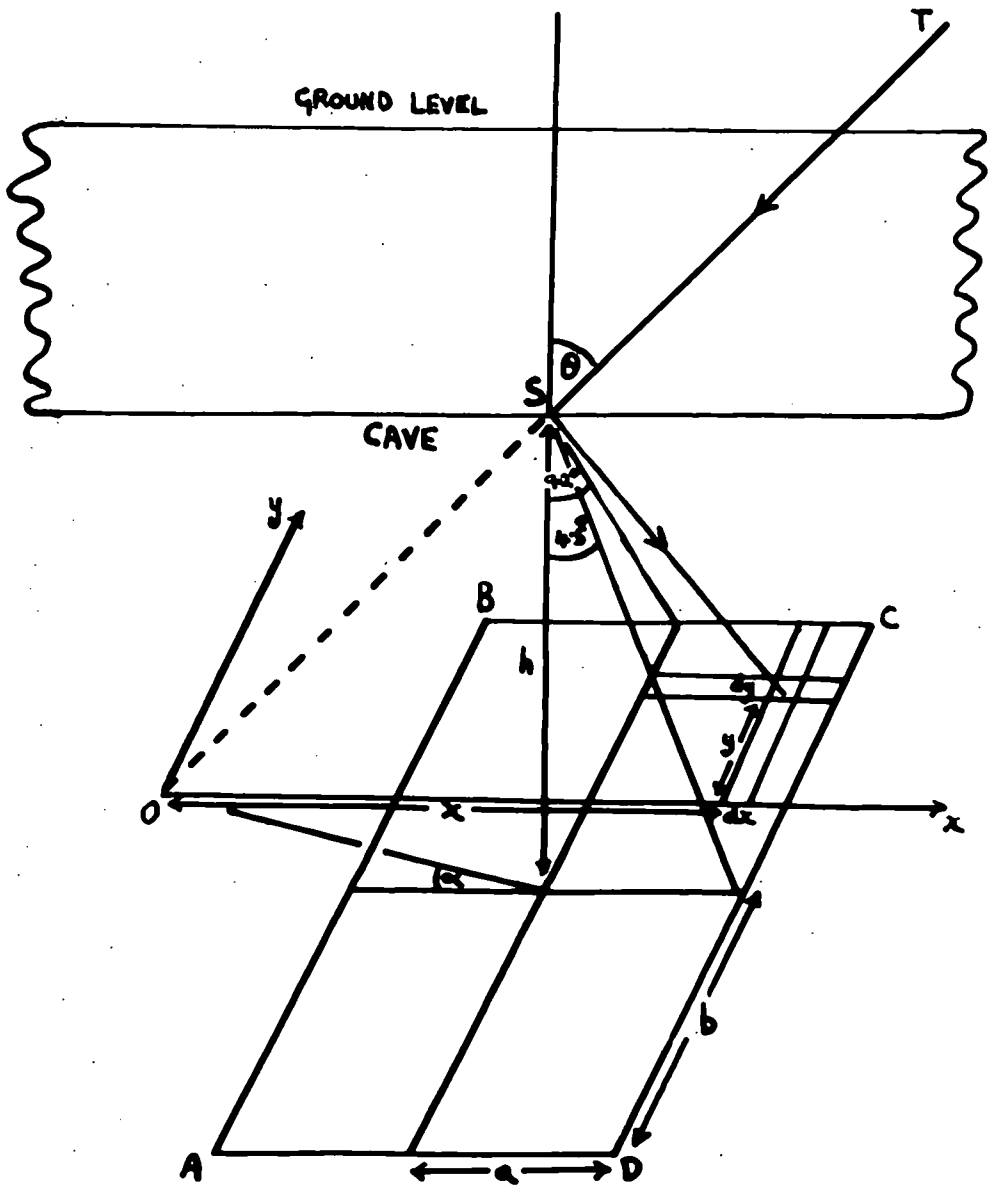

Figure 4.8 Scattering in the rock

probability that it will be scattered into the area defined by the rectangle ABCD corresponding to the acceptance of the spectrograph. Suppose $\sigma = h \tan \langle\beta\rangle$, the probability that the particle will be scattered into the element of area dx dy is given by

$$P(x)dx\ P(y)dy = \frac{1}{\sqrt{2\pi}\sigma} \exp\left(-\frac{x^2}{2\sigma^2}\right) dx \ \frac{1}{\sqrt{2\pi}\sigma} \exp\left(-\frac{y^2}{2\sigma^2}\right) dy$$

The probability that it will be scattered into the rectangle ABCD

$$= \frac{1}{2\pi\sigma^2} \int_{h\tan\theta\cos\alpha - a}^{h\tan\theta\cos\alpha + a} \exp\left(-\frac{x^2}{2\sigma^2}\right) dx \int_{-(h\tan\theta\sin\alpha + b)}^{b - h\tan\theta\sin\alpha} \exp\left(-\frac{y^2}{2\sigma^2}\right) dy$$

If p is the momentum of a particle at 37.7 m.w.e. which is incident at an angle θ to the vertical at sea-level then its momentum at sea-level is given by $\frac{p_0}{\cos\theta} + p$. The rate of such particles across an area of 1 cm.^{2} at S is

$$N\left(\frac{p_0}{\cos\theta} + p\right) \cos^n\theta\ 2\pi \sin\theta\, d\theta \cos\theta$$

Where $N\left(\frac{p_0}{\cos\theta} + p\right)$ is the vertical spectrum at sea-level and n is the zenith-angle dependence of the sea-level radiation of momentum $\frac{p_0}{\cos\theta} + p$ (Budini and Moliere, 1952). The total flux of particles of momentum p in the required solid angle is given by

$$\frac{1}{2\pi\sigma^2} \int_{h\tan\theta\cos\alpha - a}^{h\tan\theta\cos\alpha + a} \exp\left(-\frac{x^2}{2\sigma^2}\right) dx \int_{-(h\tan\theta\sin\alpha + b)}^{b - h\tan\theta\sin\alpha} \exp\left(-\frac{y^2}{2\sigma^2}\right) dy \ N\left(\frac{p_0}{\cos\theta} + p\right) \cos^n\theta\ 2\pi \sin\theta\cos\theta\, d\theta$$

where the sum is also taken over all α and θ. The limits in the integrals are for $b > h \tan\theta > a$. Taking this

into account the equation has been integrated numerically. A correction factor defined as the flux of particles of momentum p crossing 1 cm.^{2} at S, taking scattering into account, to the flux with no scattering has been calculated and the result is shown in figure 4.9.

(d) The sea-level spectrum

When this experiment was commenced the most accurate measurements of the sea-level spectrum were those of Owen and Wilson (1955), referred to as the O spectrum, and Caro, Parry and Rathgeber (1951), referred to as the C spectrum. Owen and Wilson measured the momenta of 60,000 particles with a spectrograph of m.d.m. 31 GeV/c; using the same apparatus Rodgers (1956) increased the m.d.m. to 240 GeV/c and measured 4,566 particles. Caro, Parry and Rathgeber measured the momenta of 6,056 particles with a spectrograph of m.d.m. 100 GeV/c. In figure 4.10 these two spectra are shown and it is seen that there is a discrepancy between them. Below 7 GeV/c the C spectrum lies above the O spectrum while above 7 GeV/c the C spectrum falls off more rapidly than the O spectrum. More recent work by Pine et al. (1959) and the author on the sea-level spectrum have shown good agreement with the O spectrum and not with the C spectrum and there is good evidence that the C spectrum is in error. For completeness all the calculations that follow have been made for both the O spectrum and the C spectrum.

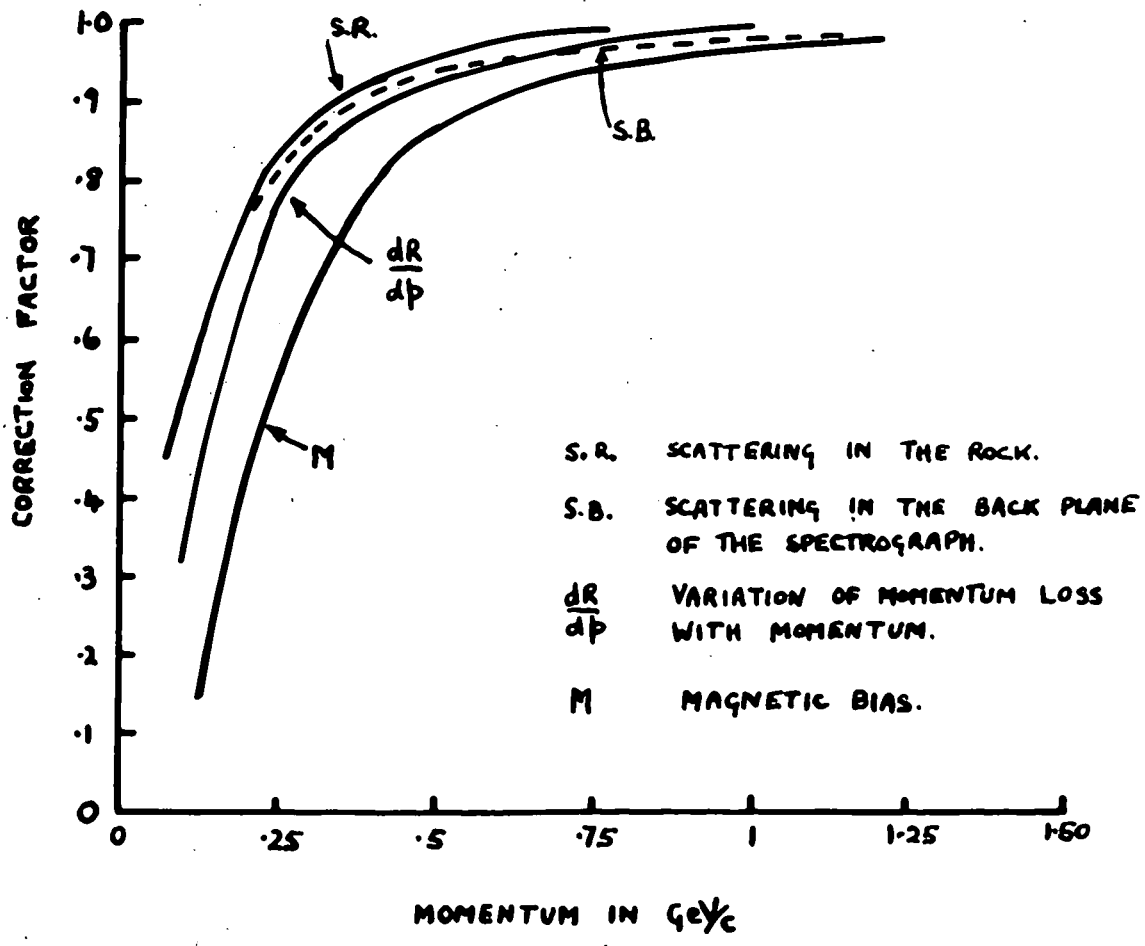

Figure 4.9 Corrections to be applied at low momenta

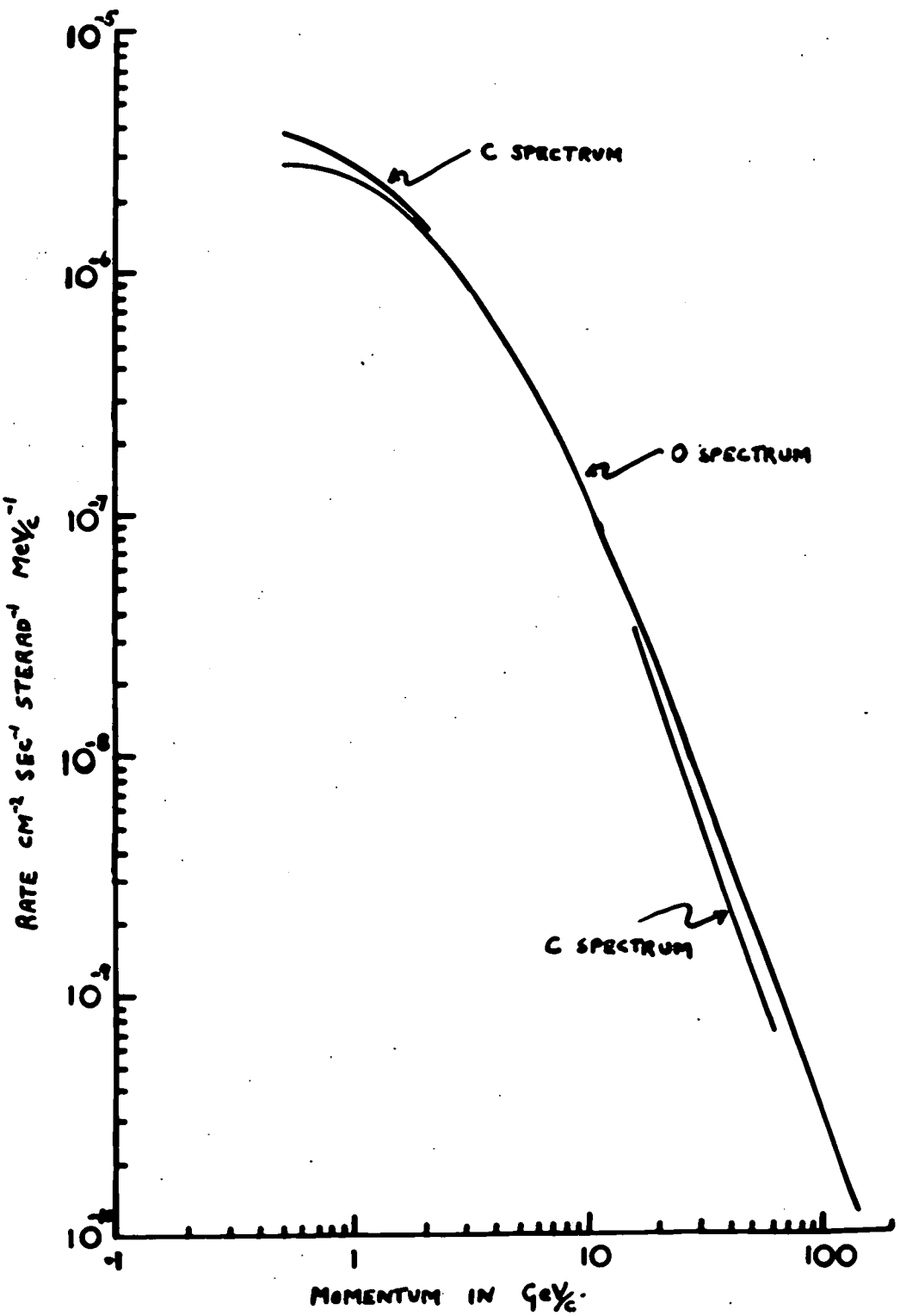

Figure 4.10 The sea-level spectrum

In the region of interest in the present experiment the sea-level spectrum has a continuously increasing slope in the range 6 - 20 GeV/c and cannot be represented by any simple analytic function. The trial spectrum at 37.7 m.w.e. was therefore derived numerically from the curves of figure 4.10 the following steps being made in the calculation.

1. The spectrum at 37.7 m.w.e. was predicted assuming a constant momentum loss for all particles.

2. Corrections were applied to this spectrum to account for the variation of $\frac{dp}{dx}$ with p at low momentum and scattering in the rock. This is the predicted spectrum incident on the top of the spectrograph.

3. A correction was applied to account for experimental bias in the spectrograph due to scattering in the back plane. The resulting momentum spectrum was converted to a deflection spectrum using the relation $p\Delta = 2.84$ GeV/c cm. and the deflection spectrum was broadened with the known experimental errors shown in figure 4.4. If $S(\Delta)$ is the predicted deflection spectrum then the broadened deflection spectrum will be $S(y)$ where

$$S(y) = \int_0^\infty S(\Delta) \frac{1}{\sqrt{2\pi}\,\sigma_M} \exp\left\{-\frac{(\Delta-y)^2}{2\sigma_M^2}\right\} d\Delta$$

This equation was solved by numerical integration.

4. Finally, the broadened spectrum was converted back to a momentum spectrum and corrected for magnetic bias. On normalising to the number of measured particles this spectrum was compared with the measured spectrum of particles traversing the

apparatus.

4.7 Deduction of the spectrum at 37.7 m.w.e.

The momentum loss in the rock, p_o, was used as a variable parameter to alter the trial spectrum until a good fit with the measured spectrum was obtained. To test the goodness of fit between the measured and predicted spectrum two methods were investigated.

(a) The ratio of the number of particles expected in the momentum interval 0.25 to 4 GeV/c to that expected in the interval 4 GeV/c to infinity was calculated for various values of p_o. The measured ratio of 0.97 ± 0.06 then determined the value of p_o which gave the best fit. The best values of p_o determined by this method for both the O spectrum and the C spectrum are shown in table 4b.

Sea-level spectrum	p_o
O spectrum	6.6 ± 0.8 GeV/c
C spectrum	7.6 ± 0.9 GeV/c

Table 4b

(b) The data was divided into 12 cells and the goodness of fit between the measured spectrum and the predicted spectrum was found by the χ^2 test. This method is superior to the previous one as it tests the goodness of fit over 12 cells instead of two cells. Also by using a contingency table (Moroney 1954) to calculate χ^2 allowance is made for the finite statistical accuracy of the O spectrum and the C spectrum as

well as that of the present results. This was particularly necessary in the case of the C spectrum which contained fewer than 1,000 particles in the common region of the spectra, i.e. $p > 7$ GeV/c at sea-level. In figure 4.11 χ^2 is plotted against p_o for both the O spectrum and the C spectrum. For the O spectrum the best fit (minimum χ^2) is at $p_o = 6.4$ GeV/c and the 16% level of significance, corresponding to the standard deviation limits of the best p_o, are at 5.4 GeV/c and 7.4 GeV/c. The results of the χ^2 calculation for both the O spectrum and the C spectrum are summarised in the table 4c.

Sea-level spectrum	Most probable momentum loss, p_o	Degree of Significance	16% limits of p_o
O spectrum	6.4 GeV/c	42%	5.4 GeV/c 7.4 GeV/c
C spectrum	7.3 GeV/c	53%	5.6 GeV/c 9.5 GeV/c

Table 4c

It is seen that the best value of p_o determined by the ratio method and the χ^2 method are consistent. In all later computations the values determined by the χ^2 method have been used.

In figure 4.12 the measured deflection spectrum is compared with that calculated from the sea-level spectrum of Owen and Wilson with $p_o = 6.4$ GeV/c, and in figure 4.13

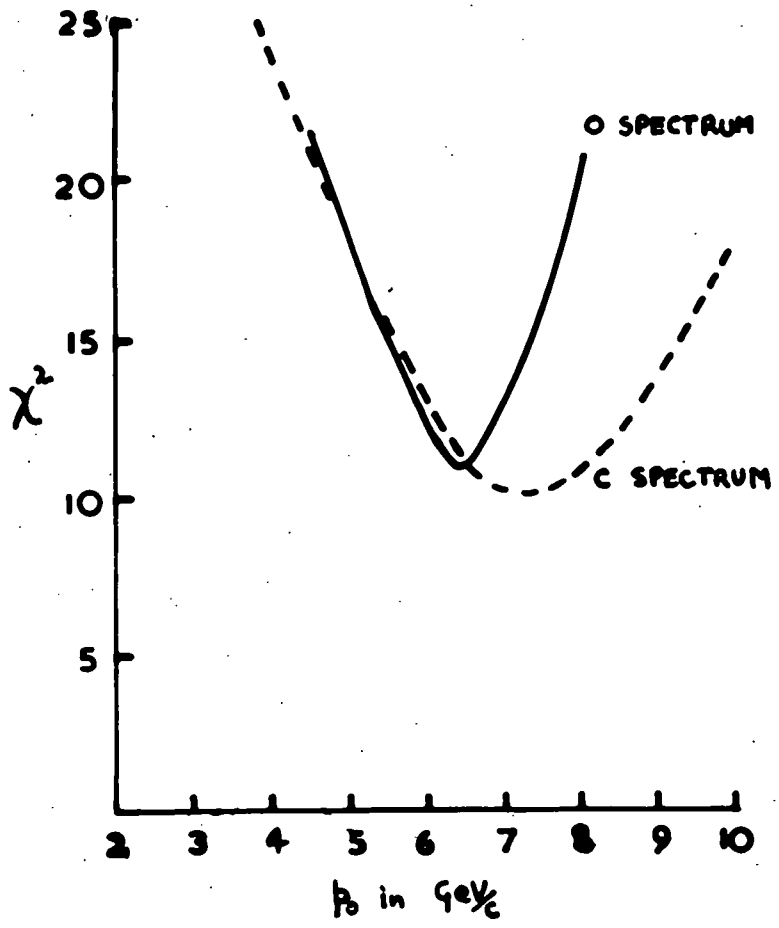

Figure 4.11 χ^2 - p_o plot for the O spectrum and C spectrum

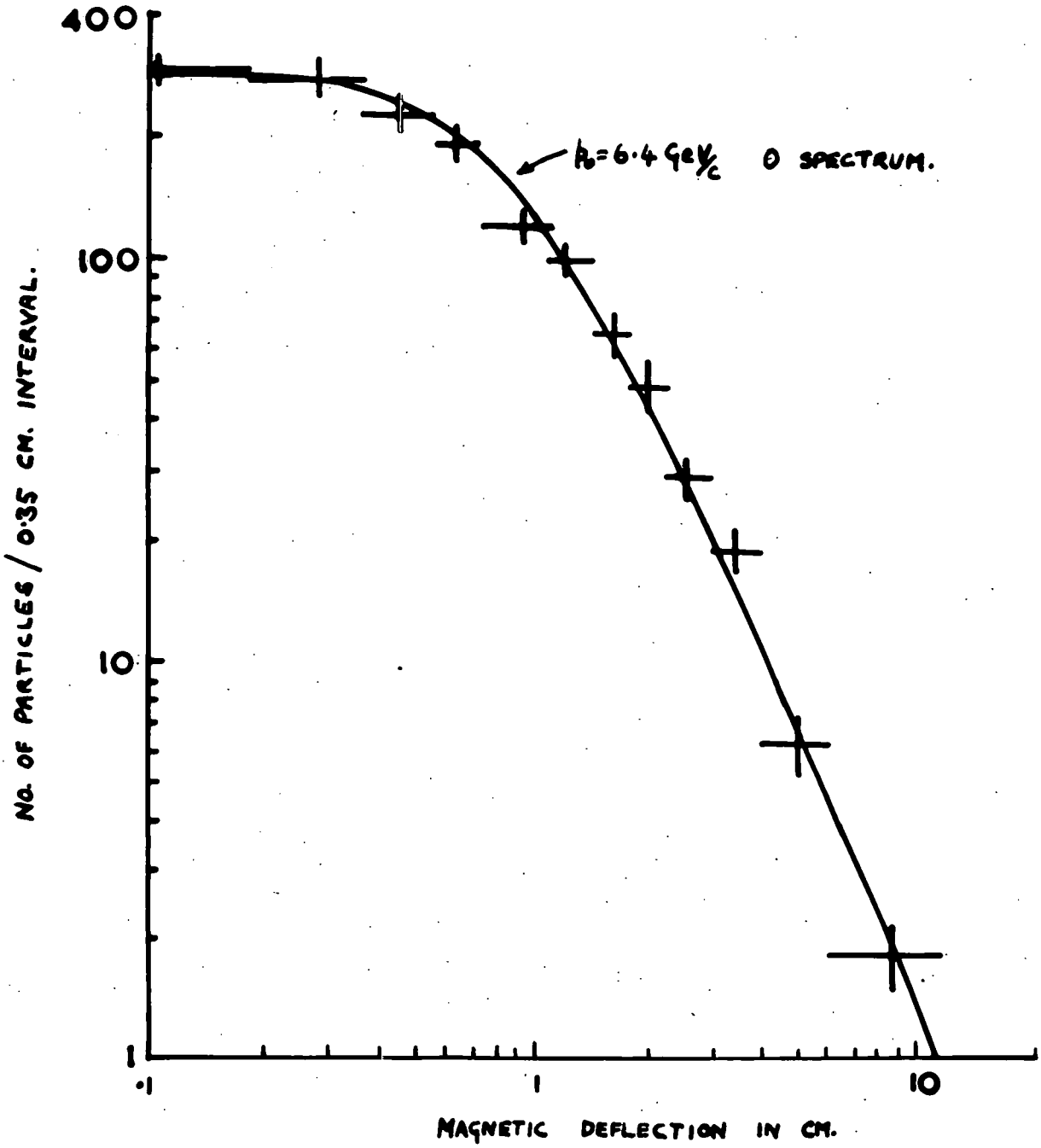

Figure 4.12 The measured deflection distribution compared with that expected for $p_0 = 6.4$ GeV/c and the O spectrum at sea-level

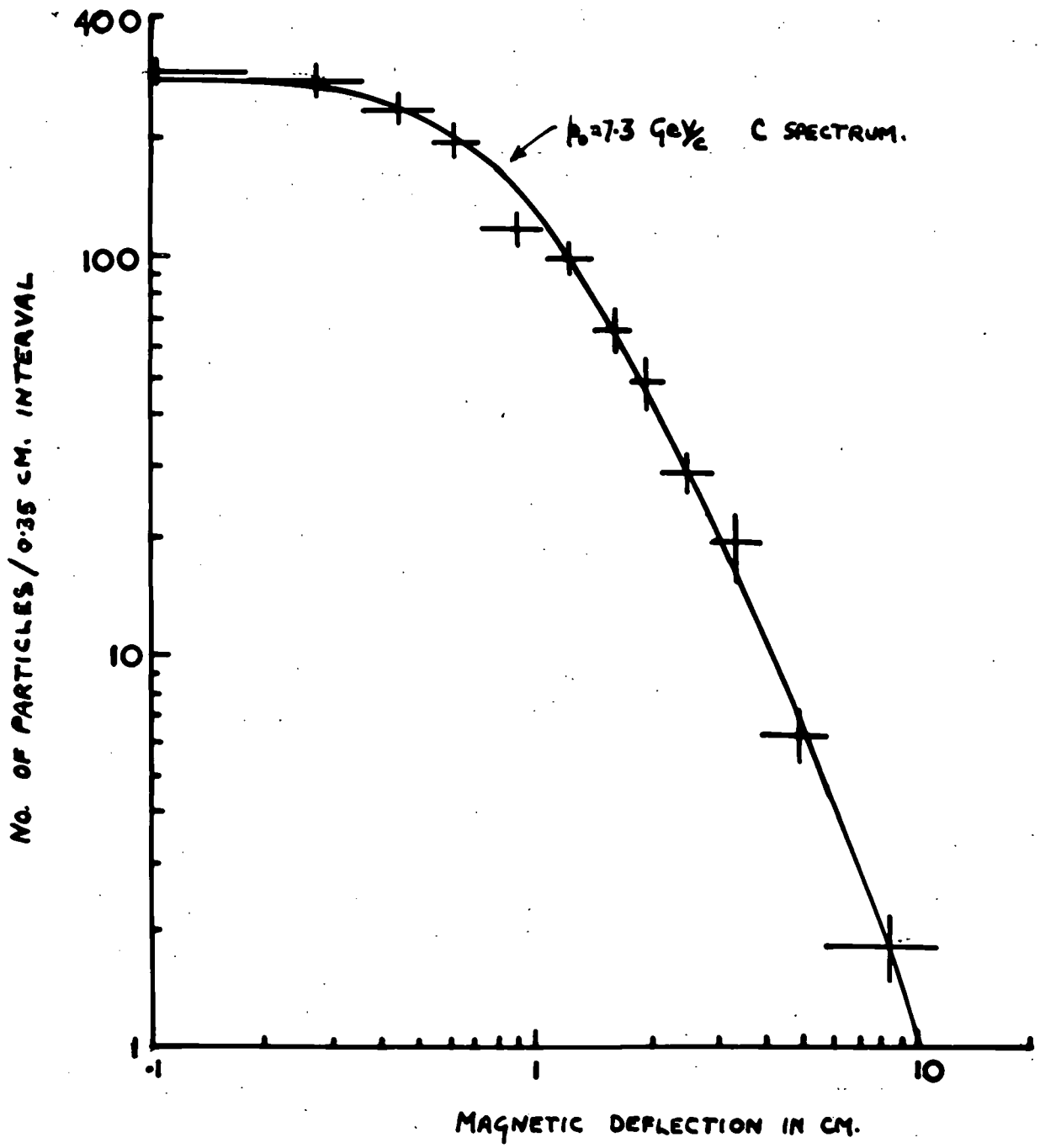

Figure 4.13 The measured deflection distribution compared with that expected for $p_0 = 7.3$ GeV/c and the C spectrum at sea-level

the analagous curve is shown for the sea-level spectrum of Caro et al. with p_o = 7.3 GeV/$_c$. In table 4d the basic data of the underground spectrum measurements are given together with the expected distributions giving the best fit to the observed distributions.

The trial spectrum of Owen and Wilson, with p_o = 6.4 GeV/$_c$, has been used to give the best estimate from this experiment of the vertical spectrum of cosmic rays at 37.7 m.w.e. and this is shown in figure 4.14. The spectrum of Owen and Wilson has been used because as explained previously, there is reason to believe that the C spectrum is in error. The experimental points shown in figure 4.14 have been plotted at the same percentage distance from the unbroadened spectrum as the broadened points were from the measured spectrum.

It will be shown in the next section that p_o = 6.4 GeV/$_c$ corresponds to a mean energy loss of μ-mesons which is less than that expected theoretically. However the significance level of this discrepancy is not high. Therefore for comparison the shape of the predicted spectrum at 37.7 m.w.e. is also shown in figure 4.14 for the sea-level O spectrum and the theoretically expected value of p_o, 7.9 GeV/$_c$. To obtain the absolute rates for p_o = 7.9 GeV/$_c$ the ordinates of figure 4.14 should be multiplied by 0.77.

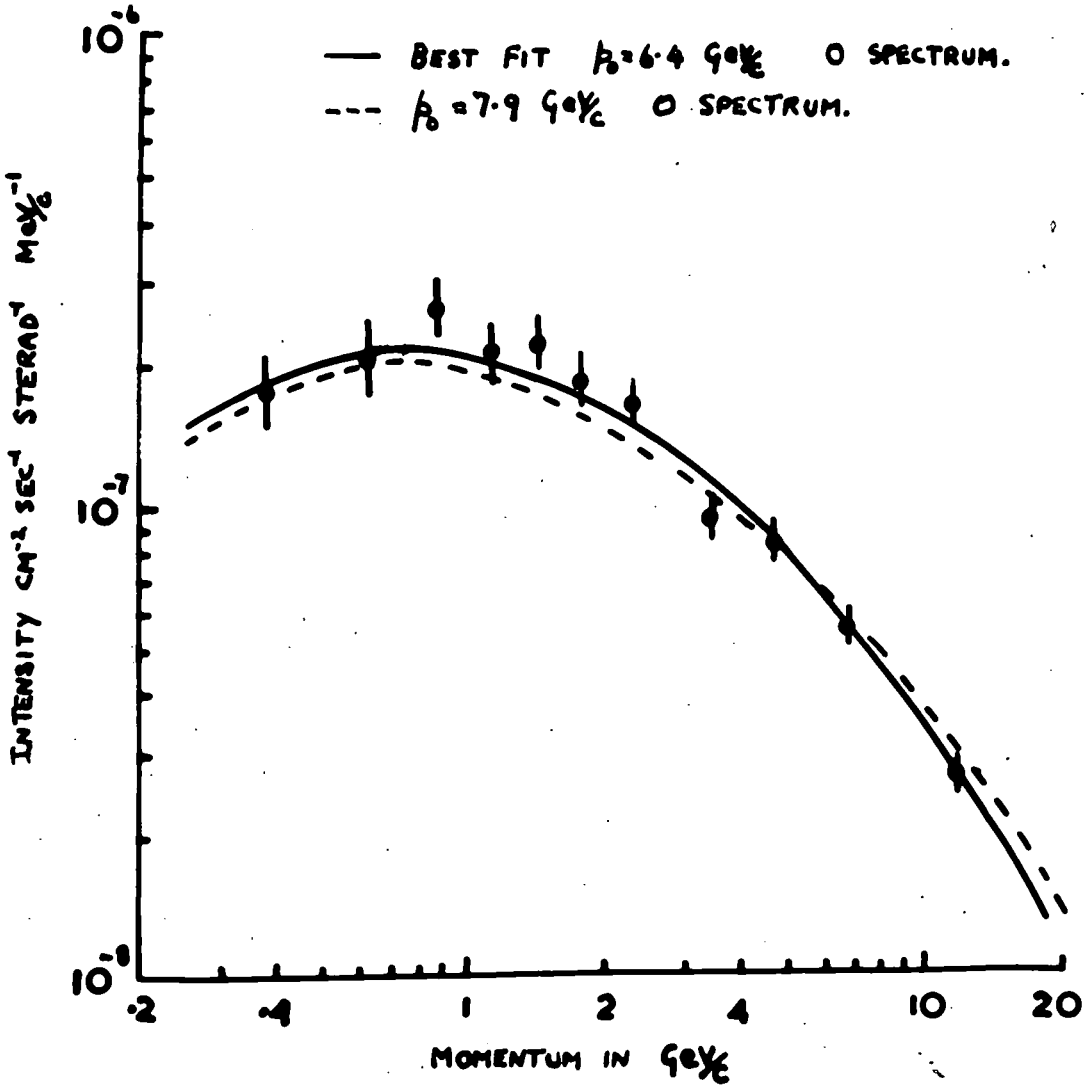

Figure 4.14 The momentum spectrum of cosmic rays at 37.7 m.w.e.

Momentum Interval GeV/c	Deflection Interval cm.	Observed Number	Expected Number O-spectrum p_o = 6.4 GeV/c	Expected Number C-spectrum p_o = 7.3 GeV/c
.25- .50	11.36-5.68	29	30	27
.50- .75	5.68-3.78	34	36	39
.75- 1.01	3.78-2.80	54	44	42
1.01-1.35	2.80-2.10	58	54	56
1.35-1.62	2.10-1.75	49	40	46
1.62-2.03	1.75-1.40	66	61	65
2.03-2.70	1.40-1.05	100	91	98
2.70-4.05	1.05-0.70	119	146	151
4.05-5.35	0.70-0.53	95	99	98
5.35-8.10	0.53-0.35	119	126	121
8.10-15.80	0.35-0.18	135	137	130
15.80 -	0.18-0	152	146	137
		1,010	1,010	1,010

Table 4d

4.8 The rate of energy loss of μ-mesons in the energy range 3-12 GeV/c

(a) The measured rate of energy loss

From the best value of p_o already determined and a knowledge of the depth of the cave below sea-level, (37.7±0.6) m.w.e., the mean rate of energy loss of μ-mesons can be calculated. The values obtained for both the O spectrum and the C spectrum are shown in table 4e.

	p_o GeV/c	$-\frac{dE}{dx}$ MeV/gm.cm.$^{-2}$	Mean Energy GeV	Energy range GeV
O spectrum	(6.4±1.0)	(1.70±0.27)	5.6	3.45-11.20
C spectrum	$(7.3^{+2.2}_{-1.7})$	$(1.94^{+0.58}_{-0.45})$	6.05	3.90-11.65

Table 4e

The mean value of $\frac{dE}{dx}$ obtained above is that of the μ-mesons when half way through the rock between sea-level and the cave. The best estimate of this energy is given by $\frac{p_o c}{2}$ plus the median energy, 2.4 GeV of particles in the measured spectrum between 0.25 GeV/c and the maximum detectable momentum, 8 GeV/c. The range of energy over which $\frac{dE}{dx}$ is an estimate of the energy loss is also shown in table 4e.

The measured rate of energy loss can now be compared with theory.

(b) The expected rate of energy loss of μ-mesons

The energy loss of μ-mesons has been considered by George (1952) and Barrett et al. (1952). The equation of George contains two terms which should be omitted in the light of later work; one term concerns the production of penetrating secondaries by μ-mesons which has been shown to be much less important than originally thought (Braddick and Leontic 1954), while the term due to Cerenkov radiation is already included in the energy loss due to ionisation. It will be useful to review the energy loss equation.

The known energy loss processes of high energy μ-mesons are listed below.

(i) Ionisation
(ii) Cerenkov radiation
(iii) Bremsstrahlung
(iv) Electron pair production
(v) Nuclear interaction

(i) Ionisation

A charged particle traversing matter loses energy to the electrons of the medium the coupling being via the Coulomb fields of the particles. The electrons can be either raised to excited states in their parent atom or can be ejected completely from the atom. In either case the

increment of energy is taken from the energy of the incident particle.

(a) Large energy transfers $>\eta$.

For large energy transfers the electrons of the medium can be considered as free but for small energy transfers the transition probability for the system formed by the primary particle and the atom as a whole must be considered.

For a μ-meson of spin $\frac{1}{2}$ and energy E, Bhabha 1938, Massey and Corben, 1939 give the probability per gm. cm.$^{-2}$ of producing an electron of energy E' as

$$\chi(E, E')dE' = \frac{2\mu_e}{\beta^2}\frac{\pi N\left(\frac{Z}{A}\right)r_0^2}{(E')^2}\left\{1 - \beta^2\frac{E'}{E'_m} + \frac{1}{2}\left(\frac{E'}{E+\mu}\right)^2\right\}$$

where μ_e, r_0 are the mass and classical radius of the electron and E'_m is the maximum transferable energy to an electron. Using this equation the mean energy loss for energy transfers $>\eta$ is given by

$$K(>\eta) = \int_{\eta}^{E'_m}\chi(E, E')dE'$$

$$= 0.0766\left\{\ln\left(\frac{E'_m}{\eta}\right) - 1 + \frac{1}{4}\left(\frac{E'_m}{E+\mu}\right)^2\right\} \text{ MeV/gm cm}^{-2}$$

(b) Small energy transfers $<\eta$

The energy loss for energy transfers $<\eta$, $K(<\eta)$ has been calculated by Bethe (1930, 1932, 1937).

$$K(<\eta) = \frac{2\mu_e}{\beta^2}\left(\frac{\pi NZ}{A}\right)r_0^2\left\{\ln\left(\frac{2\mu_e\beta^2\eta}{(1-\beta^2)I^2(z)}\right) - \beta^2\right\}$$

where $I(z) = Z\,13.5\text{ev}$

$$K(<\eta) = 0.0766\left\{\ln\left(\frac{2\mu_e\beta^2\eta}{(1-\beta^2)I^2(z)}\right) - \beta^2\right\} \quad \text{MeV/gm.cm.}^{-2}$$

In figure 4.15 $K(<\eta)$ and $K(>\eta)$ are plotted as a function of energy for η = 10 KeV, ρ = 1.9 gm./cc. Z = 10 and A = 20. The energy range 10^9 - 10^{12} ev is considered here as the variation at high energy is required in Chapter 7 where the rate of energy loss of high energy μ-mesons is determined from the sea-level integral spectrum and the depth-intensity curve. The reason for the increase of $K(>\eta)$ with energy is due to the increase in the maximum transferable energy which means that there are more final energy states available to the knock on electron.

The increase in $K(<\eta)$ with energy is due to the relativistic increase in the electric field perpendicular to the direction of motion by a factor $\frac{E}{\mu c^2}$. However, Swann (1938) pointed out that the above equation should be modified for condensed materials since the increase in the electric field at large impact parameters would tend to be opposed by the polarization of the medium. This effect was first quantitatively investigated by Fermi (1940) and later by Halpen and Hall (1940), Wick (1940) and Sternheimer (1956). According to Halpern and Hall the density correction Δ which must be subtracted from $K(<\eta)$ is given by

$$\Delta = \frac{2\mu e}{\beta^2} \frac{\pi N Z}{A} r_0^2 \left\{ \ln\left(\frac{\varepsilon - 1}{1-\beta^2}\right) - 1 \right\}$$

for $\beta > \frac{1}{\sqrt{\varepsilon}}$ (i.e. p > 415 MeV/c for μ-mesons) where ε is the equivalent dielectric constant of the medium.

$$\varepsilon = 1 + \frac{Z}{A} \rho r_0 \left(\frac{137}{I(z)}\right)^2 N_0 e^4 4\pi$$

= 1.06 for rock with ρ = 1.90 gm./cc., Z=10, A=20.

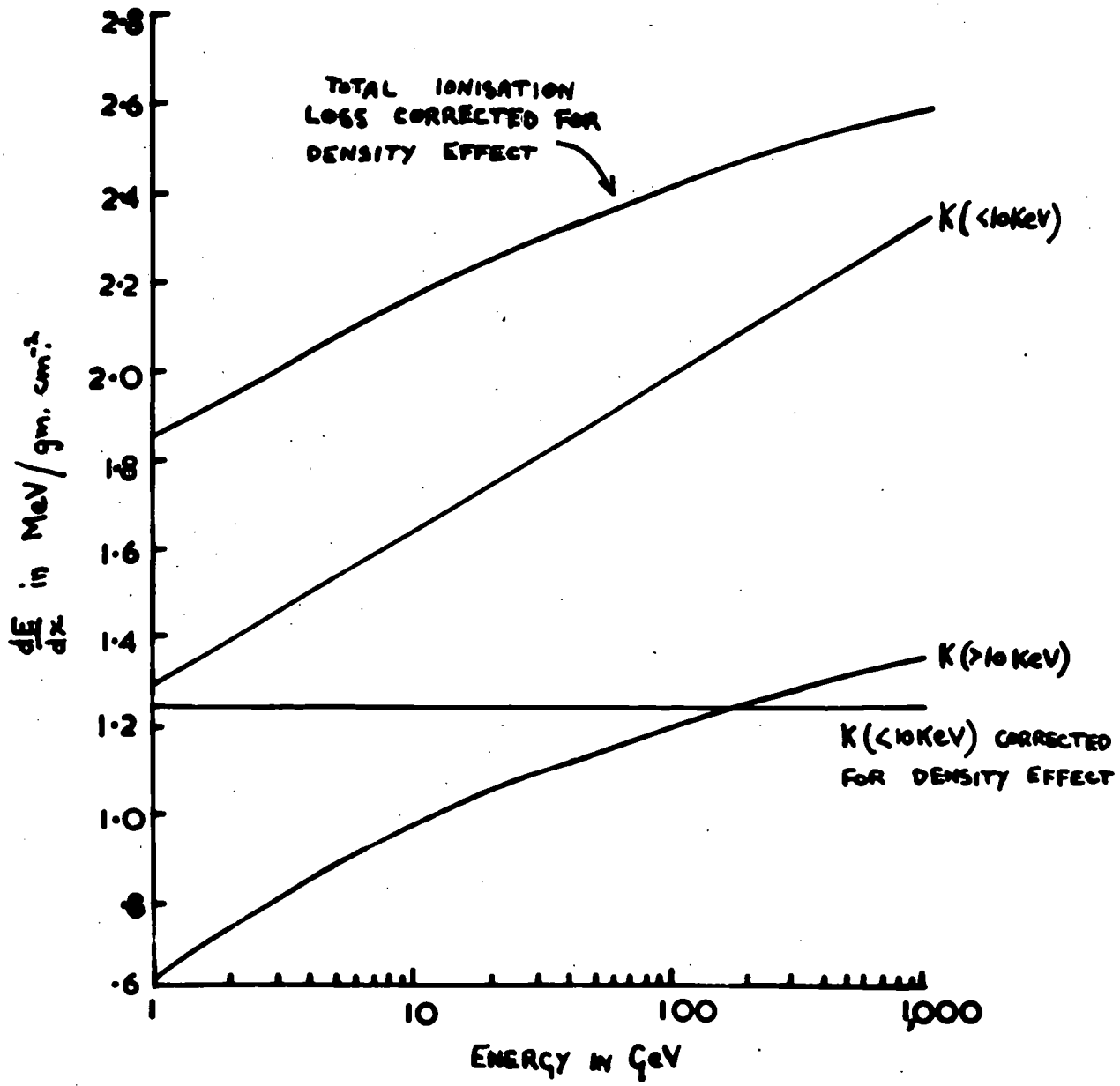

Figure 4.15 The theoretical energy loss, due only to ionisation, for μ-mesons

$$\Delta = 0{\cdot}0766 \left\{ \ln\left(\frac{0{\cdot}06}{1-\beta^2}\right) - 1 \right\} \text{ MeV/gm.cm.}^{-2}$$

When Δ is subtracted from $K(<\eta)$ it is seen that the relativistic increase of energy loss is exactly balanced out by the reduction due to the density effect. Also shown in figure 4.15 is the total ionisation loss of μ-mesons when correction is made for the density effect. Here the increase in energy loss with energy is due entirely to knock on electrons with energy >10 KeV.

(ii) Cerenkov radiation

If a particle traverses a medium with a velocity greater than the velocity of light in the medium then radiation is emitted only on the surface of a cone of half angle $\cos^{-1}\left(\frac{1}{\beta n}\right)$ where n is the refractive index of the medium. This radiation results from the interaction of the electric field of the moving charged particle with the atoms of the medium at large impact parameters. The extraction of energy from the μ-meson due to this process therefore saturates at high energy and has already been included in the term $K(<\eta)$ in considering ionisation loss.

(iii) Bremsstrahlung

The cross section for the production of a photon of energy E' to $E'+dE'$ by a μ-meson of energy E and spin $\frac{1}{2}$ (Christy and Kusaka, 1941) is

$$\sigma(E,E')dE' = \alpha Z^2 r_0^2 \left(\frac{m_e}{\mu}\right)^2 \frac{16}{3}\left\{\frac{3}{4}\frac{E'}{E} + \frac{E-E'}{E'}\right\}\left\{\ln\left(\frac{12}{5}\frac{E}{\mu Z^{1/3}}\frac{E-E'}{E'}\right) - \frac{1}{2}\right\}dE'$$

Using this result the mean energy loss per MeV/gm. cm.$^{-2}$ is given by

$$\frac{dE}{dx} = \int_0^{E-\mu c^2} \sigma(E,E')\frac{N_0}{A}E'dE'$$

$$= 1{\cdot}5.10^{-7}E\left\{\ln\left(\frac{E}{\mu c^2}\right) - \frac{1}{2}\right\} \text{ MeV/gm. cm.}^{-2}$$

(iv) Pair production

The cross section for the production of electron pairs by μ-mesons has been calculated by Bhabha (1935). The equations are more complicated than for bremsstrahlung and they give for the mean energy loss

$$\frac{dE}{dx} = 1.6 \cdot 10^{-6} E. \quad \text{MeV/ gm. cm.}^{-2}$$

(c) Nuclear interaction

Observations in nuclear emulsions exposed underground (George and Evans, 1950) have suggested that the cross section for the production of stars releasing energy in the limits $E' \text{ to } E'+dE'$ by a μ-meson of energy E is of the form

$$\sigma(E,E')dE' = \frac{2\alpha}{\pi} \sigma_{h\nu} \frac{dE'}{E'} \ln\left(\frac{E}{E'}\right)$$

where $\sigma_{h\nu} \sim 10^{-29}$ cm.$^{-2}$. The energy loss by nuclear interaction obtained from this cross section is

$$\frac{dE}{dx} = 5.0. \quad 10^{-7} \quad E \quad \text{MeV/ gm. cm.}^{-2}$$

In figure 4.16 the relative importance of these processes is shown for the energy range 1 - 1,000 GeV. The total energy loss for μ-mesons is the sum of the five independent energy losses and this is also shown.

In figure 4.17 the experimental data of table 4e on the energy loss of μ-mesons in the energy range 3 - 12 GeV is compared with theory. From figure 4.16 it is seen that at 20 GeV, ionisation loss contributes 97.6% to the total energy

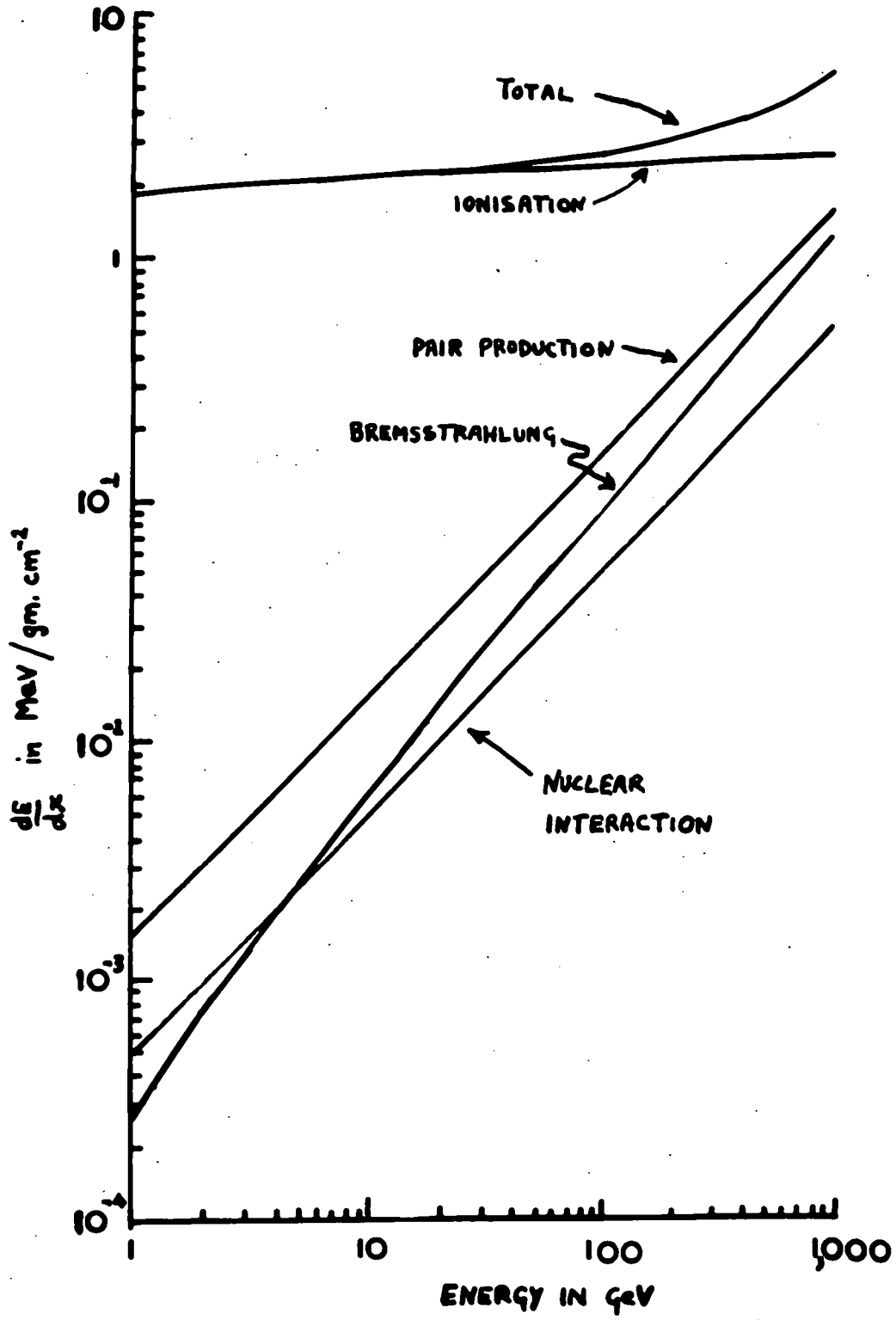

Figure 4.16 The theoretical energy loss of μ-mesons

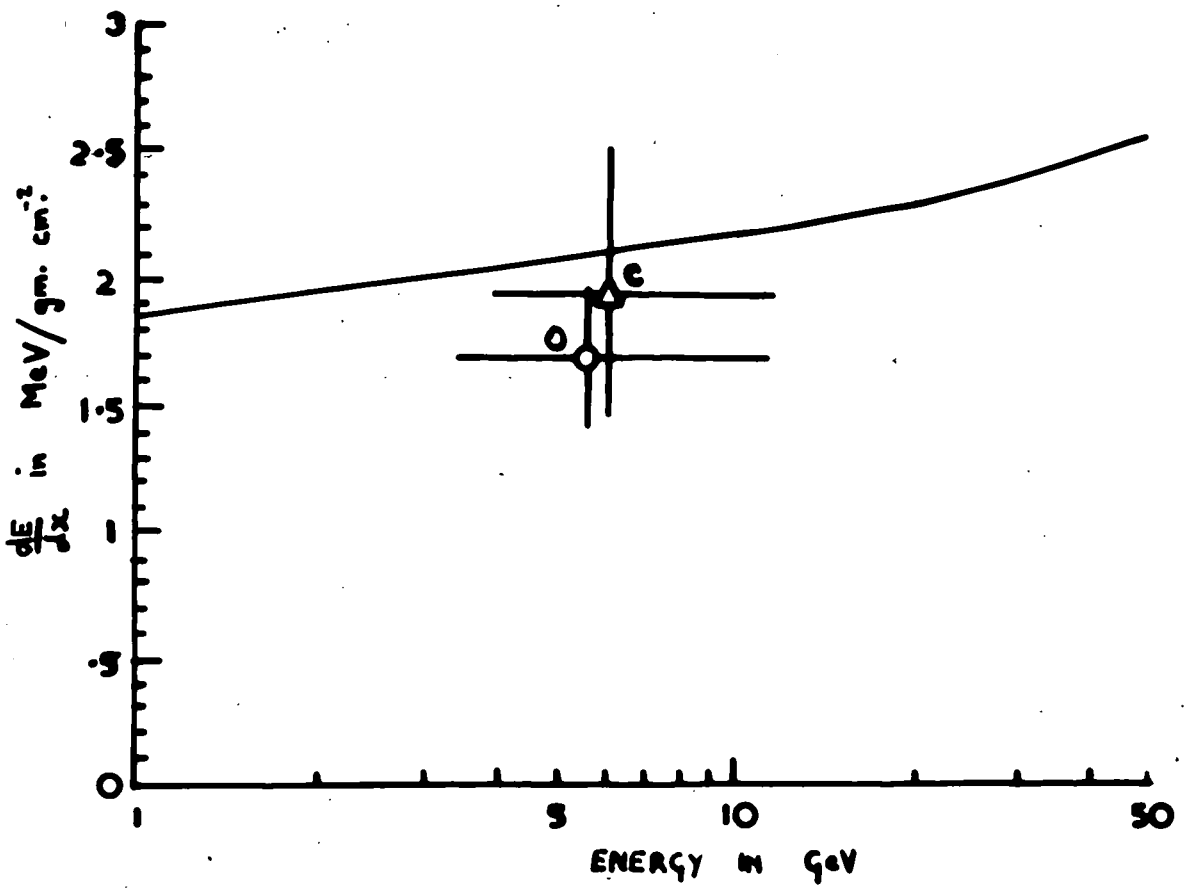

Figure 4.17 Comparison between the measured rate of energy loss of μ-mesons and the theoretical value

loss. The point O refers to the value of $\frac{dE}{dx}$ found using the O spectrum at sea-level while C is that for the C spectrum. Both points lie below the expected curve but the accuracy of determining $\frac{dE}{dx}$ is not high. In table 4e the chance that the two experimental points are consistent with the theoretical curve is given.

	$\frac{dE}{dx}$ Experimental Mev/gm.cm.$^{-2}$	$\frac{dE}{dx}$ Expected Mev/gm.cm.$^{-2}$	Probability of experimental pts. being consistent with theory
O spectrum	(1.70 ± 0.27)	2.10	8%
C spectrum	$(1.94 \begin{smallmatrix} + 0.58 \\ - 0.45 \end{smallmatrix})$	2.10	37%

Table 4e

It must therefore be concluded from this experiment that in the energy range 3 - 12 GeV the energy loss of μ-mesons is due predominantly to ionisation loss and that there is no significant disagreement between experiment and theory.

4.9 Comparison with other work on underground spectra

Recently Dayon and Potapov (1959) have made an accurate measurement of the spectrum at a depth of ~ 40 m.w.e., based on 26,000 events. They employed a magnetic spectrograph with geiger counters at the detecting levels and achieved an m.d.m. of 14.9 GeV/c. In figure 4.18 their adopted spectrum (dashed line) is compared with the experimental points obtained in the present experiment. As they did not measure their depth accurately no precise comparison can be made but it can be seen that there is no gross discrepancy.

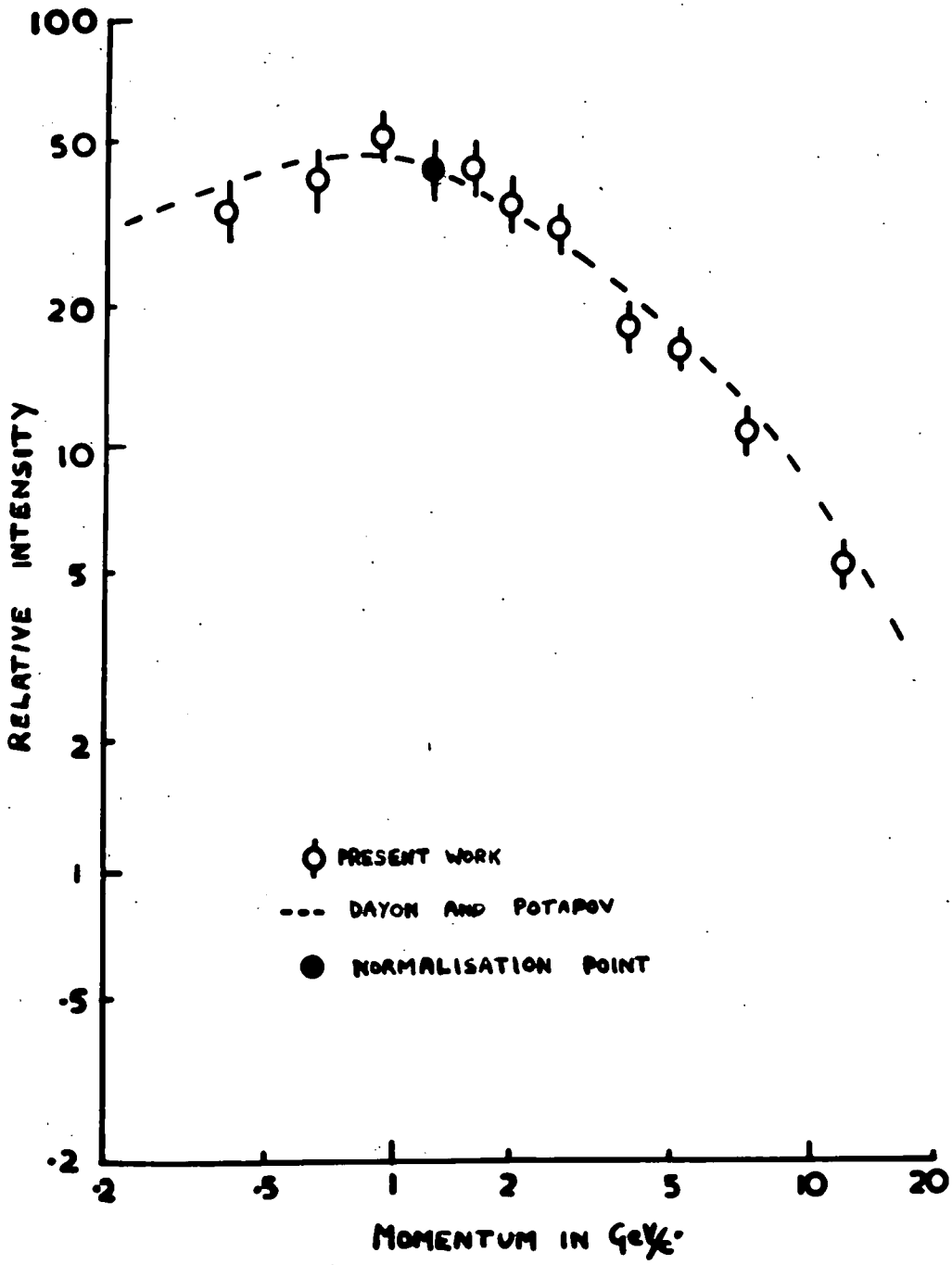

Figure 4.18 Comparison between the present work and that of Dayon and Potapov

George and Shrikantia (1956) exposed nuclear emulsions at a depth of 57 m.w.e. and derived a momentum spectrum from measurements on the multiple scattering of 317 particles in the emulsion. Comparison is made with the spectrum expected from an extrapolation of the sea-level spectrum of Owen and Wilson and the expected momentum loss in the rock. The fit with this spectrum is not good but the authors conclude that it is not in significant disagreement with expectation.

Nash and Pointon (1950) measured the scattering distribution of particles in two lead plates in a cloud chamber in the same location as the present experiment. The nature of the method precluded an accurate determination of the spectrum and the conclusion was that for $p < 1$ GeV/c there was no evidence to support a large divergence from the spectrum expected from an extrapolation of that of Owen and Wilson.

4.10 Conclusions

The momentum spectrum of cosmic rays at 37.7 m.w.e. has been measured. From a comparison of the sea-level spectrum and the spectrum at 37.7 m.w.e. it is concluded that the energy loss of μ-mesons in the range 3 - 12 GeV does not differ significantly from that predicted by theory. Thus it is clear that underground spectra at moderate depths derived from an extrapolation of the sea-level spectrum are accurate. In particular it is apparent that the low momentum end of the spectrum is quite accurately represented. It is this region that is important in the analysis of underground scattering

experiments so it can be concluded that there is no objection to the results of these experiments on the grounds of inaccurate spectra.

CHAPTER 5

The Durham High Energy Spectrograph

5.1 Description of the spectrograph

The spectrograph is similar in design to that described by Hyams et al. (1950), the main improvement over the former instrument being its much greater rate and the use of arrays of neon flash-tubes rather than cloud chambers for measuring high momentum particles. A scale diagram of the spectrograph is shown in figures 5.1 and 5.2. The detailed design was based on the performance of the prototype spectrograph. As the Durham instrument has already been described by Kisdnasamy (1958) only a brief description of its mode of operation will be given here.

The magnet is a large electromagnet of the Blackett type and the spectrograph contains two types of detectors, geiger counters and neon flash-tubes. The geiger counters alone are used in studying low momentum particles while the flash-tubes are used in conjunction with the counters to give a greater precision of measurement at high momentum.

(a) The geiger counter system

A particle traversing the spectrograph is registered by a fivefold coincidence from the geiger counters G_A, G_B, G_G, G_C, G_D. Hence if the counters through which the particle has passed can be identified the magnetic deflection can be computed. In the spectrograph of Hyams at al. this was done by hodoscoping the counters but in the present apparatus the

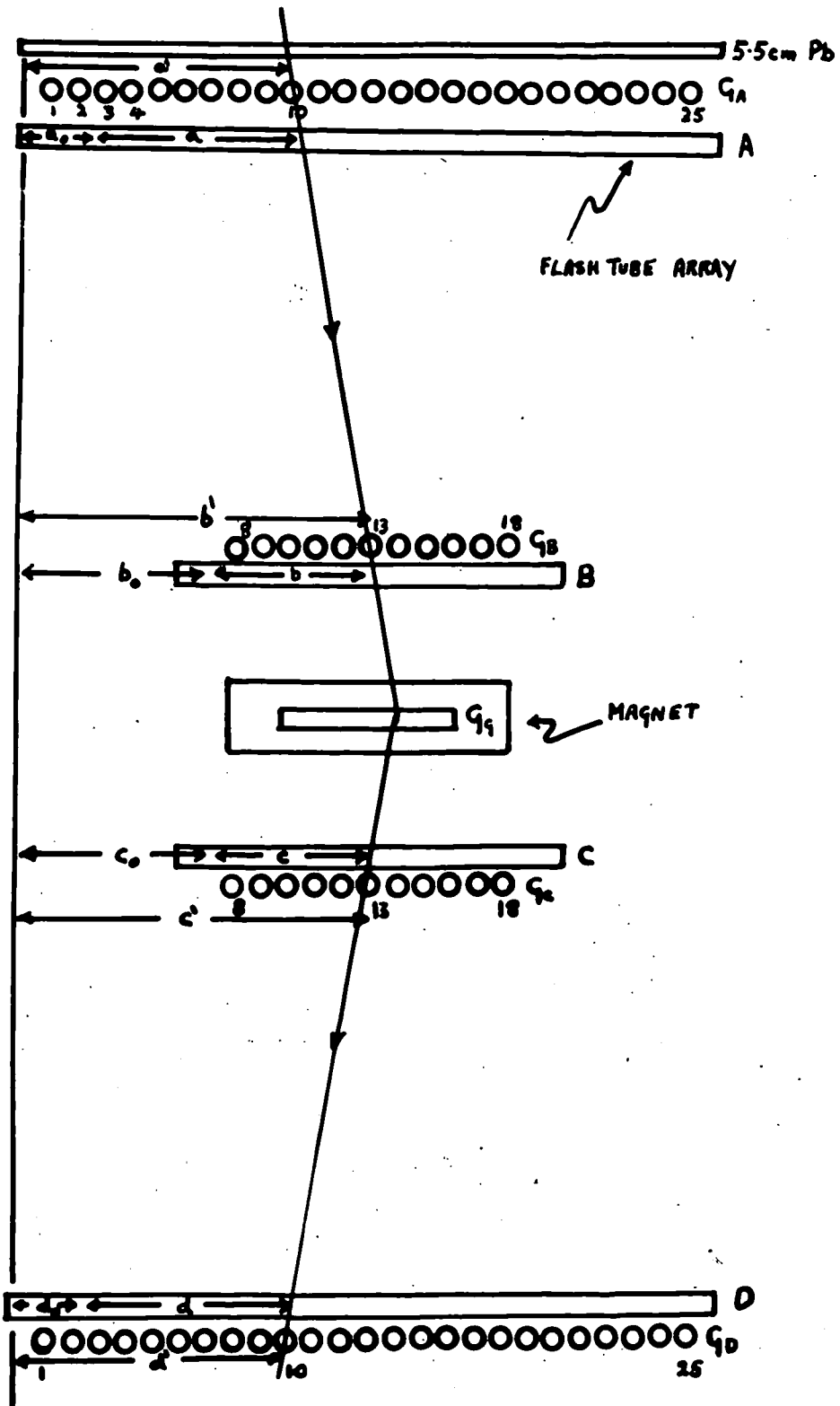

Figure 5.1 The Durham Spectrograph. Front elevation. Vertical scale = 1/30 full size except for geiger counters. Horizontal scale = 1/10 full size.

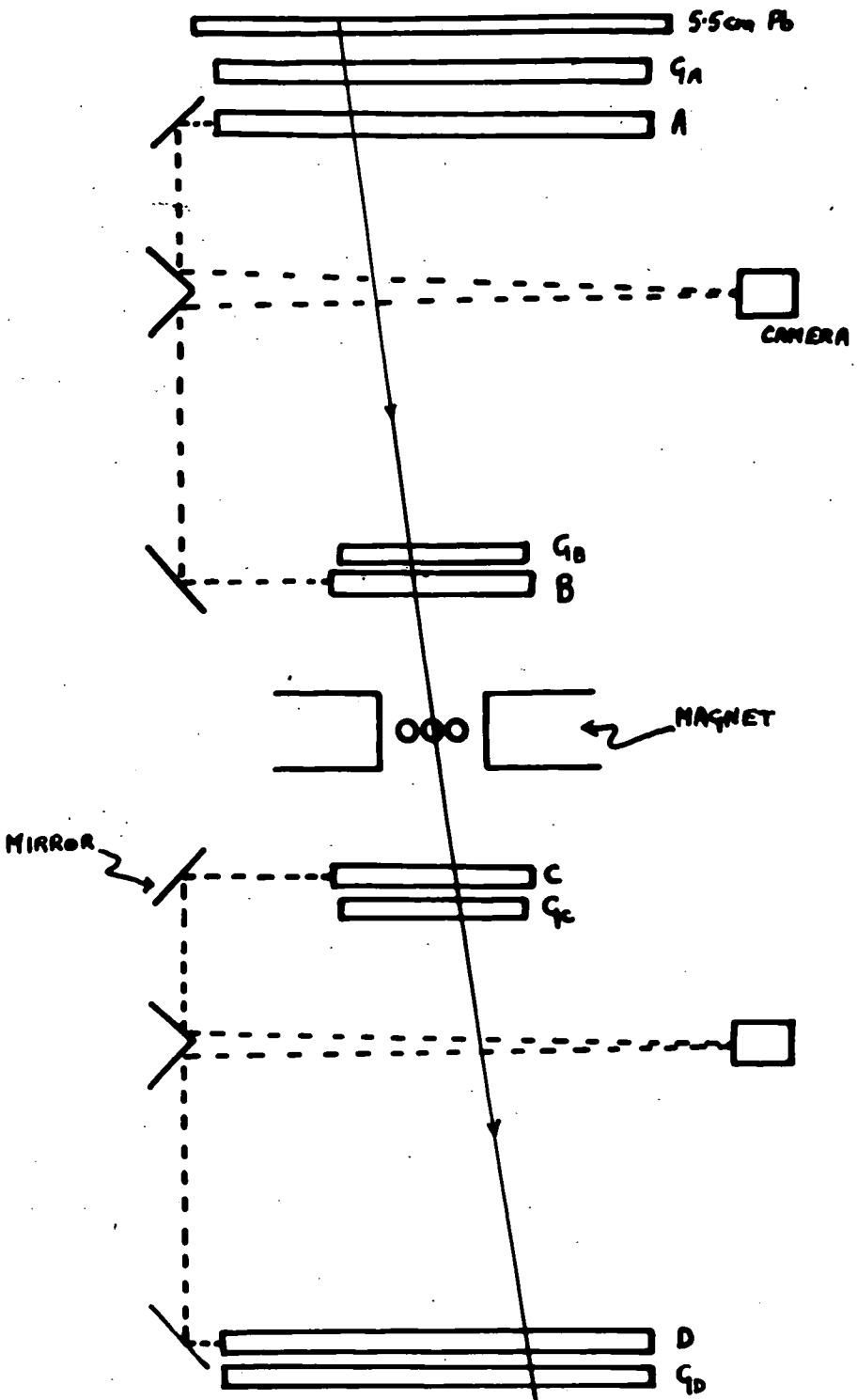

Figure 5.2 The Durham Spectrograph. Side elevation. Vertical scale = 1/30 full size except for geiger counters. Horizontal scale = 1/10 full size.

computation is performed automatically by an electrical analogue computer referred to as a momentum analyser

From figure 5.1 it can be seen that the computation required is (a'-b') - (c'-d') where a' is the distance from the reference line to the centre of the geiger counter that has been discharged in G_A, etc. Thus if each counter which discharges in trays other than G_G is caused to produce a voltage pulse of magnitude proportional to its distance from the reference line then a voltage proportional to the magnetic deflection can be generated by adding the appropriate voltages in the correct phase. The final voltage pulse is displayed on an oscilloscope and photographed. This technique assigns a particle to a certain deflection category rather than determining its deflection uniquely, due to the finite diameter of the geiger counters. For example, the trajectory shown in figure 5.1 would be assigned to category -6. As the geiger counters are accurately located such that the perpendicular distance between the axes of adjacent counters is 3.8 cm. the nominal deflection of a category n particle is n. 3.8 cm. In all there are 45 categories ranging from -22 to + 22.

If more than one particle traverses any of the geiger counter trays (other than G_G) this method breaks down but such events can be recognised electronically and either marked or rejected. In this manner Jones and Gardener (private communication) have measured 200,000 particles traversing the spectrograph; the spectrum in the range 0.5 - 15 GeV/c is at present being evaluated.

(b) The neon flash-tube system

The spectrograph contains four arrays of flash-tubes A, B, C, D. The flash-tubes are of internal diameter 5.9 mm. and external diameter 7.3 mm. Each tube is filled with neon at 3 atmospheres pressure and on the passage of a particle through the spectrograph a pulse, of time delay 6 μs, rise time 0.5 μs, length 5 μs and height 8 KV/cm., is applied across each layer of flash-tubes. Under these conditions the mean layer efficiency of all the layers is (60 ± 1)%. Each array contains 8 layers of tubes and the tubes are mounted in accurately milled slots such that the separation of the centres of adjacent tubes is 8 mm. The tubes are staggered in such a way that it is not possible for a particle to traverse an array without producing a flash.

The arrays A, B and C,D are photographed through mirrors (figure 5.2). A typical record obtained with the flash-tubes is shown in figure 5.3.

The sequence of operation after a five-fold coincidence is

(i) The coincidence circuit is paralysed

(ii) The voltage pulse is applied to the flash-tubes and the flashes are recorded

(iii) A control motor is set in motion which causes two small reference bulbs attached to each array of flash-tubes to glow; the clocks are illuminated

(iv) The camera is wound on and the paralysis is removed leaving the system ready for the next event to be recorded.

Figure 5.3 Typical record - Durham Spectrograph

The extreme images on each of the records, figure 5.2, are due to the reference bulbs.

5.2 Measurement of the trajectories

The arrays of flash-tubes are aligned by plumb lines which pass through small holes in templates attached to each array. The plumb lines cannot be photographed with the flashes so it is only possible to determine from the photographic record the projected distance of the trajectory to a fixed point on the front plane of the flash-tube array. Referring to figure 5.1 if a, b, c, d are the distances from the trajectory to the fixed points on the arrays and a_o, b_o, c_o, d_o are the distances from the fixed points to the plumb line then the magnetic deflection is given by, $\Delta = \{(a+a_o)-(b+b_o)\} - 0.972\{(c+c_o)-(d+d_o)\}$ The factor 0.972 reduces the measurements in the bottom half of the spectrograph to the same arm as those measured in the top. In making the measurements a, b, c, d difficulties arose due to distortion produced by the mirrors. This was overcome by projecting the films onto a screen on which was drawn a complete diagram of the tube system for each array. The diagrams were drawn using photographs in which all the tubes had flashed, these having been taken when the tubes were irradiated by a γ-ray source and a succession of high voltage pulses applied. The diagrams also gave the positions of the reference bulbs so that each photograph taken during the actual experiment could be aligned. The reference scale coincided with the centre of the fourth layer of tubes from

the top for each array. In this way all the measurements were made in units of 8 mm. The scale diagrams for the top and bottom halves of the spectrograph were drawn on screens constructed from separate sheets of hardboard, painted white.

Reprojection took place through a system of mirrors so that the image was formed on the surface of a table whence the measurements could be made in comfort.

5.3 The determination of Δ_o

The magnetic deflection of a particle traversing the spectrograph can be written $\Delta = \Delta_o + \{(a-b) - 0.972(c-d)\}$ where $\Delta_o = (a_o-b_o) - 0.972(c_o-d_o)$ and is a constant for all trajectories. From each record only the quantities a, b, c, d were determined and it was necessary to keep a continuous check on the alignment of the systems to make sure that the quantity Δ_o remained constant.

a_o, b_o, c_o, d_o were measured directly on the spectrograph to high accuracy and these gave $\Delta_o = (65.04 \pm 0.03)$ units of 8 mm. An experimental check was also made by operating the spectrograph with zero magnetic field. The frequency distribution of (a-b) - 0.972 (c-d) for the 311 measured trajectories is shown in figure 5.4. The mean of this distribution gives $\Delta_o = (64.94 \pm 0.13)$ units of 8 mm. The finite width of the distribution is due to multiple scattering in the spectrograph and errors of measurement. The agreement between these quantities is regarded as satisfactory. The value of Δ_o used in the computations was the former since this

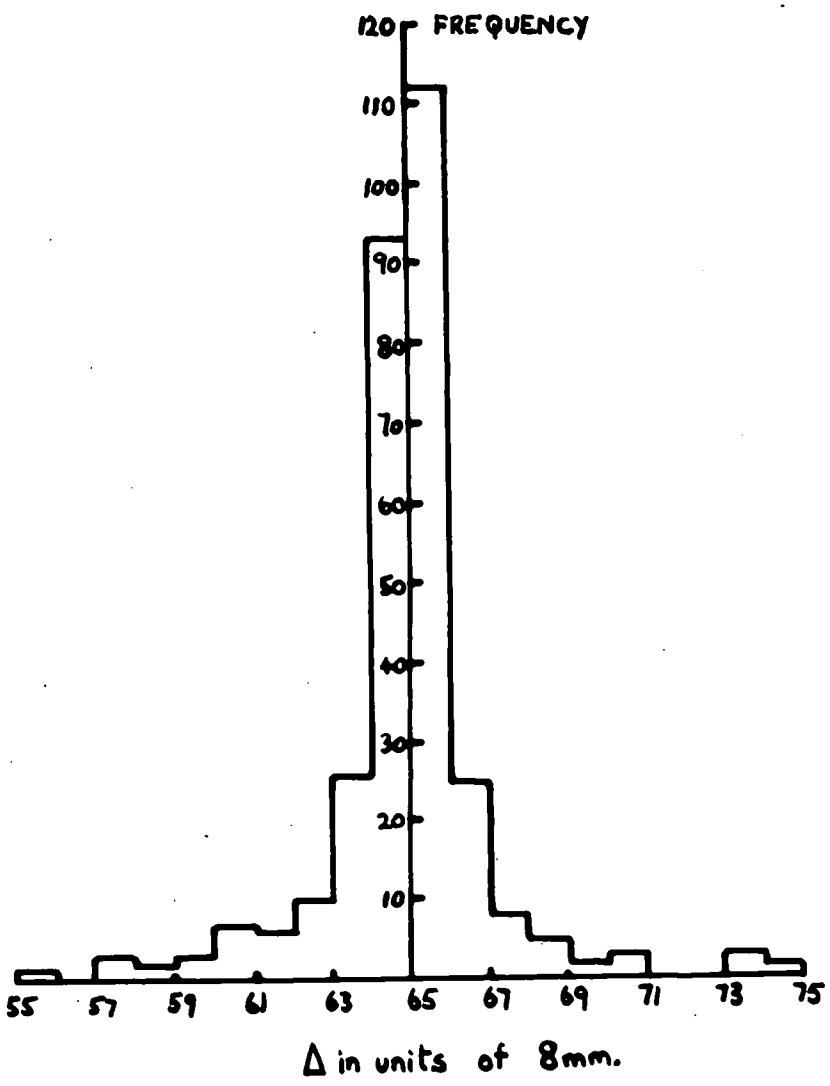

Figure 5.4 Zero magnetic field distribution

is more accurate.

CHAPTER 6

The momentum spectrum of cosmic rays at sea-level

6.1 Introduction

There have been several measurements of the sea-level spectrum with magnet cloud chambers for momenta less than 15 GeV/$_c$ but the most recent and statistically accurate are those of Owen and Wilson (1954) and Caro et al. (1951). The various spectra differ from one another and in particular the Owen and Wilson spectrum is significantly different from that of Caro et al. A χ^2-test shows that the probability of their being consistent is less than 1%. The work to be described here forms the first part of an extended programme at Durham to measure the sea-level spectrum in the range 0.5 - 1,000 GeV/$_c$ to high accuracy.

The sea-level spectrum can be regarded as one of the constants of the cosmic radiation and from it various results of interest can be derived. Starting with a primary cosmic ray spectrum at the top of the atmosphere, a model for meson production and the diffusion equation for the cosmic ray beam in the atmosphere, the sea-level spectrum of μ-mesons can be predicted and compared with experiment. It is clear that in this way information can be gained which can be correlated with other measurements such as extensive air showers and the characteristics of high energy interactions in nuclear emulsions exposed at the top of the atmosphere. Also by comparing the integral spectrum of μ-mesons with the depth-intensity curve information can be gained on the

range-energy relation for high energy μ-mesons. The positive-negative ratio and its variation with momentum is also of interest. From this, information can be gained on the multiplicity of meson production in high energy collisions.

6.2 The experimental technique

During the course of the experiment to be described the magnet current was stabilised at its maximum value, 63 amps., giving $\int H d\ell = 6.22.\ 10^5$ gauss cm. Thus for the arm separating the A and B flash-tube measuring levels the relation between magnetic deflection and momentum is $p\ \Delta = 42.95$ with Δ in units of 8 mm. and p in GeV/c.

The collection of the experimental data was divided into two parts. In the first part all events which produced a five-fold coincidence were used to trigger the flash-tubes so that particles were recorded with momentum greater than 0.39 GeV/c. This experiment was performed to give a check on the spectrum at low momentum which will be found from the geiger counter data.

In the second part only particles were recorded with momenta greater than 3.44 GeV/c. This was achieved by the use of a momentum selector constructed by Mr.D.G.Jones. As mentioned earlier the momentum analyser indicates to which deflection category a particle belongs by producing a voltage pulse of height characteristic of this category. Thus to select particles of a particular momentum band it is necessary to have a gate which will only let through pulses characteristic

of this band. The basic data obtained with all five-fold coincidences and with the momentum selector are shown in tables 6a and 6b.

6.3 The trial spectrum

In evaluating the spectrum it is convenient to have some form of trial spectrum which is of the form of the expected sea-level spectrum and then vary some parameter until a good fit with the measured data is obtained. At the moment suitable trial spectra can be obtained for $p < 20$ GeV/c and $p > 20$ GeV/c but there is no suitable analytical function for the whole momentum range. The reason for this is that for $p < 20$ GeV/c ionisation loss and μ-e decay in the atmosphere are dominant factors, while for $p > 20$ GeV/c π-meson interaction becomes important while ionisation loss and μ-e decay can be neglected. Accordingly the evaluation of the spectrum has been split into two parts, i.e. $p < 20$ GeV/c and $p > 20$ GeV/c.

(i) The trial spectrum for $p < 20$ GeV/c

The form of this spectrum has already been given by Owen and Wilson (1954). Suppose the μ-mesons are all produced at the 100 gm. cm.$^{-2}$ level in the atmosphere with a spectrum of the form $(p+p_t)^{-\gamma}$. Here p_t is the momentum loss of a μ-meson in traversing the atmosphere from the production level to sea-level and p is its momentum at sea-level. The sea-level spectrum is given by $(p+p_t)^{-\gamma} P(t,p)$ where $P(t,p)$, the probability of a μ-meson reaching sea-level with momentum p, is given by

$$P(t,p) = \left\{ \frac{t_0}{t}\left(1+\frac{p_0}{p}\right) - \frac{p_0}{p} \right\}^{-\frac{h}{c\tau}\frac{\mu c}{p+p_0}}$$

Momentum Interval GeV/c	H^+ N^+	H^+ N^-	H^- N^+	H^- N^-	Total
.39-.5	1	3	2	2	8
.5 -.75	17	12	24	17	70
.75-1	30	21	30	22	103
1-1.5	69	51	89	73	282
1.5-2	64	53	83	60	260
2-3	108	74	101	67	350
3-3.98	56	61	71	53	241
3.98-5	49	30	57	43	179
5-5.96	34	22	29	27	112
5.96-7.04	26	17	47	27	117
7.04-7.95	20	16	21	12	69
7.95-10	21	26	34	19	100
10-13	18	17	25	25	85
13-20	26	18	29	13	86
20-30	19	10	15	13	57
30-40	2	5	6	7	20
40-59.6	2	1	6	1	10
59.6-79.5	1	0	2	0	3
79.5-100	2	2	2	0	6
100-154	0	0	2	1	3
154-204	1	0	0	0	1
204	1	0	0	0	1
	567	439	675	482	2,163

Table 6a The basic data obtained with all 5 fold coincidences

Momentum Interval GeV/c	N^+	N^-	Total
3.44-4.1	32	13	45
4.1-5.4	107	53	160
5.4-7.2	180	107	287
7.2-9.55	231	139	370
9.55-12.3	198	114	312
12.3-17.2	171	134	305
17.2-20	56	47	103
20-30	123	79	202
30-40	49	35	84
40-59.6	24	30	54
59.6-79.5	17	10	27
79.5-100	8	3	11
100-154	10	4	14
154-204	4	5	9
204	5	8	13
	1,215	781	1,996

Table 6b The basic data obtained with the momentum selector

Here t_o is the total mass thickness of the atmosphere, p_o is the ionisation loss through the whole atmosphere, h the scale height of the atmosphere and T, μ the lifetime and mass of the μ-meson.

(ii) The trial spectrum for $p > 20$ GeV/c

The form of this spectrum is based on a model proposed by Greisen (1948). Suppose the primary radiation is absorbed exponentially in the atmosphere with a mean free path λ giving rise to a π-meson production spectrum of the form $p^{-\gamma}$. Also assume that the π-mesons are absorbed exponentially with a mean free path λ. The increase in number of π-mesons, dn, in a depth dx gm. cm.$^{-2}$ at a distance x gm. cm.$^{-2}$ from the top of the atmosphere can be written

$$dn_\pi = \frac{1}{p^\gamma} e^{-x/\lambda} \frac{dx}{\lambda} - n_\pi \frac{dx}{\lambda} - n_\pi \frac{dx}{x} B$$

where $B = \frac{H m_\pi c^2}{pc\tau_o}$, H = 6.46. 10^5 cm. and the other symbols have their usual meaning. In the above equation the first term represents the number produced in dx, the second the number lost by interaction and the third the number lost by decay. By integration the number of π-mesons of momentum p at atmospheric depth x is:

$$n_\pi(p,x) = \frac{1}{p^\gamma} \frac{1}{\lambda} \frac{e^{-x/\lambda} x}{1 + \frac{H m_\pi c^2}{pc\tau_o}}$$

From this equation the number of μ-mesons of momentum p at a given depth can be derived, assuming that a π-meson on decaying gives a fraction r of its momentum to the μ-meson.

The number of μ-mesons produced in the element dx at atmospheric depth x is given by

$$dn_\mu = \eta_\pi(p,x)\,\frac{dx}{x}\,B$$

Integrating gives $$\eta_\mu(p,x) = \frac{1}{p^\gamma}\,\frac{1}{\left(1+\frac{pcT_0}{Hm_\pi c^2\tau}\right)}\,r^\gamma\left(1-e^{-x/\lambda}\right)$$

Substituting numerical values in the equation gives the expected form of the high energy sea-level μ-meson spectrum, N(p), as

$$N(p) = \frac{1}{p^\gamma}\,\frac{1}{1+\frac{p}{91}}$$

where p is in GeV/c.

6.4 Experimental bias

(a) Scattering bias

The bias imposed by multiple scattering of particles in the back plane of the spectrograph has been calculated in a manner similar to that for the prototype spectrograph. The magnitude of this bias is 0.97 at 0.39 GeV/c, the minimum detectable momentum of the spectrograph for the conditions of the present measurements. As this bias will decrease with increasing momentum it is concluded that the effect is negligible.

(b) Magnetic bias

The magnetic bias for no momentum selection is determined by the geometry of the geiger counter selection system. The variation of the bias with momentum is shown in figure 6.1.

The magnetic bias for the experiment in which the momentum selector was used is a function both of the geometry of the geiger counter system and the momentum selector itself.

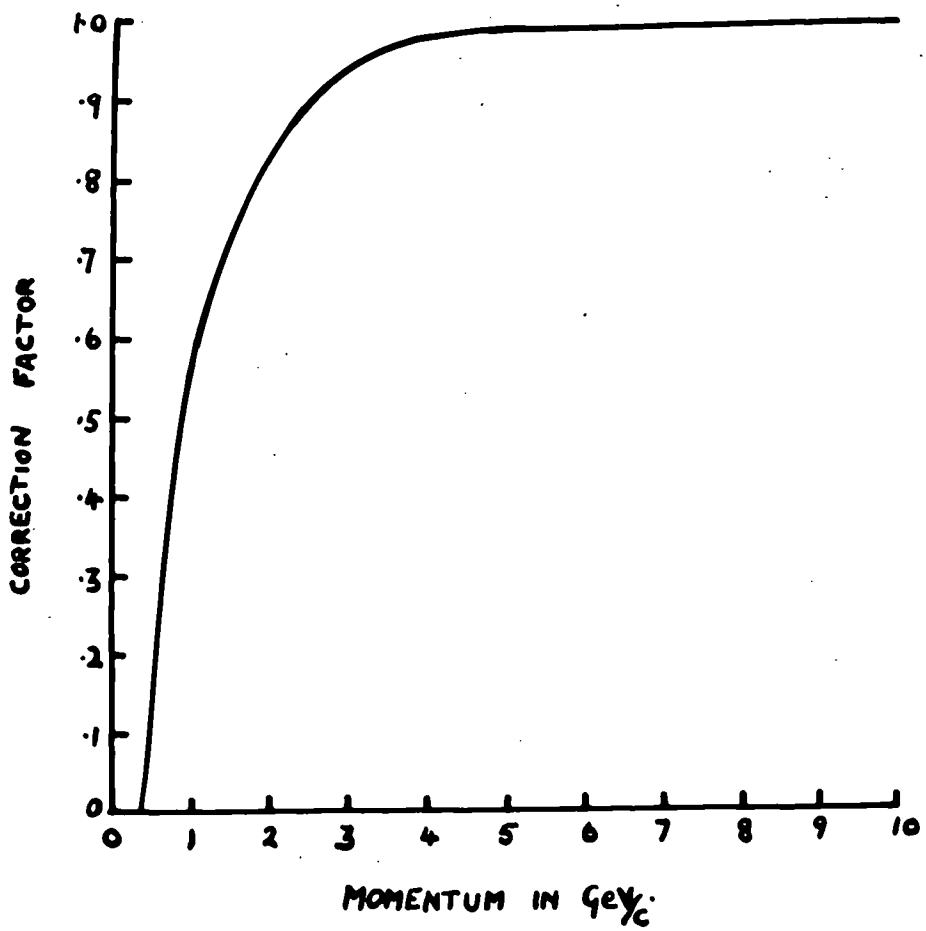

Figure 6.1 Magnetic bias for no momentum selection

An attempt was made to select all particles which traversed categories +1, 0 and -1. However because of the properties of the selector it was found that although the momentum selector was 100% efficient for category 0 events the efficiency for categories +1 and -1 was less. Actually this is an ideal characteristic as it means that high momentum particles, of which there are few, are all accepted while low momentum particles are accepted with decreasing efficiency. This enables the high momentum spectrum to be established with reasonable statistical precision without having to measure a very large number of low momentum particles.

The acceptance function for any momentum category has been considered by Lloyd and Taylor (private communication). This is shown in figure 6.2 for the case of detecting levels G_A, G_B, G_G, G_C, G_D which are infinite in extent. To obtain the acceptance function for a category n under the conditions of operation of the spectrograph the mean of this curve should be moved to n 3.8 cm. and then weighted according to the probabilities of acceptance given in figure 6.1. The deflections given in figure 6.2 are for the geiger counter arm of 192.9 cm.

The acceptance function of the momentum selector was calibrated at the beginning of each run and checked at the end to make sure that its characteristic had not altered. The calibration was performed by feeding in artificial pulses of variable height at a constant rate and determining the rate of pulses transmitted by the selector. A typical calibration

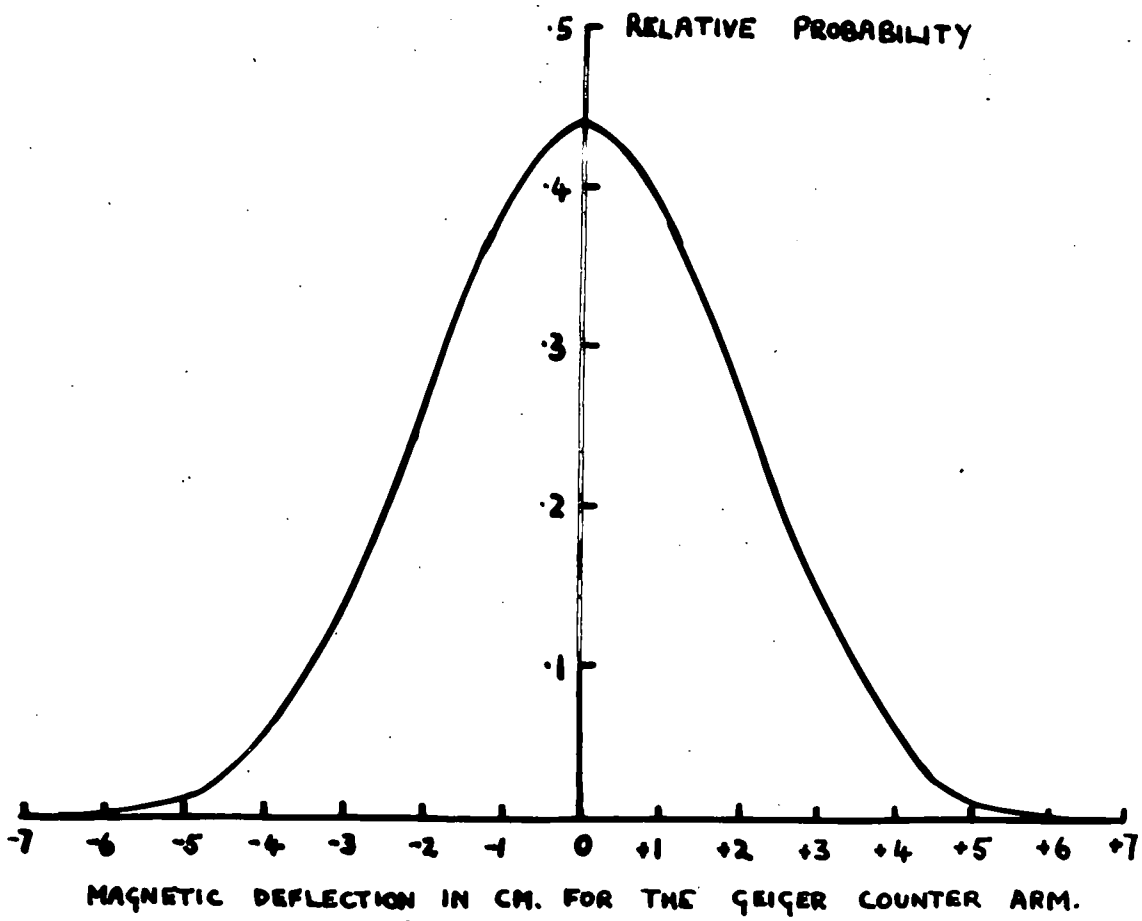

Figure 6.2 The acceptance function for category 0 for geiger trays that are infinite in extent

curve is shown in figure 6.3. In order to determine the relative numbers of particles in categories +1, 0, -1 passed by the momentum selector from the calibration curve it is required to know the distribution of pulse heights about the ideal value which occur for a particular category. It is found that this distribution can be represented by a function which is flat to a distance 0.15 category from the ideal value and then falls linearly to zero at 0.25 category. These functions centred about +1, 0, -1 are also shown in figure 6.3. The distribution of pulse heights about the ideal value arises from inaccuracies in the networks which produce the pulses characteristic of each geiger counter. The relative probabilities of category +1, 0, -1 events being passed by the momentum selector is determined by multiplying the ordinates of the two curves together and taking the ratios of the areas of the dashed curves.

During the experiment with the momentum selector events were gathered during ten separate runs. As the momentum selector characteristic varied slightly from run to run the procedure described was repeated for each one and finally a figure for the ratio +1 : 0 : -1 was calculated which was representative of the total number of events gathered during the ten runs. The momentum selector characteristic shown in figure 6.3 is asymmetric so that for a given magnetic field direction there is a greater probability of recording particles of one sign rather than the other. This effect was balanced out somewhat by reversing the magnetic field for some of the

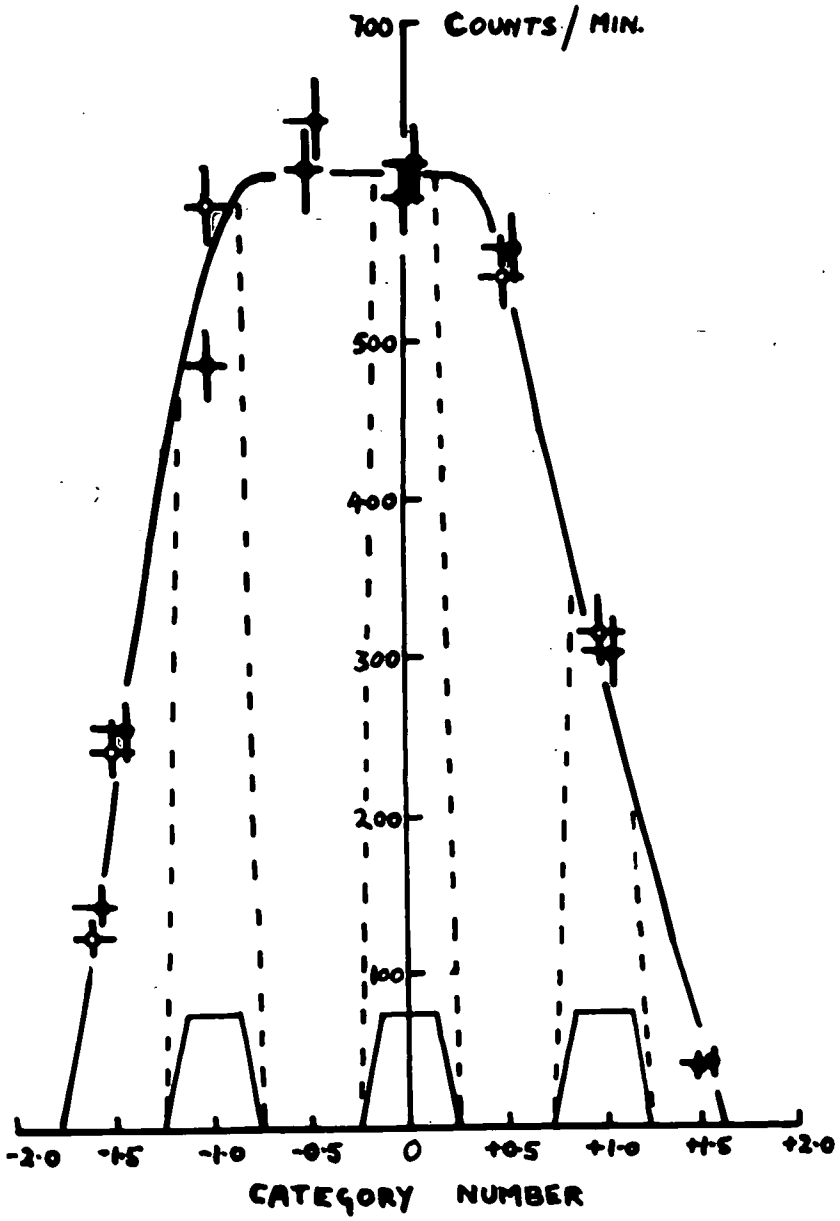

Figure 6.3 A typical momentum selector calibration curve

runs but as more particles were gathered on one direction of the field than the other the final data were biassed against particles of negative sign. The weighted acceptance functions for positive and negative particles obtained with the momentum selector are shown in figure 6.4. This curve has been found using figure 6.1, figure 6.2 and the data obtained from the momentum selector calibrations.

6.5 The errors of momentum determination

There is an uncertainty in the measured magnetic deflection due to scattering in the spectrograph and also due to the location error associated with the flash-tubes. The magnitude of these effects has been determined from the distribution of the separation of the trajectories at the centre of the magnetic field in exactly the same way as for the prototype spectrograph in chapter 4. The result for the scattering constant is $(5.65 \pm 0.06)\%$ compared with the expected value of 5.6%. Also the location error at each level is found to be (1.10 ± 0.07) mm. corresponding to an uncertainty in Δ of 2.17 mm. and a maximum detectable momentum of 158 GeV/$_c$.

The location error at each level of (1.10 ± 0.07) mm. has been obtained by making independent measurements on the trajectory at each of the levels A, B, C, D. Considerably increased accuracy of location is expected when more refined measurements are made in which greatly enlarged replicas of the arrays are used. Such measurements, which are in progress at the present time, should lead to an m.d.m. approaching 1000 GeV/$_c$.

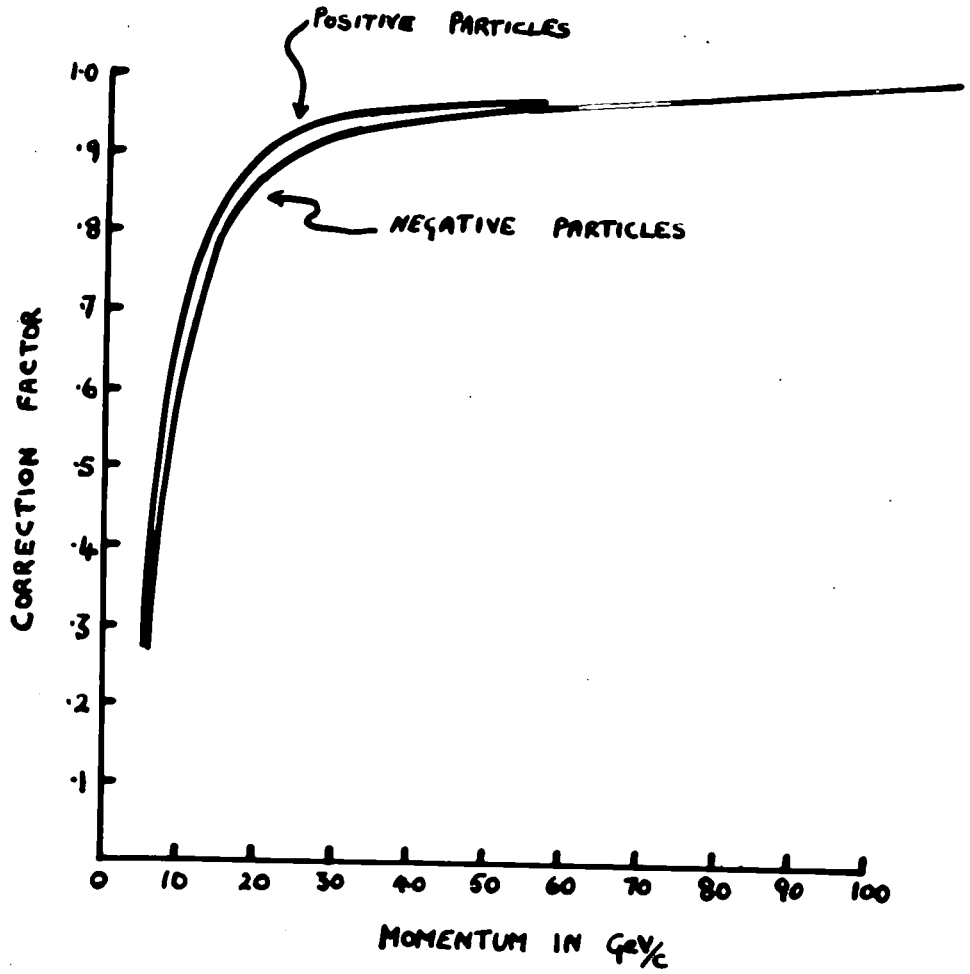

Figure 6.4 Magnetic bias for positive and negative particles for the momentum selector basic data

6.6 The evaluation of the spectrum

(a) Momenta < 20 GeV/c

As mentioned earlier both Owen and Wilson (1954) and Caro et al. (1951) have measured the spectrum accurately in this region. The O spectrum is based on ~ 60,000 events and the C spectrum on ~ 6,000. A comparison between the present data and these spectra has been made by calculating the expected number of events occurring in the momentum cells shown in table 6a. The goodness of fit between the observed distribution and the expected one has been made using the χ^2 test and the result is shown below.

Comparison spectrum	Significance level
O spectrum	90%
C spectrum	15%

From this it is concluded that the present data are in good agreement with the O spectrum and not in significant disagreement with the C spectrum. Pine et al. (1959) on the other hand, working at Cornell University, have measured the spectrum accurately in this region and conclude that their data are in good agreement with the O spectrum but definitely in disagreement with the C spectrum.

In table 6c the observed and expected distribution of particles for the O spectrum is shown together with the rates at which the experimental points should be plotted. Following Owen and Wilson the rates have been normalised to the rate

Momentum Interval GeV/c	$\bar{p}$ GeV/c	Observed	Expected	Rate at $\bar{p}$ cm.$^{-2}$ sec.$^{-1}$ sterad^{-1} MeV/c^{-1} x 10^{-6}	S.D.%
.39- .5	.46	8	9	2.40	35.0
.5 - .75	.63	70	69	2.73	12.0
.75-1	.86	103	117	2.29	9.9
1-1.5	1.25	282	264	2.30	6.0
1.5-2	1.75	260	242	1.76	6.2
2-3	2.5	350	270	1.05	5.3
3-3.98	3.49	241	244	.69	6.4
3.98-5	4.49	179	182	.47	7.5
5-5.96	5.48	112	122	.31	9.5
5.96-7.04	6.50	117	100	.30	9.6
7.04-7.95	7.50	69	68	.202	12.0
7.95-10	8.98	100	98	.133	10.0
10-13	11.5	85	86	.080	10.8
13-20	16.5	86	91	.032	10.8
		2,062	2,062		

Table 6c Evaluation of the spectrum in the range 0.39-20 GeV/c from the basic data obtained with no momentum selection. The 'expected' column is for the Owen and Wilson comparion spectrum.

given by Rossi (1948) of 2.45. 10^{-6} cm.$^{-2}$ sec.$^{-1}$ sterad.$^{-1}$ MeV/c^{-1} at 1 GeV/c. This is necessary since absolute rates were not determined in the experiment.

In table 6d the observed and expected distribution of particles for the 0 spectrum for $p < 20$ GeV/c is shown for the results obtained with the momentum selector. The χ^2 test gives a goodness of fit corresponding to the 33% significance level. It is concluded that there is satisfactory agreement in this overlap region.

(b) Momenta > 20 GeV/c

It has been stated earlier that the expected form of the spectrum for $p > 20$ GeV/c is $p^{-\gamma}\left(1+\frac{p}{q_1}\right)^{-1}$ where p is in GeV/c. For comparison with the observed data the expected distribution of particles for several values of γ were calculated. The steps in the calculation were

(i) The comparison spectrum was corrected for magnetic bias.

(ii) The resulting spectrum was converted into a deflection spectrum and this was broadened with the known uncertainty in the magnetic deflection. To do this the errors were assumed to be Gaussian, the justification being that the distribution of the separation of the trajectories at the centre of the magnetic field was well fitted by this distribution.

(iii) The expected distribution of particles was then computed and compared with observation.

For each value of γ the goodness-of-fit between the observed and expected distributions was studied using the χ^2-test and in figure 6.5 χ^2 is plotted against γ. From

Momentum Interval GeV/c	$\bar{p}$ GeV/c	Observed	Expected	Rate at $\bar{p}$ $cm.^{-2}$ $sec.^{-1}$ $sterad^{-1}$ $MeV/c^{-1} \times 10^{-6}$	S.D.%
5.4-7.2	6.3	287	298	.264	5.9
7.2-9.55	8.4	370	331	.174	5.1
9.55-12.3	10.9	312	313	.090	5.7
12.3-17.2	14.8	305	318	.041	5.7
17.2-20	18.6	103	117	.023	9.8
		1,377	1,377		

Table 6d The momentum selector overlap data. The 'expected' column is for the Owen and Wilson comparison spectrum

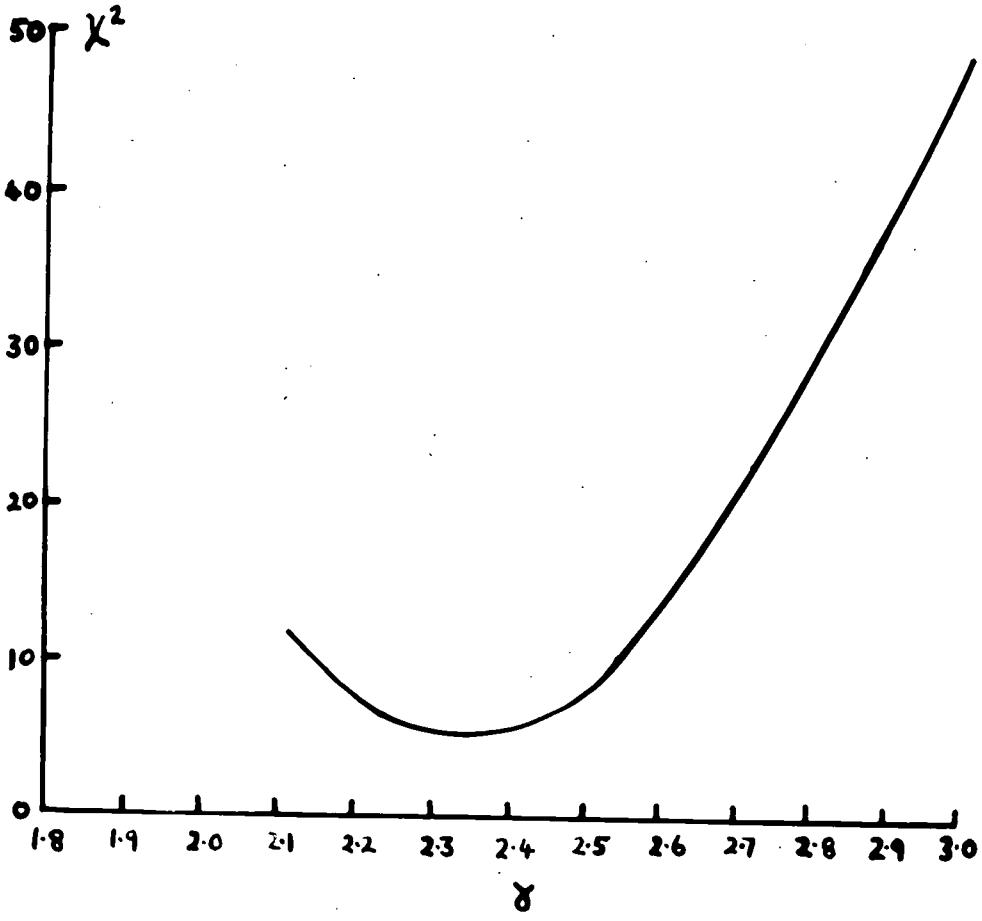

Figure 6.5 Determination of the best fit comparison spectrum for $p > 20$ GeV/$_c$

Momentum Interval GeV/c	$\bar{p}$ GeV/c	Observed	Expected	Rate at $\bar{p}$ cm.$^{-2}$ sec.$^{-1}$ sterad^{-1} MeV/c^{-1}	S.D. %
20-30	25	259	257	$1.21.\ 10^{-8}$	6
30-40	35	104	92	$6.21.\ 10^{-9}$	10
40-59.6	49.8	64	80	$1.60.\ 10^{-9}$	12.5
59.6-79.5	69.6	30	31	$7.49.\ 10^{-10}$	18
79.5-100	89.6	17	16	$4.14.\ 10^{-10}$	24
100-154	127	17	18	$1.36.\ 10^{-10}$	24
154-204	179	10	8	$5.75.\ 10^{-11}$	31
204	358	14	13	$7.08.\ 10^{-12}$	26
		515	515		

Table 6e Evaluation of the spectrum for $p > 20$ GeV/c. The 'expected' column is for the comparison spectrum $p^{-2.34}\left(1+\frac{p}{91}\right)^{-1}$

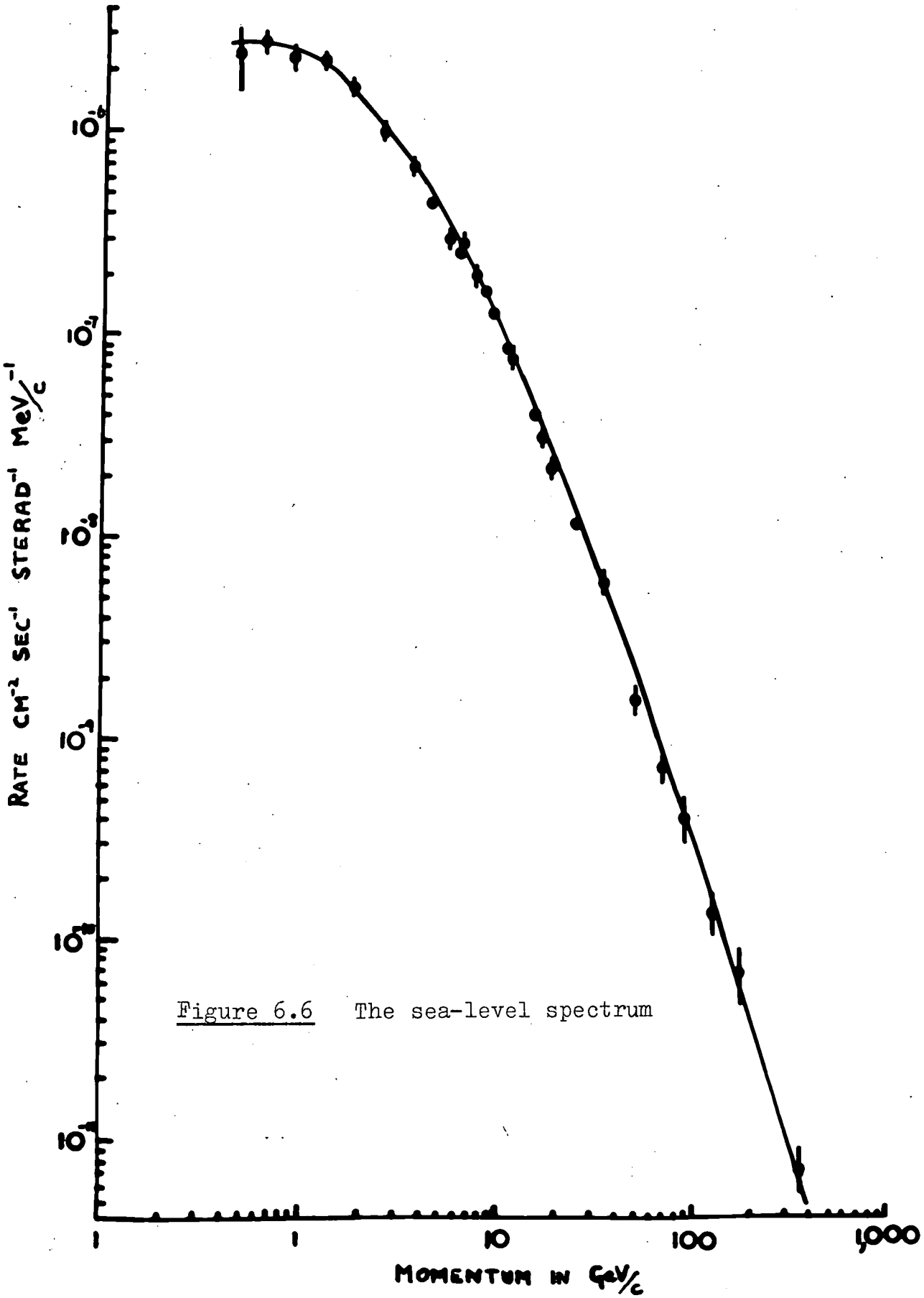

Figure 6.6 The sea-level spectrum

from run to run. Accordingly the positive-negative ratio was calculated using the acceptance functions for positive and negative particles shown in figure 6.4.

In table 6f the calculations on the positive-negative ratio are summarised and in figure 6.7 the ratio is plotted as a function of momentum. Also shown are the results of other workers. It is concluded that the present measurements are not in disagreement with other work but the statistical accuracy is not good enough to establish the form of the variation of the ratio with momentum.

6.8 Comparison with other work on the sea-level spectrum

In figure 6.8 the spectrum obtained from the present experiment is compared with that of Caro et al. (1951), Rodgers (1956) and Pine et al. (1959). For $p < 20$ GeV/c the present work and that of Pine et al. is in good agreement with the Owen and Wilson spectrum but not with that of Caro et al. It is concluded that the best estimate of the sea-level spectrum in this momentum range is that of Owen and Wilson and that the Caro et al. spectrum is possibly in error. For $p > 20$ GeV/c the experimental points of Rodgers are in good agreement with the present data up to the maximum detectable momentum of 158 GeV/c while above this they lie above an extrapolation of the best estimate of the spectrum from the present work. However it should be pointed out that both of the last points of Rodgers are above his m.d.m. of 240 GeV/c. The experimental points of Pine at al. are in good agreement with the present

No momentum selection

Momentum Interval GeV/c	Median Momentum GeV/c	N^+/N^-
.39-2	1.3	1.33 ± 0.10
2-5	3.1	1.35 ± 0.10
5-10	7.3	1.39 ± 0.14
10-30	15.9	1.37 ± 0.17

Momentum selection

Momentum Interval GeV/c	Median Momentum GeV/c	N^+/N^-
3.44-9.55	6.8	1.27 ± 0.09
9.55-30	14.8	1.37 ± 0.09
30-100	40.7	1.29 ± 0.18

Table 6f The positive-negative ratio

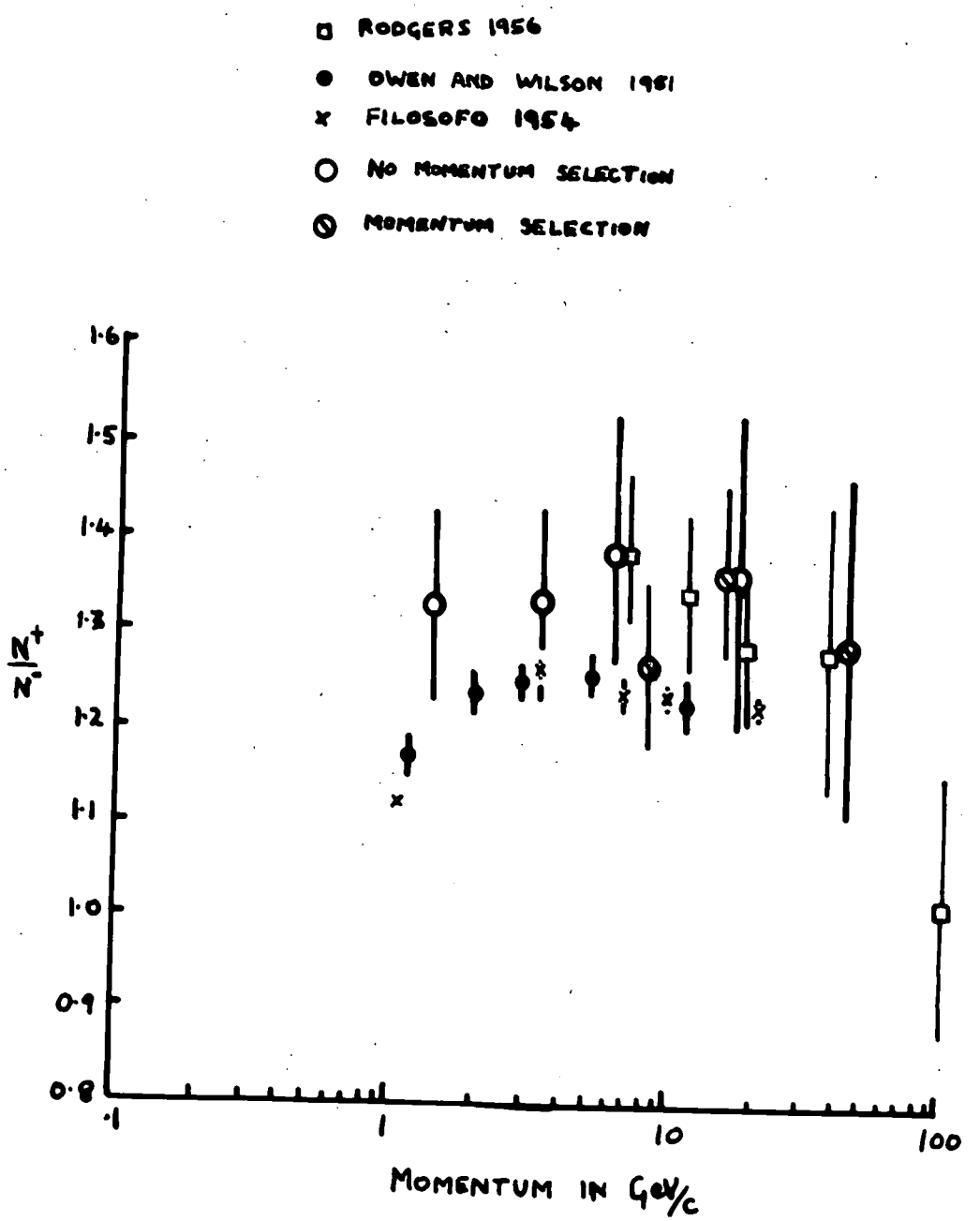

Figure 6.7 The positive-negative ratio

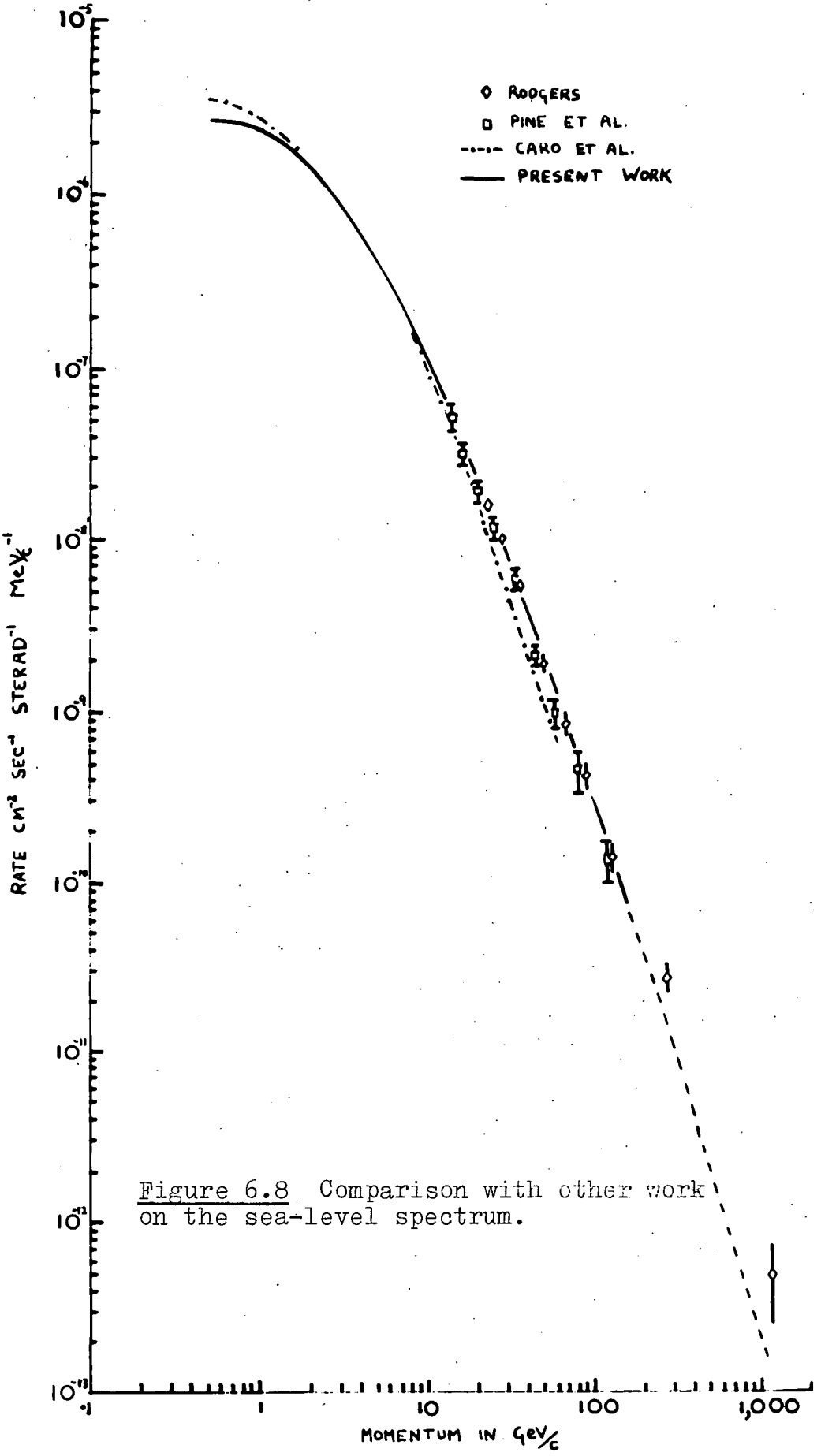

Figure 6.8 Comparison with other work on the sea-level spectrum.

work up to 40 GeV/c and above this they lie slightly below the curve. However nowhere are they significantly different from the present work.

The relative statistical weights of the various experiments, in the high energy region, can be seen from table 6g.

Workers	m.d.m. GeV/c	No. of events with p >20 GeV/c
Caro et al. (1951	100	167
Rodgers (1956)	240	905
Pine et al. (1959)	175	230
Present experiment	158	515

Table 6g

Shower bias

It has been suggested that some of the differences between various measurements of the sea-level spectrum are due to bias effects arising from extensive showers. The general problem of shower bias will now be discussed.

The μ-mesons observed at sea-level are the result of interactions of the primary cosmic rays with air nuclei near the top of the atmosphere. In this interaction approximately equal numbers of π^+, π^- and π° mesons are produced. The π° mesons decay into two γ rays which

initiate an electron-photon cascade. At low energies this cascade is rapidly absorbed but at high energies it reaches sea-level and constitutes the observed extensive air showers. In addition the showers contain a small percentage of μ-mesons derived from the π-mesons produced in the nucleon cascade and an even smaller percentage of nucleons. Thus at high μ-meson energies at sea-level there is a possibility that the μ-mesons are accompanied by electrons. The probability of accompaniment would be expected to increase with energy. As explained earlier the momentum analyser can only indicate the momentum of single unaccompanied particles traversing the spectrograph so a high momentum bias may be present in the basic data obtained with the momentum selector. This is not so in the data obtained from all five-fold coincidences as in this case the μ-mesons can be identified as long as not too many particles traverse any given flash-tube array.

The expected magnitude of the effect can be estimated. Assuming the Fermi theory of meson production, where the number of π-mesons produced by a primary of energy E_p is given by $2.10^{-2}\ E_p^{1/4}$ where E_p is in eV, the average energy, E, of the secondaries can be derived, $E = 50\ E.^{3/4}$, for secondaries of energy 10^{11}eV this gives a multiplicity of 24. Assuming that only π^+, π^-, π° mesons are produced in the collision the number of π_o mesons produced is 8. Also assuming that the collision takes place at the 100 gm. cm.$^{-2}$ level and using the cascade development curves of Greisen (1956) the average number of electrons that reach sea-level is ~ 8. As these

will be spread over the area of a circle of radius ~ 80 metres, Brennan et al. (1958), the chance of an electron striking one of the geiger counter trays is negligible.

A similar calculation for a μ-meson energy of 8.10^{11} eV shows that ~ 510 electrons are expected to reach sea-level. Using the structure function given by Brennan et al. this corresponds to an electron density of ~ 1 per sq. metre at the core.

Barrett et al. (1952) working at 1600 m.w.e. below sea-level have observed the coincidence between μ-mesons underground and electrons at sea-level. Their observations are not inconsistent with these approximate calculations. The effect of air showers on the present measurements can now be assessed. The area of G_A, G_D is 0.57 sq. metres and that of G_B, G_C 0.11 sq. metres. As the energy of shower electrons at sea-level is in the region of the critical energy (~ 98 MeV) and since G_A is shielded by 5.5. cm. Pb and G_C by the yoke of the magnet no bias is expected up to the m.d.m., 158 GeV/c of the present measurements.

6.9 Conclusions

The differential spectrum of cosmic rays at sea-level has been measured up to a momentum of 158 GeV/c. Below 20 GeV/c it can be represented by the form $(p+p_t)^{-2.85} P(t,p)$ where the symbols are defined in section 3 of this chapter. Between 20 GeV/c and 158 GeV/c it can be represented by $p^{-2.34}\left(1+\frac{p}{91}\right)^{-1}$ where p is in GeV/c.

CHAPTER 7

The range-energy relation of high energy μ-mesons

7.1 Introduction

Direct information on the range-energy relation for high energy μ-mesons can be obtained from a comparison of the integral spectrum at sea-level with the depth-intensity curve. That protons are negligible in the cosmic ray beam at sea-level has been established by Mylroi and Wilson (1951) and an estimate of the flux of π-mesons can be made from the equations for the π-meson and μ-mesons flux developed in chapter 6, section 6.3. The result of this calculation is that at 100 GeV/c the π-meson flux is ~ 0.1% of the μ-meson flux and at 1,000 GeV/c it is ~ 1%.

7.2 The depth-intensity curve

Many workers have measured the rate of cosmic rays underground and George (1952) has collected the data for a wide range of depths. Barrett et al. (1952) have also made a similar survey for depths greater than 100 m.w.e. In figure 7.1 the experimental points given by George are shown. In order to draw a smooth curve through the points George and Barrett et al. corrected the rates for the angular distribution of particles to obtain the vertical intensity and also corrected the rates for showers. In figure 7.2 the best estimate of the variation of the vertical intensity of μ-mesons with depth is shown. The curve of George has been taken for depths between sea-level and 100 m.w.e. and for

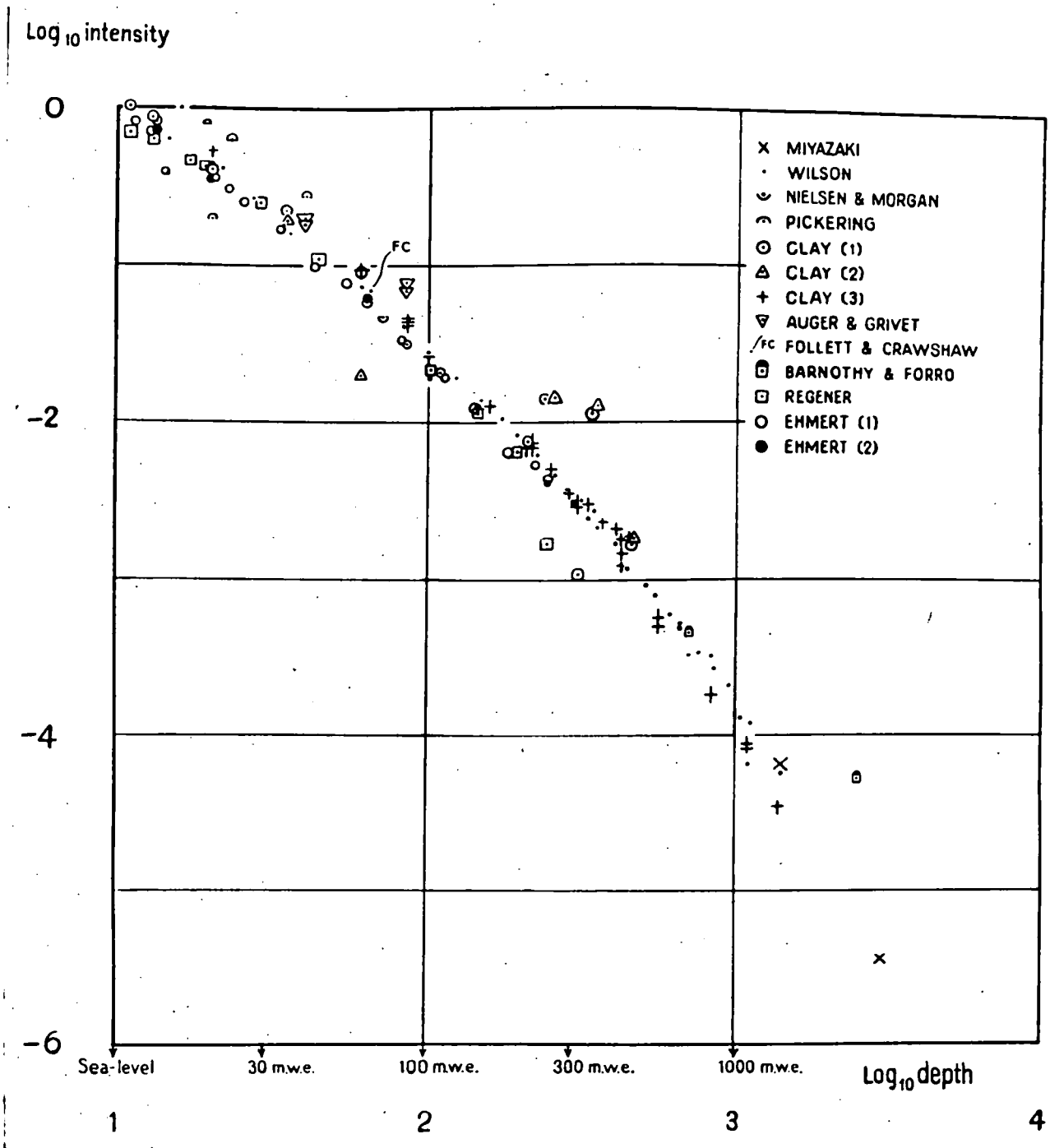

Figure 7.1 The depth-intensity curve, George (1952)

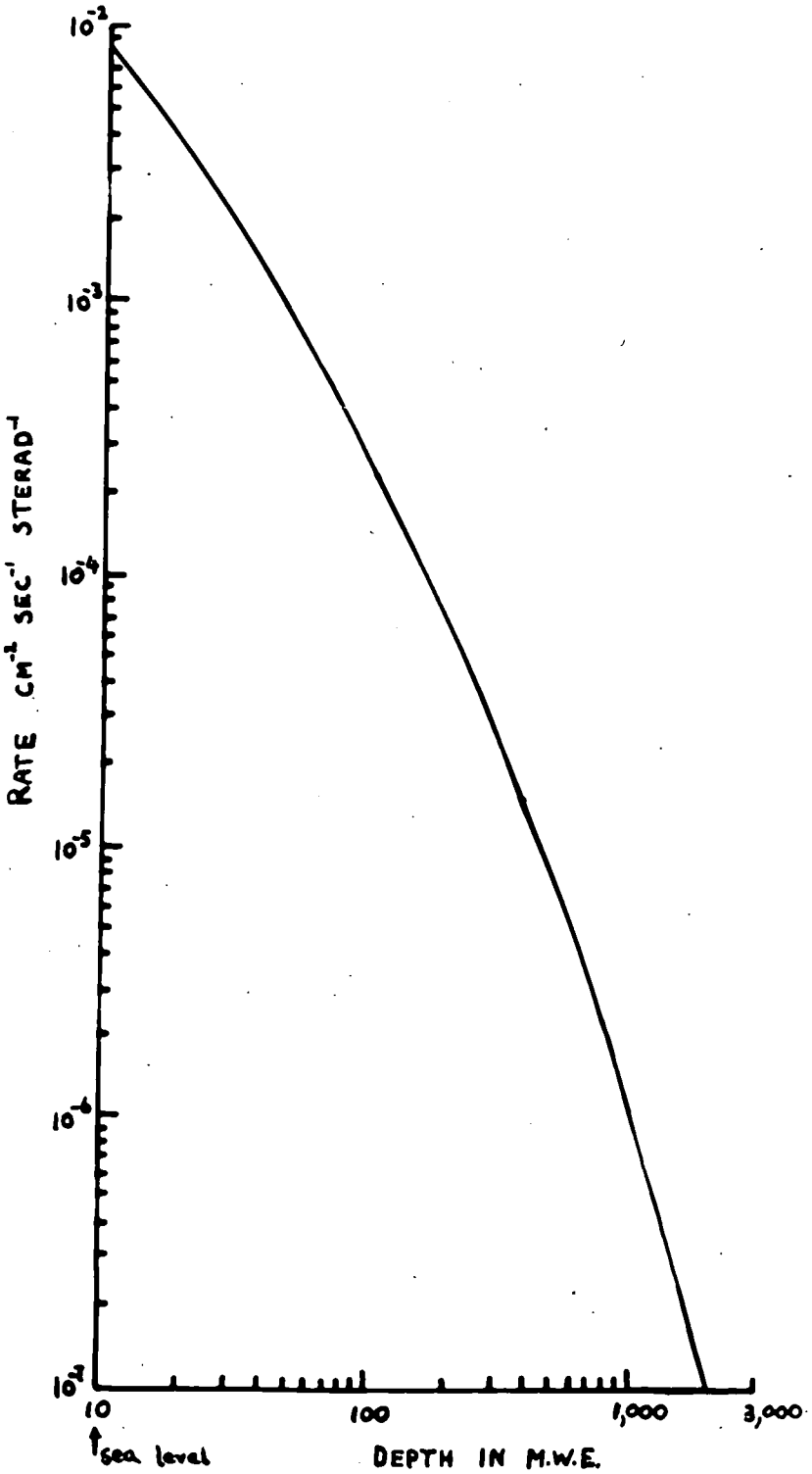

Figure 7.2 Best estimate of the depth-intensity curve

greater depths the curve of Barrett at al. has been used. At great depths Barrett at al. had at their disposal some accurate results of Bollinger (1951). At the moment the depth-intensity curve can be considered well established down to 1900 m.w.e. below sea-level below which there is only the inaccurate measurement of Miyazaki at 3,000 m.w.e.

7.3 The integral spectrum

The integral spectrum of figure 7.3 is derived directly by numerical integration of the differential spectrum shown in figure 6.6. It should be noted that only the last point at high momentum is statistically independent of the rest.

7.4 The theoretical range-energy relation

The rate of energy loss of μ-mesons due to ionisation, Cerenkov radiation, bremsstrahlung, electron pair production and nuclear interaction has already been considered in chapter 4. Summing all the terms gives

$$\frac{dE}{dx} = 1.52 + 0.0766 \ln E'_m + 0.15 \left\{ \ln\left(\frac{E}{\mu c^2}\right) - \frac{1}{2} \right\} E + 2.1\ 10^{-6} E \quad \text{MeV/gm cm}^{-2}$$

where E is in MeV and $E'_m = \dfrac{E^2}{E + \frac{\mu^2 c^2}{2\mu_e}}$

From this equation the range-energy relation can be calculated:

$$R = \int_E^0 -\frac{1}{\frac{dE}{dx}}\, dE$$

The integration has been performed numerically and figure 7.4 shows the range-energy relation obtained. For μ-meson energies greater than 1 GeV momentum and energy are

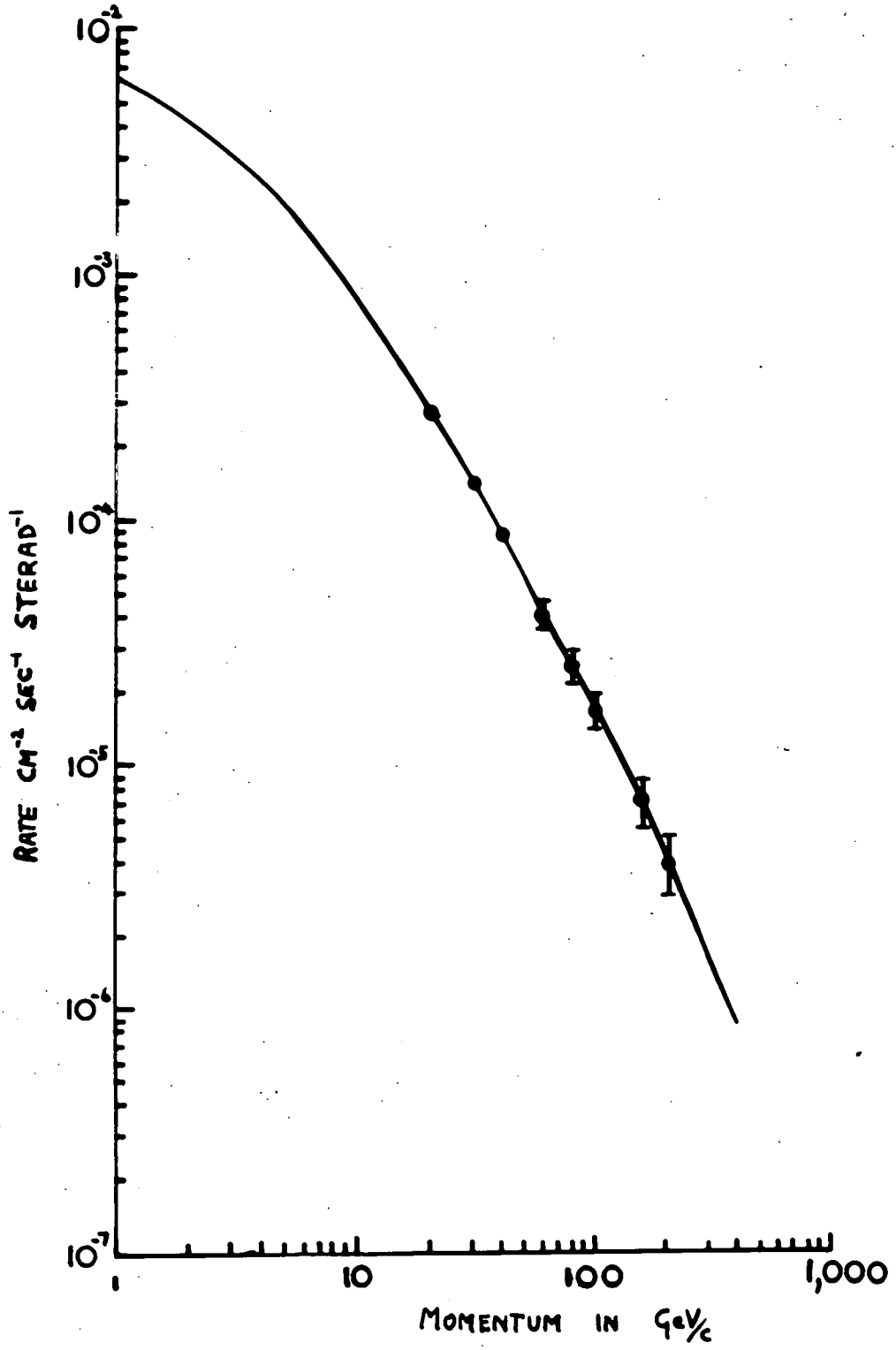

Figure 7.3 The integral spectrum at sea-level

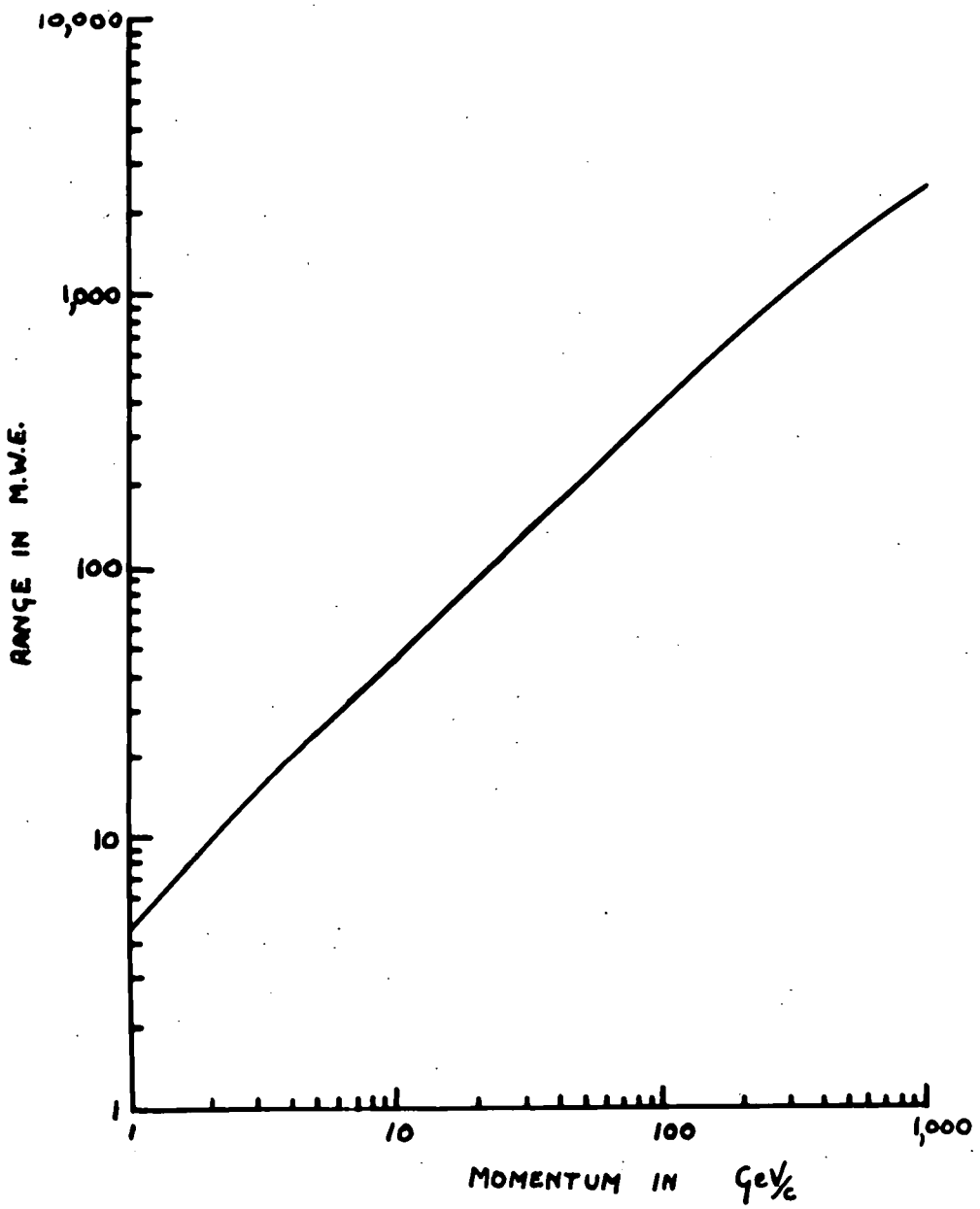

Figure 7.4 Theoretical range-energy relation for μ-mesons

interchangeable as the rest energy of the μ-meson is small compared with the total energy.

The validity of the range-energy relation derived in this manner using the mean energy loss for bremsstrahlung has been checked by Bollinger (1951) in a Monte Carlo calculation. He concluded that for energies up to 10^{12} eV the range-energy relation derived in the above way was accurate. This result can be accounted for in contrast to the behaviour of electrons because of the relative importance of direct pair production. Whenever bremsstrahlung is an important process of energy loss for μ-mesons, direct pair production is equally important. The latter involves more numerous transfers of comparatively low energy than does bremsstrahlung, hence fluctuations are not large in pair production losses. These losses prevent any mesons from experiencing ranges much larger than those which correspond to the mean rate of energy loss. For electrons on the other hand the fluctuations in range are considerable since direct pair production is not responsible for much of the energy loss.

7.5 Comparison of the integral spectrum and the depth-intensity curve

From the integral spectrum and the range-energy relation the expected rates at various depths underground have been calculated and these are shown in figure 7.5. The rates underground have been normalised so that the predicted rate at 10 m.w.e. below sea-level is the same as the rate given by George at this depth. Allowing for the fact that the

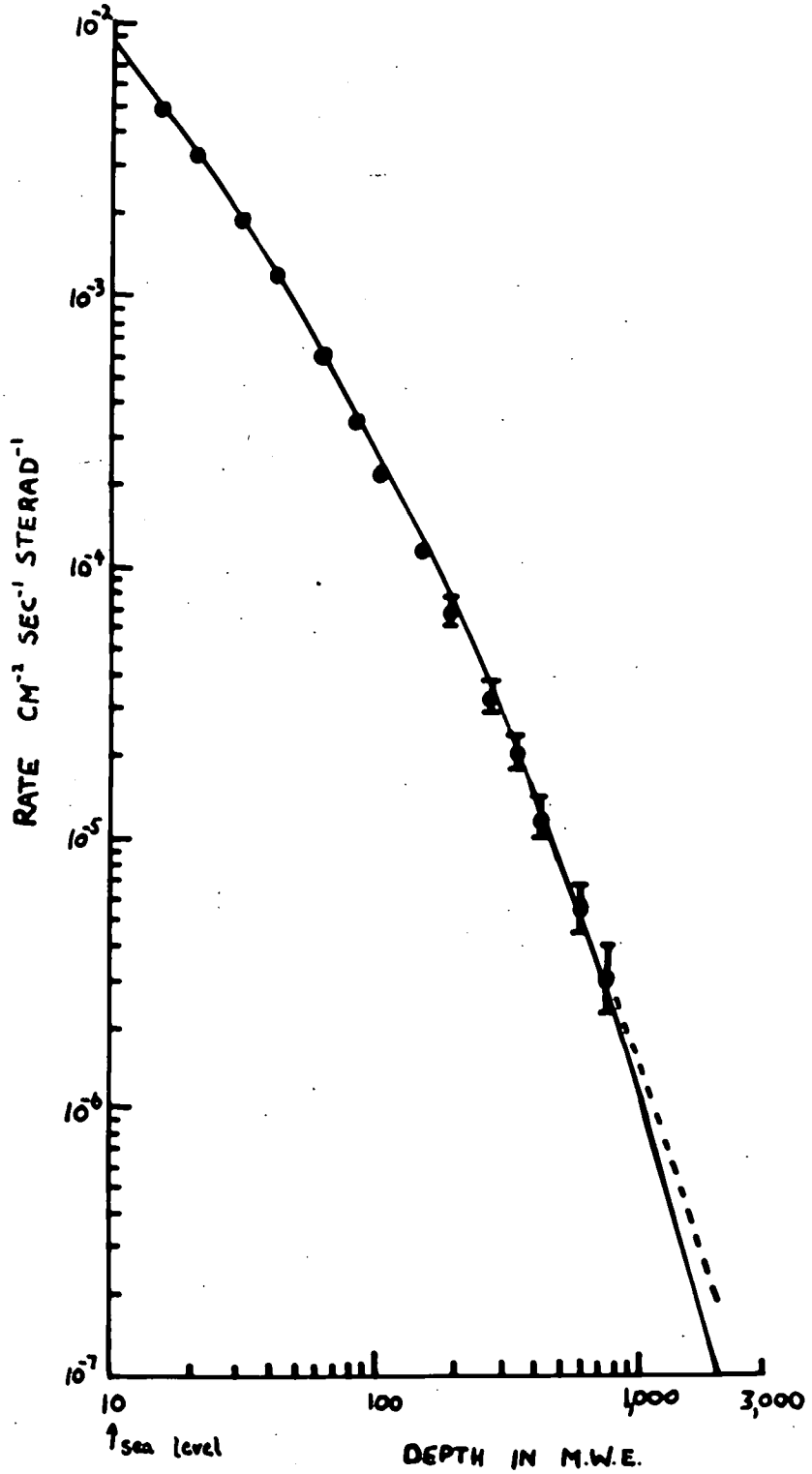

Figure 7.5 The depth-intensity curve. The experimental points refer to rates calculated from the sea-level integral spectrum and the theoretical range-energy relation.

experimental rates measured underground are distributed somewhat about this curve the fit is good. In particular for depths less than 100 m.w.e. the fit is excellent and there is no indication of an energy loss different from that expected theoretically. From a comparison of the spectrum at 37.7 m.w.e. below sea-level with the sea-level spectrum discussed in chapter 4 it was found that the best fit between the two spectra occurred for an energy loss which was less than the expected loss. However the result was not statistically inconsistent with the expected loss and it is now concluded that in this energy region the energy loss is in accord with theory.

For depths greater than 100 m.w.e. a trend is noticed in so far as the points between 100 m.w.e. and 300 m.w.e. lie just below the curve while the two points at a depth greater than 300 m.w.e lie just above it. Extrapolating the integral spectrum gives the dashed curve which lies above the intensity-depth curve. It is found that a differential spectrum of the form $p^{-2.6}\left(1+\frac{p}{91}\right)^{-1}$ for $p > 20$ GeV/c at sea-level would give good agreement between the sea-level integral spectrum and the depth-intensity curve down to 2,000 m.w.e. using the range-energy relation calculated above. From the χ^2, γ plot shown in figure 6.5 it is found that the chance that the present data is consistent with an exponent of 2.6 is 5%. Thus the present results are not entirely inconsistent with such an exponent. However, it should be pointed out that an extrapolation of the sea-level spectrum to momenta much greater than the maximum

detectable momentum is not justifiable and in fact the sea-level spectrum may increase in exponent for $p > 158$ GeV/$_c$. Measurements at momenta greater than 150 GeV/$_c$ are required to resolve this question and these are at present in progress at Durham.

7.6 Comparison with other work

Rodgers (1956) has compared his sea-level spectrum with the depth-intensity curve and reported an indication of larger energy losses than indicated by theory for energies >50 GeV. However Rodgers took the theoretical energy loss of μ-mesons of all energies to be 2.2 MeV/ gm. cm.$^{-2}$ and this is now known to be in error. A reanalysis of his results using the range-energy relation of figure 7.4 shows that the energy loss of μ-mesons is consistent with theory up to 150 GeV and above this value his last two experimental points lie above the depth-intensity curve. The last two points on his sea-level spectrum are above his m.d.m. of 240 GeV/$_c$ and hence little weight can be attached to them. The results of Rodgers are thus in good agreement with the present work.

Pine et al. (1959) have also compared their integral spectrum with the depth-intensity curve and conclude that the range-energy relation of μ-mesons is consistent with theory up to an energy of 150 GeV. The extrapolation of their integral spectrum also indicates increased energy losses at high energy.

7.7 Conclusions

Both the present experiment and those of Rodgers and Pine et al. show that the range-energy relation for μ-mesons is consistent with theory up to the maximum momentum that has been reliably measured experimentally. An extrapolation of all three spectra to higher momenta shows that the sea-level spectrum, the depth-intensity curve and the theoretical range-energy relation of μ-mesons are not consistent with one another. Whether this is due to an increase in energy loss over the theoretical loss for energies > 150 GeV or whether it is due to a change in slope of the sea-level spectrum for energies > 150 GeV cannot be decided from the present experimental evidence. More experimental data at high energy are required to resolve this point.

ACKNOWLEDGEMENTS

The author wishes to acknowledge the support given and the facilities provided by Professor G.D.Rochester, F.R.S. He would also like to thank his supervisor, Dr.A.W.Wolfendale, for his help and encouragement at all stages of the work.

The experiment at 37.7 m.w.e. below sea-level was performed in the Nottingham University Underground Cosmic Radiation Laboratory and he would like to express to the Nottingham group, Dr.W.F.Nash, Mr.J.E.Cousins and Mr.D.Coates, his appreciation for their hospitality and cooperation.

The work at sea-level was carried out with the help of Messrs. J.L.Lloyd, D.G.Jones, F.E.Taylor and P.J.Hayman. The author is grateful for their cooperation.

Messrs. M.Crossland and A.Bryce of the laboratory staff assisted in the reduction of experimental data at various stages of the work.

He is indebted to the D.S.I.R. for the provision of a Research Studentship which enabled this work to be carried out.

REFERENCES

Apostolakis A.J. and Macpherson I., 1957, Proc.Phys.Soc., A70, 146 and 154.

Ashton F, Kisdnasamy S and Wolfendale,A.W., 1958, Nuovo Cimento, 8, 615.

Barrett P.H., Bollinger L.M., Cocconi G., Eisenberg Y., and Greisen K. 1952, Rev.Mod.Phys., 24, 133.

Bethe H. 1930, Ann. d. Physik, 5, 325.
1932, Zeits f.Physik, 76, 293.
1937, Rev.Mod.Phys., 9, 245.

Bhabha H.J., 1935, Proc.Roy.Soc., A152, 559.
1938, Proc.Roy.Soc., A164, 257.

Bollinger,L.M., 1951, Ph.D. Thesis, Cornell University.

Braddick H.J. and Leontic B., 1954, Phil.Mag., 45, 1287.

Brennan M.H., Millar D.D., and Wallace C.S., 1958, Nature, 182, 905.

Budini and Moliere G., 1952 "New Research Techniques in Physics" p.59.

Caro D.E., Parry J.K and Rathgeber H., 1951, Aust.J.Sci.Res., A4, 16.

Christy R.F. and Kusaka S., 1941, Phys.Rev., 59, 414.

Conversi M., Focardi S., Franzinetti C., Gozzini A., and Murtas P., 1955, "Proceedings of the Pisa Conference on Elementary Particles"

Dayon M.I. and Potapov L.I., 1959, Z.E.I.T.F., 36, 697.

Fermi E., 1940, Phys.Rev., 57, 485.

Filosofo I., Pohl E and Pohl-Ruling J., 1954, Nuovo Cimento, 12, 809.

Gardener M., Kisdnasamy S., Rössle E. and Wolfendale A.W., 1957, Proc.Phys.Soc., B60, 687.

George E.P. and Evans J., 1950, Proc.Phys.Soc., A63, 1248.

George E.P., 1952, P.C.R.P., Vol.I.

George E.P. and Shrikantia G.S., 1956, Nuclear Physics, I, 54.

Greisen K., 1948, Phys.Rev., 73, 521.
1956, P.C.R.P., Vol. III.

Halpern O.and Hall H., 1948, Phys.Rev., 73, 477.

Hyams B.D., Mylroi M.G., Owen B.G., and Wilson J.G., 1950, Proc.Phys.Soc., A63, 1053.

Janossy L., 1948, "Cosmic Rays" p.177, Clarendon Press, Oxford.

Kisdnasamy S., 1958, Ph.D. Thesis, Durham University.

McDiarmid I.B., 1954, Phil.Ma., 45, 933.

Moroney M.J., 1954, "Facts from figures" p.246, Penguin Books Ltd., London.

Massey H.S.W. and Corben H.C., 1939, Camb.Phil.Soc., 35, 463.

Mylroi M.G., andWilson J.G., 1951, Proc.Phys.Soc., A64, 404.

Nash,W.F. and Pointon A.J., 1956, Proc.Phys.Soc., A69, 725.

Owen B.G., and Wilson J.G., 1951, Proc.Phys.Soc., A64, 417.
1955, Proc.Phys.Soc., A68, 409.

Pine J, Davisson R.J. and Greisen K., 1959, Private Communication.

Rodgers A.L., 1956, Ph.D. Thesis, Manchester University.

Rossi B. and Greisen K., 1941, Rev.Mod.Phys., 13, 240.

Rossi, B., 1948, Rev.Mod.Phys., 20, 537.

Sternheimer R., 1956, Phys.Rev., 103, 511.

Swann,W.F., 1938, J.Frank.Inst., 226, 598.

Wick, G.C., 1940, Ricerca. Scient. 11, 273.